Abstract book

The 19th international symposium on

Biomechanics in Vascular Biology and Cardiovascular Disease

16 – 17 May 2024

Thursday May 16th

08.00 – 08.50	Registration, coffee, poster set-up
08.50 – 09.00	Opening
09.00 – 09.30	**Keynote Blanca Rodriguez, University of Oxford, Oxford, United Kingdom** *Digital twins for cardiovascular disease investigations: modelling, simulation, and big data* *Chair: Frank Gijsen*
09.30 – 10.40	**Session Fluid Mechanics and Pathology** *Chair: Philippe Bijlenga and Jolanda Wentzel*
09.30 – 09.50	Peter Stone, Harvard Medical School, Boston, USA *Widening the Lens for Risk-Stratification of High-Risk Plaques Likely to Cause Future MACE: From Invasive IVUS/OCT to Non-Invasive CCTA*
09.50 – 10.10	Ryan Pedrigi, University of Nebraska, Lincoln, USA *Normal Blood Flow plus Atorvastatin Promotes Regression of Unstable Plaques*
10.10 – 10.25	Peter Weinberg, Royal Brompton Hospital, London, United Kingdom *Relative Residence Time can account for half of the anatomical variation in fatty streak prevalence within the right coronary artery*
10.25 – 10.40	Diego Gallo, Politecnico di Torino, Turin, Italy *Functional and Hemodynamic Assessment in Elderly Patients with Myocardial Infarction and Multivessel Disease. A Longitudinal Study*
10.40 – 11.10	Coffee break
11.10 – 12.40	**Session Mechanotransduction I** *Chair: Paul Evans and Tzung Hsiai*
11.10 – 11.30	Suowen Xu, University of Science and Technology of China, Hefei, China *Endothelial IGFBP6 Suppresses Vascular Inflammation and Atherosclerosis*
11.30 – 11.50	Young-June Jin, Max Planck Institute for Heart and Lung Research, Bad Nauheim, Germany *Endothelial protein kinase N1 (PKN1) mediates phosphorylation of histone H3.3 for rapid disturbed flow-induced gene activation*
11.50 – 12.10	Graeme Birdsey, Imperial College London, London, United Kingdom *Loss of ERG function contributes to lymphatic vessel malformations and primary lymphoedema*
12.10 – 12.25	Daniela Pirri, Imperial College London and Mary University of London, London, United Kingdom *EPAS1 maintains endothelial homeostasis and is atheroprotective via lipid metabolism at sites of disturbed flow.*
12.25 – 12.40	Eulashini Chuntharpursat, University of Leeds, Leeds, United Kingdom *Mechanosensing at endothelial cell-cell junctions*
12.40 – 14.00	Lunch - posters
14.00 – 15.25	**Session Aneurysms** *Chair: Peter Weinberg and Selene Pirola*
14.00 – 14.20	Philippe Bijlenga, Geneva University Hospital, Genève, Switzerland *Navigating the Mist: Unveiling the Mysteries of Intracranial Aneurysm*
14.20 – 14.40	Michela Bozzetto, Mario Negri Institute for Pharmacological Research, Milan, Italy *Do Vascular Wall Vibrations Play a Role in Vascular Disease? The Case of Cerebral Aneurysm and Arteriovenous Fistula*

14.40 – 14.55	Mannekomba Diagbouga, University of Geneva, Genève, Switzerland *Exploring endothelial dysfunction and mechanical forces in intracranial aneurysm pathogenesis: insights from transcriptomic studies*
14.55 – 15.10	Beatrice Bisighini, University of Lyon and University of Jean Monnet, Saint-Etienne, France *Coupling finite element and machine learning modelling for the real-time simulation of intracranial aneurysms endovascular treatment*
15.10 – 15.25	Janneck Stahl, University of Magdeburg, Magdeburg, Germany *Can black blood MRI indicate unstable neurovascular pathologies? A hemodynamic analysis of wall and intraluminal enhancement*
15.25 – 16.00	Coffee break - posters
16.00 – 17.15	**Session Digital twin of (congenital) heart disease** *Chair: Blanca Rodriguez and Michele Conti*
16.00 – 16.20	Wouter Huberts, TU Eindhoven, Eindhoven, the Netherlands *An efficient uncertainty and sensitivity analysis approach to direct personalization and assess the credibility of digital human twins*
16.20 – 16.40	Nele Famaey, KU Leuven, Leuven, Belgium *A multi-scale, multi-physics approach to understand and prevent cardiovascular maladaptation in the Ross procedure*
16.40 – 17.00	Arno Roest, Leids Universitair Medisch Centrum, Leiden, the Netherlands *The incremental value of computational fluid dynamics (CFD) in single ventricle congenital heart disease*
17.00 – 17.15	Sander Schomaker, University of Groningen, Groningen, the Netherlands *Efficient personalized lumped parameter modeling of pulmonary arterial hypertension*
17.15 – 17.30	Closing day 1
19.00	Conference dinner

Friday May 17th

08.00 – 09.00 Registration - coffee

09.00 – 10.25 Session Mechanotransduction II

Chair: Hanjoong Jo and Graeme Birdsey

09.00 – 09.20 Ellie Tzima, University of Oxford, Oxford, United Kingdom
Mechanisms of endothelial flow sensing

09.20 – 09.40 Caroline Cheng, UMC Utrecht, Utrecht, the Netherlands
Mechanosensing and regenerative medicine for human IPCs vascular cells

09.40 – 09.55 Tzung Hsiai, UCLA, Los Angeles, USA
Multi-Scale Mechano-OMIC Interactions to Uncover Molecular Transducers for Vascular Protection

09.55 – 10.10 Elizabeth Jones, KU Leuven, Leuven, Belgium
Acetylation permits arterial gene expression in a SMAD1/5-dependent manner in the pre-flow embryo

10.10 – 10.25 Rob Krams, Queen Mary University London, London, United Kingdom
A.I. driven RNA therapeutics. Validation with a new CRISPR high throughput platform

10.25 – 11.00 Coffee break – posters

11.00 – 12.10 Session Wall mechanics

Chair: Michela Bozzetto and Umberto Morbiducci

11.00 – 11.20 Ali Akyildiz, Erasmus Medical Centre, Rotterdam, the Netherlands
Role of Mechanical Wall Stress in Coronary Atherosclerosis

11.20 – 11.40 Koen Reesink, Maastricht University, Maastricht, the Netherlands
The Maastricht acquisition platform for studying mechanisms of cell-matrix crosstalk (MAPEX): Emerging insights on ascending thoracic aortic aneurysm formation

11.40 – 11.55 Farhad Nezami, Harvard Medical School, Boston, USA
Real-Time Quantification of Patient-specific Wall Stress in Diseased Coronary Arteries

11.55 – 12.10 Virginia Fregona, Politecnico di Milano, Milan, Italy
Impact of thrombus mechanical properties on virtual thrombectomy procedures

12.10 – 13.45 Lunch - posters XXXX

13.45 – 14.15 NHS Lecture Hanjoong Jo, Emory University of Medicine, Atlanta, USA
Disturbed Flow-Induced Reprogramming of Endothelial Cells (FIRE) in Atherosclerosis

Chair: Jolanda Wentzel

14.15 – 15.45 Session Human disease models

Chair: Ton van der Steen and Behrooz Fereidoonnezhad

14.15 – 14.35 Pat McGarry, University of Galway, Galway, Ireland
Microstructually based biomechanical models for human thrombi

14.35 – 14.55 Abdul Barakat, Ecole Polytechnique, Palaiseau, France
Role of Endothelial Cell Shape and Orientational Order in Angiogenic Sprouting

14.55 – 15.15 Michele Conti, University of Pavia, Pavia, Italy
Bioprinting of 3D vascular models. Biofabrication Process and Preliminary Results using FRESH technique

15.15 – 15.30 Frank Gijsen, Erasmus Medical Center, Rotterdam, the Netherlands
A tissue-engineered model of the atherosclerotic plaque cap with microcalcifications

15.30 – 15.45	Gábor Závodszky, University of Amsterdam, Amsterdam, the Netherlands *Image-based flow and structural simulation of platelet aggregates under low, medium, and high shear flow conditions*
15.45 – 16.30	Awards, closing remarks, drinks

Abdel-Raouf, Yousof	27	Examining the range of Constrained Mixture Modelling in predicting Adaptation and Maladaptation in Arterial Mechanics
Armour, Chloe	25	The importance of patient-specific boundary conditions when modelling the pulmonary artery
Berghout, Brian	8	Biomechanical exploration of ischemic stroke risk among atherosclerotic carotids – a BRISKNESS pilot study
Bontempi, Luca	26	Aortic Annuloplasty: a Methodology to integrate Experimental Data, In-silico Analysis, and 4D-flow MRI Validation
Caballero, Ricardo	9	In-Silico Modeling of Atherosclerosis: An Agent-Based Modeling Approach
Çelikbudak Orhon, Cemre	5	Stiffening of the Large Arteries in Healthy Aging
Cruts, Janneke	24	Fibrin clot formation modeling: from in vitro validation to 3D simulations
De Nisco, Giuseppe	6	Lipid-Rich Plaque Progression in Human Coronary Arteries can be Predicted Combining Multimodal Imaging and Computational Hemodynamics
Fontana, Federica	32	Impact of calcifications on the hemodynamics of the intracranial internal carotid artery
Garreau, Morgane	12	In-silico modelling of cerebral vasculopathy among pediatric patients with sickle cell disease
Gijsen, Frank	28	Thrombus composition and mechanical properties
Gijsen, Frank	29	Thrombus imaging properties and mechanical properties
Kolega, John	1	Spatial transcriptomics of remodeling brain arteries reveals potential molecular signals for dystrophic versus eutrophic responses to flow
Krams, Rob	18	A fully automated vulnerable plaque classifier for OCT accurately predicts vulnerable plaques in human coronary arteries.
Kuijk, Sanne van	30	Mechanical characterization of thrombi by studying shear and friction
Kuppers, Wieger	22	Arterial arcades and collaterals regress under hemodynamics-based diameter adaptation: a computational and mathematical analysis
Lin, Daigi	31	CFD assisted Machine Learning for blood flow prediction in patient-specific aorta geometries
Lissoni, Vittorio	7	Fluid-structure interaction simulations for the investigation of coronary artery disease
Manenti, Mattia	15	In Vitro Model Mimicking Early-Stage Tissue Formation in in situ Tissue-Engineered Vascular Access Grafts
Mannekomba, Diagbouga	21	Characterizing TWIST1 signalling pathway in atheroprogression
Murali, Amal Roy	17	Gaussian processes improve rapid estimates of physics-based artificial intelligence predictors of 3D velocity, shear

		stress and pressure fields in pig and human coronary arteries.
Ruisch, Janna	4	In vivo evaluation of the hemodynamic consequences of carotid endarterectomy by using ultrafast ultrasound-based blood flow imaging
Rutten, Lisa	23	Optical Coherence Tomography versus Computed Tomography Angiography in the stented femoropopliteal tract for Computational Fluid Dynamics
Sengupta, Sampad	13	Complex Aortic Arch Repair: a Fluid-Structure Interaction analysis
Suk, Julian	10	Machine Learning-Based Estimation of Wall Shear Stress using Small Data
Tardajos Ayllón, Blanca	19	Twist1 deletion influences atherosclerotic plaque size and composition
Tian, Siyu	20	Endothelial GATA4 in Atherosclerosis Progression
Tziotziou, Aikaterini	2	Mechanical wall stress and wall shear stress are associated with atherosclerosis development in coronary arteries
Tziotziou, Aikaterini	3	In-depth calcification morphometrics in carotid arteries are associated with cerebrovascular events, sex and cardiovascular risk factors
Wang, Tianai	14	Altercations of aortic hemodynamics during aortic valve stenosis leading to subclinical hemolysis: A subject-specific analysis using 4D Flow MRI-based CFD techniques
Zambon, Sara	11	Mechanical stress in coronary atherosclerotic plaques: Comparison of 2D vs. 3D computational strategies
Zwaan, Robert	16	The left ventricular strain-volume loop in a healthy Dutch population: age- and sex related differences

Conference dinner

21 Pinchos

Starts at:

19:00 hrs

Location:

Nico Koomanskade 1024 3072 LM Rotterdam

21 PINCHOS

TAPAS BAR

Widening the Lens for Risk-Stratification of High-Risk Plaques Likely to Cause Future MACE: From Invasive IVUS/OCT to Non-Invasive CCTA

Peter H. Stone, Mona Ahmed, Diaa Hakim, David Molony, Nicholas V. Cefalo, Ahmet U. Coskun, Dave Engberg, Melissa Aquino, Rob Jennings, James Earls, Habib Samady, James K. Min
on behalf of the ICONIC Investigators

Vascular Profiling Research Laboratory, Cardiovascular Division, Brigham & Women's Hospital,

Harvard Medical School, Boston, MA, USA

Introduction
Local hemodynamic blood flow patterns (endothelial shear stress, ESS) surrounding coronary plaques drive atherosclerosis behavior to progress, destabilize or remain quiescent. The presence of high-risk hemodynamic ESS patterns affecting coronary artery plaques, derived from invasive intravascular ultrasound (IVUS) or optical coherence tomography (OCT) imaging, significantly enhances risk-stratification of coronary plaques likely to destabilize and cause acute coronary syndromes (ACS). Coronary computed tomography angiography (CCTA) can identify anatomical high-risk coronary plaque features in patients with suspected/known coronary artery disease (CAD), but detailed evaluation of prognostic accuracy of biomechanical variables derived from CCTA imaging has not been studied. We investigated if adverse ESS metrics, derived from CCTA images, can accurately predict plaques that will develop future ACS.

Methods
We first compared the accuracy of Computational Fluid Dynamics (CFD) computation of local ESS metrics by CCTA vs IVUS imaging in 59 patients. We then evaluated 447 patients, with 3,574 lesions, from 2,084 arteries, from the ICONIC study, a nested case-control study within the CONFIRM registry of stable patients without known CAD, who had a CCTA at baseline, and subsequently did/did not experience a blinded core lab-adjudicated ACS at 3.4 years follow-up. CCTA images were automatically segmented using Cleerly Labs AI software. ESS metrics (minESS, maxESS, maxESS gradient [ESSG; low ESS immediately adjacent to high ESS]) were calculated by CFD. Investigators were blinded to outcome data.

Results
Anatomical plaque characteristics (vessel, lumen, plaque area and minimal luminal area) were correlated when measured with IVUS and CCTA. ESS metrics of local minimal, maximal, and average ESS were also moderately correlated when measured with IVUS and CCTA (2.0±1.4 vs 2.5±2.6 Pa, r=0.28; 3.3±1.6 vs 4.2±3.6 Pa , r=0.42; 2.6±1.5 vs 3.3±3.0 Pa, r=0.35, respectively). CCTA-based computation accurately identified the spatial localization of local ESS heterogeneity compared to IVUS.

The available CCTA cohort for plaque-based prognostic assessment consisted of 220 ACS patients vs. 222 non-ACS control patients. In analysis of ACS patients vs. non-ACS control patients, 162 culprit lesions were compared to 1,707 non-culprit lesions: minESS 0.80±1.16 vs. 1.27±1.83 Pa ($p<0.0001$), maxESS 27.48±93.19 vs. 7.13±22.87 Pa ($p<0.005$), maxESSG 40.85±169.2 vs. 9.31±47.52 Pa/mm ($p<0.0178$). In analysis within patients who developed an ACS, 162 lesions were adjudicated as culprit lesions vs.1,591 non-culprit lesions. ESS metrics in ACS culprit lesions vs. non-culprit lesions: minESS 0.80±1.16 vs. 1.50±7.13 Pa ($p<0.0007$), maxESS 27.48±93.19 vs. 7.24±21.70 Pa ($p<0.005$), maxESSG 40.85±169.24 vs. 9.07±44.33 Pa/mm ($p<0.0159$). Similar results were observed in maxESSGaxial upslope, maxESSGaxial downslope, maxESSG circumferential, maxVorticity, max APSupslope, maxAPSdownslope, and maxAreaStenosis.

Conclusions
We demonstrate here, for the first time, that CCTA-derived high-risk ESS metrics (minESS, maxESS, maxESSG in all directions) identify plaques and patients associated with future ACS. Our future studies will assess synergistic or additive prediction of adverse outcomes combining a broad range of high-risk ESS metrics with a broad range of high-risk anatomic/plaque metrics. The implications are enormous for non-invasive, population-based, CCTA screening of individuals around the world with, or at risk of, high-risk coronary artery disease, to enable, and potentially justify, highly targeted, preemptive intervention strategies to prevent plaque destabilization and MACE.

Normal Blood Flow plus Atorvastatin Promotes Regression of Unstable Plaques

Ian S. McCue, Morgan A. Schake, Ryan M. Pedrigi

Department of Mechanical and Materials Engineering, University of Nebraska-Lincoln, USA

Introduction

Blood flow is a key regulator of atherosclerotic plaque development [1]. Disturbed flow that is multidirectional at a low magnitude promotes plaque development, while normal flow that is unidirectional at a normal magnitude protects against plaque development. Although these relationships are well established, there remains a need for complementary studies of the potentially therapeutic effects of normal blood flow. In this study, we tested the hypothesis that restoration of normal blood flow plus daily administration of atorvastatin promotes plaque regression.

Methods

A total of 75 female mice were instrumented with a blood flow-modifying cuff around the left carotid artery [1]. Mice were randomly assigned to one of four experimental groups: (1) untreated with the cuff maintained for nine weeks, (2) treated with decuffing (to restore normal blood flow) after five weeks of cuff placement and maintained without the cuff for an additional four weeks, (3) treated with atorvastatin daily after five weeks of cuff placement and maintained with the cuff for an additional four weeks, and (4) treated with the combination of atorvastatin plus decuffing. Magnetic resonance imaging (MRI) and Doppler ultrasound were used to quantify lumen patency at the point of maximum artery stenosis and peak blood velocity, respectively. At the endpoint of each experiment, carotid arteries were excised and serially cryosectioned at 8 μm thickness to evaluate: lipids (oil red O), collagen (picrosirius red), and macrophages (CD68). The stained sections were imaged and analyzed with custom software to quantify stain area to intima area. All quantities are reported as mean ± standard deviation and statistics were performed considering normality, equal or unequal variances, and multiple comparisons. An adjusted *p*-value of less than 0.05 was considered statistically significant.

Results

MRI and Doppler ultrasound demonstrated that placement of the blood flow-modifying cuff caused a significant reduction in lumen patency and blood velocity. One week after cuff placement, MRI revealed a dramatic reduction in lumen area (13.7±5.2% versus 99.6±17.4%, $p<0.0001$), which was similar at four weeks. However, two weeks after decuffing (seven weeks after initial cuff placement), the maximum stenosis had improved (74.8±21.2% versus 103.9±19.5%, $p=0.004$) and, after four weeks, there was no significant difference between the left and right carotid arteries (84.3±18.1% versus 97.3±14.6%, $p=0.07$). Blood velocity from Doppler ultrasound exhibited similar trends over time.

Histological analysis of the unstable plaques revealed that restored normal blood flow alone caused plaque stabilization and the combination with atorvastatin caused plaque regression. Decuffed mice (i.e., those treated with restored normal flow alone) exhibited significant changes in plaque composition compared to the untreated group, wherein lipid content was lower (4.8±4.5% versus 17.2±9.4%, $p=0.005$), macrophage content was lower (9.3±6.9% versus 33.8±15.5%, $p=0.001$), and collagen content was higher (9.3±3.1% versus 4.9±2.0% $p=0.005$). Similar results were seen with atorvastatin. The combination of restored normal blood flow and atoravastatin exhibited similar plaque lipid and macrophage contents, but a higher collagen content versus each therapy individually (15.7±4.2% versus 8.2±5.4% in the atorvastatin group ($p=0.01$) and 9.3±3.1% in the decuffed group ($p=0.008$)). Furthermore, the combined therapy group was the only one that exhibited a significant decrease in plaque burden from the untreated group (22.7±18.0% versus 43.5±12.8%, $p=0.02$).

Conclusions

These findings demonstrate high efficacy of normal blood flow against unstable atherosclerotic plaques and motivate development of new therapies that leverage flow sensing. Our results suggest that such therapies could provide an additive beneficial effect when administered in parallel to statins.

References

[1] Schake MA, McCue IS, Curtis ET, Ripperda TJ, Harvey S, Hackfort BT, Fitzwater A, Chatzizisis YS, Kievit FM, and Pedrigi RM, Restoration of normal blood flow in atherosclerotic arteries promotes plaque stabilization, *iScience*, 26: 106760, 2023.

Relative Residence Time can account for half of the anatomical variation in fatty streak prevalence within the right coronary artery

Pratik Kandangwa[1,2], Kevin Cheng[3] , Miten Patel[3,4], Spencer Sherwin[2], Ranil de Silva[3,4], Peter Weinberg[1]

[1]Bioengineering, [2]Aeronautics and [3]NHLI, Imperial College London, and [4]Royal Brompton Hospital, UK

Introduction

The patchy anatomical distribution of atherosclerosis has been attributed to variation in haemodynamic stresses acting on the endothelium. Although the consensus view is that low wall shear stress (WSS) and a high Oscillatory Shear Index (OSI) promote the disease, many other hypotheses have been proposed. For example, we have shown for the rabbit aorta that the transverse WSS (transWSS), which captures components of WSS vectors at right angles to the temporal mean WSS vector, spatially correlates threefold better than WSS or OSI with fatty streak prevalence [1].

Atherosclerosis of the coronary arteries has greater clinical significance than atherosclerosis of the aorta, but computation of WSS metrics is complicated by the fact that coronaries undergo substantial translation, bending and torsion during each cardiac cycle. Local values of OSI are significantly altered if such motion is not included in simulations, and we recently showed that the anatomical distribution of transWSS is even more affected [2]. Here we present the first comparison of spatial patterns of coronary lesion prevalence and flow metrics computed in dynamic models of the arteries.

Methods

Dynamic geometries of right coronary arteries (RCAs) from 10 subjects (5 male, 5 female, 44-79 years; IRAS project ID 318558) were reconstructed from angiograms acquired at 15 frames/second and with two views at an included angle of ≥30° using CAAS Intravascular Software. Time-dependent flow simulations were carried out using STAR-CCM+ as previously described [2]. Blood was modelled as a laminar incompressible Newtonian fluid. A published inlet velocity waveform and a parabolic inlet velocity profile were imposed. A mass flow rate boundary condition was applied at side branch outlets, with flow divisions calculated using an empirical power law. Maps of fatty streak prevalence were obtained by digitising figures from the PDAY study [3]. Spearman's rank correlation coefficient was calculated between maps of lesion prevalence and WSS metrics; confidence intervals were obtained by bootstrapping.

Results

The distribution of lesion prevalence was helical with the highest value at the entrance being close to the inner curvature of the vessel; the helix rotated clockwise. Maps of individual basic metrics – time average WSS, OSI, the cross-flow index (CFI) and transWSS – did not show strong correlations with the map of fatty streak prevalence: the coefficient for transWSS did not reach statistical significance (the confidence interval included zero) and although coefficients for the other basic metrics did, even the highest value of r, which was for CFI, was 0.44 (i.e. explaining <20% of the variance in lesion prevalence). Amongst other metrics, the highest correlation was for the relative residence time (RRT), a metric that decreases with WSS and increases with OSI; it gave r=0.71, and this coefficient was not changed if CFI, a non-dimensional form of transWSS, was used instead of OSI in its calculation.

Conclusions

Contrary to our previous finding in the rabbit aorta, the pattern of lesion prevalence in the human right coronary did not correlate well with the transWSS. It was better explained by the RRT, which is increased by both low WSS and high OSI. Multidirectional rather than back-and-forward flow appeared to be the primary determinant of the OSI values. (*Supported by EPSRC*)

References

[1] Mohamied Y et al. Change of Direction in the Biomechanics of Atherosclerosis. Ann Biomed Eng 2015;43:16–25
[2] Kandangwa P et al. Influence of Right Coronary Artery Motion, Flow Pulsatility and Non-Newtonian Rheology on Wall Shear Stress Metrics. Front Bioeng Biotech 2022;10:516
[3] McGill HC et al. Effects of coronary heart disease risk factors on atherosclerosis of selected regions of the aorta and right coronary artery. Arterioscler Thromb Vasc Biol 200;20:836-845

Functional and Hemodynamic Assessment in Elderly Patients with Myocardial Infarction and Multivessel Disease. A Longitudinal Study

Diego Gallo[1], Maurizio Lodi Rizzini[1], Alessandro Candreva[1,2], Jean Paul Aben[3], Claudio Chiastra[1], Barbara Stähli[2], Simone Biscaglia[4], Gianluca Campo[4], Umberto Morbiducci[1]

[1] PolitoBIOMed Lab, DIMEAS, Politecnico di Torino, Turin, Italy
[2] Department of Cardiology, University Hospital Zurich, Zurich, Switzerland
[3] Pie Medical Imaging BV, Maastricht, the Netherlands
[4] Department of Medical Science, University of Ferrara, Ferrara, Italy

Introduction

In older patients experiencing myocardial infarction (MI) and multi-vessel coronary artery disease (MVD), the capability to identify risk of future adverse events is limited. Recently, the clinical trial FIRE [1] highlighted the benefits from a physiology-guided management of these patients, suggesting the treatment with percutaneous coronary intervention not only of the lesion culprit of MI, but also of all functionally significant non-culprit lesions [1]. Here we explore the capability of advanced hemodynamic and anatomical analysis to support the identification of patients at higher risk of complications. To do that, wall shear stress (WSS) profiles from angiography-derived computational fluid dynamics (CFD) simulations and anatomical lesion parameters were calculated in functionally non-significant lesions to predict major adverse events at 1 year in a large cohort.

Methods

Patients (327) from the FIRE trial [1] were included. Non-culprit vessel geometries were reconstructed using 3D QCA (CAAS Workstation WSS software, Pie Medical Imaging). Lesions were characterized in terms of percentage area stenosis (%AS) and lesion length [2]. CFD simulations were carried out to obtain the time-average WSS (TAWSS) and the topological shear variation index (TSVI, measuring the variability of the contraction/expansion action exerted by WSS on the endothelium along the cardiac cycle) [2,3]. Outcome events were death, MI, stroke, or ischemia-driven coronary revascularization occurring within 1 year after baseline MI. These outcomes were combined to define the primary outcome. Further outcomes were contrast-associated acute kidney injury, cerebrovascular accident, and bleeding. Cox proportional-hazard models were fitted to estimate hazard ratios (HR) for “conventional” risk factors, %AS, lesion length, TAWSS or TSVI with respect to the outcomes. Variables found to be significant at the univariate analysis entered in multivariate models to identify independent predictors. The concordance index (C-index) was used to assess the predictive capacity of each model.

Results

%AS was associated with higher risk of primary outcome (HR 1.02, p=0.041). Longer lesions were associated with higher risk of all-cause death within 1 year (HR 1.04, p=0.045). Higher TSVI was associated with higher risk of MI within 1 year (HR 1.01, p=0.012), ischemia-driven coronary revascularization (HR 1.01, p=0.018), bleeding (HR 1.01, p=0.012). TAWSS was not associated with any of the outcomes. The addition of anatomic variables (%AS or lesion length) or TSVI to multivariate models based on conventional risk factors led to improvements for all predictions (Fig. 1).

C-index of multivariate models	w/o anatomic variables or TSVI	w anatomic variables or TSVI
Primary outcome	0.623	0.647
All-cause death	0.766	0.791
MI	0.692	0.730
Revascularization	0.603	0.712
Bleeding	0.781	0.826

* p < 0.05; † p < 0.01; ‡ p < 0.001

F lex) of multivariate Cox regression models

Conclusions

Lesion severity, length and TSVI represent independent predictors of clinical outcomes within 1 year in elderly patients with MI and MVD. The present findings are consistent with the previously reported ability of TSVI in predicting lesion progression over time [3], and in identifying mild lesions culprit of MI at 5-years follow-up [2]. Despite the retrospective study design, it focuses on a patient cohort of relevant clinical interest, paving the way for prospective studies including computational hemodynamics.

References

[1] Biscaglia S et al., Complete or culprit-only PCI in older patients with myocardial infarction. N Engl J Med, 89(10): 889-898, 2023.
[2] Candreva A et al., Risk of myocardial infarction based on endothelial shear stress analysis using coronary angiography, Atherosclerosis, 342:28-35, 2022.
[3] Mazzi V et al., Early atherosclerotic changes in coronary arteries are associated with endothelium shear stress contraction/expansion variability. Ann Biomed Eng, 49:2606-2621, 2021.

Endothelial IGFBP6 Suppresses Vascular Inflammation and Atherosclerosis

Suowen Xu, Meiming Su, Yun Fang, Paul C. Evans, Hanjoong Jo, Bradford C. Berk, Stefan Offermanns, Yu Huang, Jianping Weng

Clinical Research Hospital, Chinese Academy of Sciences, University of Science and Technology of China, Hefei, China

Introduction
Shear stress generated by the blood flow is important for vascular development, homeostasis, and atherosclerotic cardiovascular diseases. However, the molecular mechanisms whereby shear stress regulates vascular health and disease remain obscure.

Methods
By employing multi-layered transcriptomic profiling, we identified the downregulation of insulin-like growth factor binding protein 6 (IGFBP6) under pro-atherogenic conditions, while upregulation of IGFBP6 under atheroprotective conditions. Endothelial cell specific knockout and conditional overexpressing mice were generated. Mice were feed with high cholesterol diet or undergo partial carotid ligation to assess atherosclerosis development.

Results
We observed that global or endothelial cell (EC)-specific deficiency of Igfbp6 accelerated the progression of atherosclerosis induced by disturbed flow (DF) (using the model of partial carotid ligation) or high-cholesterol diet (HCD) feeding, whereas EC-specific overexpression of Igfbp6 ameliorated the progression of atherosclerosis. In vitro, overexpression of Igfbp6 inhibits monocyte adhesion to ECs and reduces DF- or TNF-α-mediated induction of endothelial adhesion molecules. Mechanistic studies suggested that IGFBP6 is transcriptionally regulated by krüppel-like factor 2 (KLF2) and executes anti-inflammatory effects through directly interacting with the major vault protein (MVP) and blocks Jun N-terminal kinase (JNK) dependent pro-inflammatory response. Of clinical significance, IGFBP6 protein expression was decreased in serum and atherosclerotic plaque tissues of CAD patients.

Conclusions
In summary, this study implicates IGFBP6 as a promising therapeutic target to prevent or treat atherosclerosis and associated vascular diseases.

References
[1] Nigro P, Abe J, Berk BC. Flow shear stress and atherosclerosis: a matter of site specificity. Antioxid Redox Signal. 2011;15(5):1405-14.
[2] Tamargo IA, Baek KI, Kim Y, Park C, Jo H. Flow-induced reprogramming of endothelial cells in atherosclerosis. Nat Rev Cardiol. 2023;20(11):738-753.
[3] Souilhol C, Serbanovic-Canic J, Fragiadaki M, Chico TJ, Ridger V, Roddie H, Evans PC. Share Endothelial responses to shear stress in atherosclerosis: a novel role for developmental genes. Nat Rev Cardiol. 2020;17(1):52-63.

Endothelial protein kinase N1 (PKN1) mediates phosphorylation of histone H3.3 for rapid disturbed flow-induced gene activation

Young-June Jin, Stefan Offermanns

Max Planck Institute for Heart and Lung Research, Department of Pharmacology, Bad Nauheim, Germany

Introduction
The histone H3.3 variant is expressed throughout the cell cycle in quiescent endothelial cells and is enriched in euchromatin. Its phosphorylation at serine residue 31 has been shown to lead to rapid changes in chromatin modification as well as to fast and robust induction of transcription. How H3.3S31 phosphorylation is regulated is incompletely understood.

Methods
We used different shear stress assays *in vitro* and conditional endothelium-specific knock-out mice as well as AAV-mediated gene transfer *in vivo* to study disturbed flow-induced downstream signalling, chromatin modification and gene expression in the context of disturbed flow-induced physiological regulation and pathophysiological vascular remodelling.

Results
We found that protein kinase N1 (PKN1) phosphorylates H3.3S31 in endothelial cells of blood vessels and thereby mediates endothelial inflammation and pathological vascular remodelling induced by disturbed blood flow. Endothelial PKN1 activation is mediated by integrin $\alpha5\beta1$ and results in the translocation of PKN1 to the nucleus where it directly phosphorylates H3.3S31. H3.3S31 phosphorlyation leads to fast chromatin modifications in the promoter regions and gene bodies of *FOS* and *FOSB*, resulting in the rapid induction of the expression of these AP-1 transcription factors required for endothelial inflammatory gene expression in response to disturbed flow. Endothelial loss of PKN1 or blockade of H3.3S31 phosphorylation inhibits disturbed flow-dependent endothelial inflammation and atherosclerosis progression *in vivo*.

Conclusions
Our data identify a central mechanism of disturbed flow-induced endothelial cell inflammation in vascular remodelling. We also provide evidence that PKN1-mediated H3.3S31 phosphorylation is a widely used mechanism that mediates rapid signaling-induced gene activation.

References
%

Loss of ERG function contributes to lymphatic vessel malformations and primary lymphoedema

Graeme M. Birdsey

National Heart and Lung Institute, Imperial College London, London, UK.

Introduction

Blood and lymphatic vessels form interconnected networks that are essential for transport of fluids, gases, macromolecules and cells. Endothelial cells (EC) line both vessels and are essential for maintaining tissue homeostasis through regulation of angiogenesis and lymphangiogenesis. Dysfunction of lymphatic vessels leads to disturbed tissue fluid balance and lymphoedema, a chronically debilitating disease that affects about 120,000 people in the UK. Primary lymphoedema is a rare inherited genetic condition caused by abnormal development of lymphatic vessels or failure of lymphatic function, due to mutations in key genes. Linkage analysis and exome sequencing have so far identified ~20 genes whose mutation causes hereditary lymphoedema[1]. However, coding variants in these genes only account for ~40% of primary lymphoedema cases, with the remaining patients having no genetic diagnosis. The ETS-related gene (ERG), one of the most highly expressed ETS factors in differentiated blood endothelial cells (BEC), is a master regulator of endothelial homeostasis, BEC lineage specification and angiogenesis[2]. However, ERG's role in regulating lymphatic EC (LEC) gene expression and lymphangiogenesis is unknown.

Results

We find similar levels of ERG in primary human dermal LEC compared to human umbilical vein EC (HUVEC). Comparative analysis of HUVEC and LEC high-throughput sequencing has revealed the unique epigenetic and ERG-dependent transcriptomic signatures of LEC. Inhibition of ERG in LEC leads to differential expression of genes required for lymphatic vessel development, metabolism, and homeostasis, as well as dysregulation of genes commonly altered in patients with primary lymphoedema. Functional assays show that siRNA inhibition of ERG leads to disrupted sprouting in a LEC spheroid-based lymphangiogenesis model. Using a postnatal inducible lymphatic endothelial-specific ERG-deleted mouse model (*Prox1-CreERT2-ERG flox*), we find that dermal lymphatic vessels and valves appeared malformed and disorganized compared to controls, suggesting a role for ERG in lymphangiogenesis. We analyzed genome sequencing data from the 100,000 Genomes Project, which included 100 primary lymphoedema patients, leading to the identification of variants in the ERG gene that were exclusively observed in patients[3]. These mutations in ERG were predicted to reside within variation intolerant protein domains, which was validated through in vitro assays that showed the newly identified ERG variants to be less efficient in driving transcriptional activity and lacking the ability to bind DNA.

Conclusions

Together, these studies define a novel transcriptional pathway for LEC gene expression and lymphangiogenesis under the control of the transcription factor ERG. We demonstrate that ERG is central for lymphatic homeostasis and that its loss leads to human disease and disease-associated phenotypes in rodent models. Moreover, this research provides compelling evidence to include ERG coding variants as a new pathogenic marker for primary lymphoedema.

References

1. Martin-Almedina, S., Mortimer, P.S. & Ostergaard, P. *Physiol Rev.* (2021), 101:1809-1871.
2. Shah, A.V., Birdsey, G.M. & Randi, A.M. *Vascular Pharmacology* (2016), 86:3-13.
3. Greene et al., *Nature Medicine*. (2023), 29(3):679-688.

EPAS1 maintains endothelial homeostasis and is atheroprotective via lipid metabolism at sites of disturbed flow.

Daniela Pirri[1,2], Siyu Tian[2], Blanca Tardajos Ayllon[2], Jovana Serbanovic Canic[3], Maria Fragiadaki[2], Paul C. Evans[2]

1 National Heart and Lung Institute, Imperial College London, London, UK; [2] Centre for Biochemical Pharmacology, William Harvey Research Institute, Barts and the London School of Medicine and Dentistry, Queen Mary University of London, London, UK [3] School of Medicine and Population Health, INSIGNEO Institute, and the Bateson Centre, University of Sheffield, Sheffield, UK.;

Introduction

The vascular network is characterised by an inner monolayer of endothelial cells (EC) which maintains homeostasis by the fine interplay of mechanical forces (shear stress), metabolic stimuli (glucose levels and lipids), balance of anti-oxidant species, and transcription regulation of EC gene expression [1,2]. The transcription factor EPAS1 (HIF2-α) has an essential role in vascular development, adult tissue homeostasis and pulmonary hypertension. Its involvement in cardiovascular diseases such as atherosclerosis is unexplored. This work unveils the role of EPAS1 in atherosclerosis and the contribution of obesity in regulating EPAS1-mediated homeostasis.

Methods

To assess the role of shear stress on EPAS1 levels, we performed immunofluorescence staining of the murine aorta at regions prone to atherosclerosis. To assess the contribution of obesity on arterial EPAS1 levels, mice were fed a high-fat diet (HFD) or standard chow, aortas were isolated to assess EPAS1 levels at atheroprone regions. A group of HFD mice was treated with an antioxidant compound from the cruciferous plant (sulforaphane) before measuring EPAS1 levels in isolated aortas. To uncouple the hyperglycemic component of obesity, we studied EPAS1 levels in the aortas of lean diabetic mice treated with streptozotocin. We also evaluated the levels of EPAS1 in the plasma of obese patients compared to lean controls. The role of EPAS1 in atherosclerosis was evaluated using tamoxifen-induced endothelial (*Cdh5-CreERT2*)-driven *Epas1* deletion, followed by hypercholesterolemia induction (AAV-PCSK9; HFD). The role of EPAS1 in regulating endothelial metabolism under atheroprone shear stress was investigated using isolated primary porcine aortic EC (PAEC) exposed to free fatty acid (FFA) challenge using oleic acid; bioenergetics analysis was carried out using Seahorse assay.

Results

Immunofluorescence staining of the murine aorta revealed EPAS1 enrichment at the atheroprone region of the aortic arch, a site of disturbed flow and atherosclerosis initiation. Obesity, induced by exposing C57BL/6 mice to a HFD for 25 weeks, significantly reduced the levels of EPAS1 at the atheroprone region. In contrast, diabetic mice preserved the levels of EPAS1 within the aorta when compared to their vehicle-treated controls. Sulforaphane treatment of HFD fed mice reduced triglyceride levels and restored EPAS1 expression, suggesting that triglycerides may be involved in EPAS1 suppressionObesity-associated reduction of EPAS1 was also observed in plasma from obese patients compared to lean controls. Endothelial-specific deletion of EPAS1 in mice challenged with AAV-PCSK9 and HFD exhibited increased atherosclerotic plaque formation compared to controls, indicating that EPAS-1 is atheroprotectiveGene silencing analysis in cultured PAEC revealed that EPAS1 promotes proliferation under disturbed flow. Seahorse analysis and immunoblotting revealed that EPAS1 is essential forf atty acid metabolism in PAEC via via induction of the lipid transporters CD36 and LIPG.

Conclusions

EPAS1 positively regulates endothelial homeostasis and protects the endothelium from atherosclerosis. EPAS1 contributes to the regulation of fatty acid metabolism in atheroprone endothelium to support vascular repair via promoting cell proliferation. Obesity limits EPAS1 at atheroprone regions, suggesting a novel role for EPAS1 as a therapeutic target to prevent or treat atherosclerosis.

References

1. Feng, S. *et al.* Mechanical Activation of Hypoxia-Inducible Factor 1alpha Drives Endothelial Dysfunction at Atheroprone Sites. *Arterioscler. Thromb. Vasc. Biol.* **37**, 2087–2101 (2017).
2. Wu, D. *et al.* HIF-1alpha is required for disturbed flow-induced metabolic reprogramming in human and porcine vascular endothelium. *Elife* **6**, (2017).

Mechanosensing at endothelial cell-cell junctions

Eulashini Chuntharpursat-Bon, Oleksandr Povstyan, Marjolaine Debant, David Beech

School of Medicine, University of Leeds, Leeds, UK

Introduction

Critical to blood vessel integrity is the inner lining formed by a patchwork of endothelial cells zipped together through special cell-cell junctions. Mechanical forces, for example from blood flow, activate signalling mechanisms that cause cell-cell junctions to tighten, loosen or open. We have recently shown that PIEZO1 is an integral part of this biochemical zipper [1] between cells, merging two prominent but seemingly opposed ideas for force sensing [2, 3, 4]. Key components of the junctions are adhesion molecules PECAM1 and CDH5 that bind together via extracellular homophilic domains to control the exchange of substances and cells between the blood and tissue. PECAM1 was an early candidate in mediating endothelial response to shear stress. Subsequently, came the discovery of PIEZO1 mechanosensitive ion channel that was found to be a blood flow sensor in endothelial cells [2, 3]. We were interested in how these two mechanisms intersect.

Methods

We have used multiple fluorescent microscopy approaches including stimulated emission depletion (STED) and Forster resonance energy transfer detected by fluorescence lifetime imaging (FRET/FLIM) to characterise these proteins in mouse and reconstituted models. Endogenous proteins were examined in tissue using our CRISPR-modified HA-tagged PIEZO1 mouse. We used patch clamp and fluorescent calcium recordings to determine ion channel activity and calcium switch assays to recapitulate junction formation on endothelial monolayers.

Results

We identified a pool of PIEZO1 located at cell junctions where PECAM1 and CDH5 are in complex with PIEZO1. PECAM1 formed a stable complex that leads to the dampening of PIEZO1 activity. Shear activation of PIEZO1 showed dynamic recruitment of junctional CDH5 and PIEZO1 knockdown impaired CDH5 junction formation. PIEZO1 is required in the calcium-dependent formation of adherens junctions and associated cytoskeleton, consistent with it conferring force-dependent calcium entry for junctional remodelling.

Conclusions

We propose an additional location and role for PIEZO1 in mechansensing at endothelial junctions.

References

[1] E Chuntharpursat-Bon et al., Commun. Biol. (2023) https://doi.org/10.1038/s42003-023-04706-4.
[2] J Li et al., Nature (2014) https://doi.org/10.1038/nature13701.
[3] S. S Ranade et al., Proc. Natl. Acad. Sci. (2014) https://doi.org/10.1073/pnas.1409233111.
[4] E Tzima et al., Nature (2005) https://doi.org/10.1038/nature03952.

Do vascular wall vibrations play a role in vascular disease? The case of cerebral aneurysm and arteriovenous fistula

Michela Bozzetto

Department of Bioengineering, Istituto di Ricerche Farmacologiche Mario Negri IRCCS, Bergamo, Italy

It is estimated that roughly 3% of the population harbour cerebral aneurysms, which are the most common cause of subarachnoid hemorrhage [1]. Despite a large body of research into local hemodynamic conditions, there are still no commonly accepted hemodynamic indicators of rupture risk [2]. Recently, it has been shown that turbulent-like flows and the associated high-frequency pressure fluctuations cause aneurysm wall to vibrate at high frequencies [3]. High-fidelity fluid structure interaction simulations revealed that these vibrations induce irregular, high-rate deformation of the aneurysm wall at frequencies up to 500Hz and amplitudes up to 1 μm [4]. This evidence suggests that wall vibrations can have a mechanobiological effect on the walls, but longitudinal studies in cerebral aneurysms are hindered by the fact that, in most of the cases, they are discovered incidentally and have a slow progression until a sudden unpredictable rupture.

On the contrary, arteriovenous fistula (AVF), the preferred vascular access for hemodialysis, is characterized by the formation of luminal stenosis that progresses rapidly, causing the failure of AVF in 40% of the cases within 1 year from its creation. This makes the AVF an excellent model for studying the role of mechanical stresses in vascular remodelling. Interestingly, using patient-specific high-fidelity simulations, we conducted the first investigation in 1 patient, and found that also AVF is characterized by high-frequency wall vibrations with frequencies of hundred of Hertz [5]. The model used in this first study was physiologically plausible but included few relevant limitations. Therefore, we enhanced the computational model to include patient-specific pulsatile flow rates, different thickness and stiffness for the artery and vein, and the modeling of the perivascular tissue [6]. Using this new pipeline, we studied 4 patients from the time of AVF creation over a period of 1 year. We found that the two patients who developed AVF stenosis developed higher vessel wall vibration amplitudes (up to 35 μm) and a frequency content up to 500 Hz. On the contrary, patients with preserved AVF patency at 1 year showed relatively lower vibration amplitudes and a spectral content up to maximum 70 Hz. Our preliminary findings indicate distinct vibration responses corresponding to different AVF outcomes, suggesting a relationship between high-frequency mechanical stresses within the vascular wall and adverse remodeling. If the relation between vessel wall vibrations and AVF complications will be confirmed in a larger cohort, this finding could have significant implications for clinical practice: the possibility of detecting AVFs at risk of closure allowing timely intervention, the identification of new surgical strategies and new devices to limit vibrations.

In conclusion, certain cerebral aneurysms and AVFs are characterized by similar high-frequency wall vibrations caused by turbulent-like flows, which is consistent with clinical observations of bruits and thrills. In both cases the vascular wall experiences radical wall remodeling, although in two opposite directions (excessive dilatation or stenosis). Although purely hypothetical, our preliminary computational results suggest that wall vibrations can have an overlooked mechanobiological role, potentially disrupting physiological cell biology and promoting deleterious wall remodeling.

References

[1] Vlak MHM et al. Prevalence of unruptured intracranial aneurysms, with emphasis on sex, age, comorbidity, country, and time period: a systematic review andmeta-analysis. *Lancet Neurol* 10(7):626-636, 2011

[2] Liang L et al. Towards the clinical utility of CFD for assessment of intracranial aneurysm rupture - a systematic review and novel parameterranking tool. *J. Neurointerv. Surg*. 11: 153–158, 2019

[3] Souche A & Valen-Sendstad K. High-fidelity fluid structure interaction simulations of turbulent-like aneurysm flows reveals high-frequency narrowband wall vibrations: A stimulus of mechanobiological relevance? *Journal of Biomechanics*, 145, 111369, 2022

[4] Bruneau DA et al. Understanding intracranial aneurysm sounds via high-fidelity fluid-structure-interaction modelling. *Communications Medicine* 3:163, 2023

[5] Bozzetto M et al. Flow-induced high frequency vascular wall vibrations in an arteriovenous fistula: a specific stimulus for stenosis development? *Physical and Engineering Sciences in Medicine* 47(1): 187–197*,* 2023*.*

[6] Soliveri L et al. Towards a Physiological Model of Vascular Wall Vibrations in the Arteriovenous Fistula. under review

Exploring endothelial dysfunction and mechanical forces in intracranial aneurysm pathogenesis: insights from transcriptomic studies.

Mannekomba R Diagbouga[1], Sandrine Morel[1,2], Sylvain Lemeille[1], Anne F Cayron[1,3,4], Julien Haemmerli[2], Marc Georges[2], Beerend P Hierck[5], Eric Allémann[3,4], Philippe Bijlenga[2], Brenda R Kwak[1]

1. Department of Pathology and Immunology, University of Geneva. 2. Neurosurgery Division, Department of Clinical Neurosciences, Geneva University Hospitals. 3. School of Pharmaceutical Sciences, University of Geneva. 4. Institute of Pharmaceutical Sciences of Western Switzerland. 5. Department of Anatomy and Embryology, Leiden University the Netherlands.

Introduction

Intracranial aneurysms (IAs) pose a significant risk of rupture, leading to hemorrhagic stroke and poor clinical outcomes, despite current treatment modalities. Polycystic kidney disease (PKD) patients have a high IA incidence and high risk of rupture, which is often attributed to the dysfunction of primary cilia that act as wall shear stress (WSS) sensors. However, the molecular mechanisms by which primary cilia promote IA disease remain poorly understood. In addition to WSS being a crucial factor in IA pathogenesis, cyclic circumferential stretch (CCS) may also have important implications. While IAs are typically characterized by a lack of CCS, investigations into the impact of cyclic stretch on vascular physiology and disease lag behind. Our aim was to understand the role of biomechanical forces (WSS and CCS) on the cellular and molecular mechanisms underlying IA pathogenesis.

Methods

Employing transcriptomic analyses, we investigated the role of endothelial dysfunction and mechanical forces in IA development. Firstly, we explored the impact of primary cilia dysfunction on the endothelial response to WSS. We compared wild-type and primary cilia-deficient arterial endothelial cells (ECs) under physiological and aneurysmal WSS conditions using the Ibidi *in vitro* flow system. Secondly, we investigated the influence of cyclic circumferential stretch (CCS) on EC function and its relevance to IA pathogenesis. Human umbilical vein ECs were exposed to physiological (6%) or aneurysmal CCS (0%), and differential gene expression analysis was performed using the Flexcell strain unit FX-5000T.

Results

Transcriptomic analysis revealed a fivefold increase in WSS-responsive genes in primary cilia-deficient ECs. We demonstrated that PKD ECs displayed perturbed intercellular junctions, correlating with higher endothelial permeability. Zona occludens-1 (ZO-1) was identified as a central regulator in junctional organization. Furthermore, we confirmed low expression of ZO-1 in ECs of IA domes from PKD patients. As for cyclic stretch investigations, RNA-seq analysis revealed that physiological cyclic stretch prevents significant endothelial cell deviation. Aneurysmal CCS up-regulated oxidative stress, angiogenesis, and inflammation pathways while down-regulating proliferation and extracellular matrix-receptor interaction pathways. Moreover, we highlighted differential cell junction gene expression and confirmed that the expression of GJA4 (Cx37) and GJA5 (Cx40), essential proteins for endothelial homeostasis, was down- regulated by aneurysmal CCS.

Conclusions

Altogether, our results highlighted the significance of cell junction gene expression in endothelial stability and integrity under wall shear stress and mechanical stretch conditions. The altered endothelial function we uncovered may not only contribute to the severity of IA disease observed in PKD patients, but may also serve as a potential diagnostic tool to determine the vulnerability of IAs.

Coupling finite element and machine learning modelling for the real-time simulation of intracranial aneurysms endovascular treatment

Beatrice Bisighini, Miquel Aguirre, Baptiste Pierrat, Stéphane Avril

Mines Saint-Etienne, Univ Lyon, Univ Jean Monnet, Etablissement Français du Sang, INSERM, U 1059, Sainbiose, F-42023 Saint-Etienne, France

Introduction

The current decision-making process for treating intracranial aneurysms mainly relies on measurements from medical images. However, predicting treatment outcomes is challenging due to the complex behaviour of endovascular devices, leading to potential complications during and after surgery. To assist clinicians, computational models are being developed to simulate device deployment before treatment [1]. Yet, the high computational cost of these simulations limits their clinical application. In this study, a new approach is proposed to enable real-time simulations, which consists of coupling finite element (FE) with machine learning (ML) modelling.

Methods

The proposed framework involves (1) parameterizing the anatomical structure where the stent is deployed, and (2) training a ML model to learn a mapping between these parameters and the stent deployed configuration. For the parametrisation, we relied on a statistical shape model built by performing a principal component analysis on a clinical database comprising 86 models of internal carotid arteries. The principal coefficients of the first 11 modes were then sampled to generate 3000 synthetic models. In the offline phase, the stent deployed configuration corresponding to each of these models was computed through a FE simulation. The simulations were performed using an in-house, open-source FE solver in Julia for modelling contact interactions between wire-like structures, discretised using beams, and rigid surfaces [2]. Finally, within the framework of a static, non-intrusive reduced-order model, a regression model was trained, considering the principal coefficients of the synthetic models as input and the nodal displacement vector at the end of the deployment simulation as output [3]. The model performance was assessed in terms of the relative prediction error between predicted and FE solutions.

Results

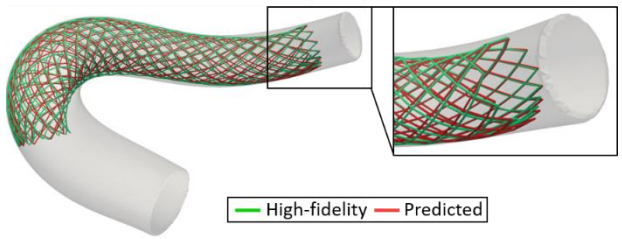

Figure 1. Predicted (red) and FE (green) solutions for a testing case with average prediction error = 0.13 mm.

With 2900 cases used for training and 100 for testing, we achieved an average prediction error of 0.19 mm on unseen cases. This error is below the spatial resolution of digital subtraction angiography (0.2 mm), commonly employed for identifying and treating intracranial aneurysms. For the cases where the prediction error is close to 0.19 mm, the predicted stent closely matches the FE stent, effectively conforming to the vessel's curvature. For cases with a larger error, the differences are mainly localised in the radial direction.

Conclusions

The successful comparison of machine learning outcomes with finite element results suggests that these techniques can accurately predict stent deployment outcomes in real time even in complex, realistic scenarios. This sets the basis for possible future adoption of these tools in clinical settings.

References

[1] B. Bisighini et al., Brain Multiphysics, vol. 5, no. June, 2023, p. 100079.
[2] B. Bisighini et al., Adv. Eng. Softw., vol. 171, no. June, 2022.
[3] B. Bisighini et al., Front. Physiol., no. March, pp. 1–18, 2023.

Can black blood MRI indicate unstable neurovascular pathologies? A hemodynamic analysis of wall and intraluminal enhancement

Janneck Stahl[1,2], Jana Korte[1,2], Franziska Gaidzik[1,2], Mariya Pravdivtseva[3], Laura Stone McGuire[4], Sylvia Saalfeld[1,5], Daniel Behme[1,6], Naomi Larsen[3], Ali Alaraj[4], Philipp Berg[1,7]

[1]Research Campus STIMULATE, University of Magdeburg, Magdeburg, Germany
[2]Department of Fluid Dynamics and Technical Flows, University of Magdeburg, Magdeburg, Germany
[3]Department of Radiology and Neuroradiology, University Clinic Schleswig-Holstein, Kiel, Germany
[4]Department of Neurosurgery, University of Illinois, Chicago, USA
[5]Department of Computer Science and Automation, Ilmenau University of Technology, Ilmenau, Germany
[6]Department of Neuroradiology, University Clinic Magdeburg, Magdeburg, Germany
[7]Department of Medical Engineering, University of Magdeburg, Magdeburg, Germany

Introduction

Signal enhancement (SE) in black blood magnetic resonance imaging (BBMRI) data may indicate inflammatory changes in cerebral vessel walls [1] as well as unstable intraluminal flow-related phenomena [2]. It has been hypothesized that SE may relate to the progression of stenoses [3] and risk of rupture [4] in the neurovasculature. In this study the relationship between hemodynamic flow patterns and SE is investigated, focusing on draining veins of arteriovenous malformations (AVM) and intracranial aneurysms (IAs).

Methods

Image-based blood flow simulations are conducted on eight AVM draining veins presenting with SE acquired on BBMRI. For the AVM draining veins the SE regions are registered and projected onto the luminal surface of the vessel walls ensuring a quantitative extraction of relevant hemodynamic parameters. Here, the parameters in the mapped enhanced areas are compared to near proximal and distal regions. For further representative IAs, intraluminal volumes of the SE and simulation results are co-registered and qualitatively compared. Time-averaged wall shear stresses (AWSS) as well as oscillatory shear indices (OSI) are calculated for the shear-related parameters. For the intraluminal flow patterns velocity, kinetic energy and oscillatory velocity indices are evaluated.

Results

The wall areas harboring SE in AVM draining veins show a significant decrease of 55 % ($p = 0.03$) for AWSS compared to non-enhanced parts. This is confirmed by an almost significant decrease of flow velocity (14 %, $p = 0.06$) in the lumen of the enhanced areas. However, oscillatory patterns of the flow in the enhanced veins are detected due to increased OSI values (32 %) at the wall and OVI (26 %) values inside the lumen, although not significant ($p = 0.3$). These findings are strengthened by the qualitative intraluminal comparisons of SE areas in the IA sacs. Here, reduced velocities causing lower kinetic energy values occur. Nevertheless, increased OVI values are found in enhanced luminal areas.

Conclusions

This multimodal investigation of hemodynamics in neurovascular pathologies harboring SE allows for precise predictions of flow patterns in BBMRI data. The results suggest that near-wall slow flow and shear rates as well as decreased but oscillating intrasaccular velocities may be associated with unstable disease conditions.

References

[1] Larsen N, Brelie C von der, Trick D, et al. Vessel wall enhancement in unruptured intracranial aneurysms: an indicator for higher risk of rupture? High-resolution MR imaging and correlated histologic findings. AJNR Am J Neuroradiol. 2018;39(9):1617-1621.
[2] Gaidzik F, Pravdivtseva M, Larsen N, Jansen O, Hövener J-B, Berg P. Luminal enhancement in intracranial aneurysms: fact or feature? - A quantitative multimodal flow analysis. Int J Comput Assist Radiol Surg. 2021;16(11):1999-2008.
[3] McGuire LS, Rizko M, Brunozzi D, Charbel FT, Alaraj A. Vessel wall imaging and quantitative flow assessment in arteriovenous malformations: A feasibility study. Interv Neuroradiol. 2022:15910199221143189.
[4] Matouk CC, Mandell DM, Günel M, et al. Vessel wall magnetic resonance imaging identifies the site of rupture in patients with multiple intracranial aneurysms: proof of principle. Neurosurgery. 2013;72(3):492-6.

An efficient uncertainty and sensitivity analysis approach to direct personalization and assess the credibility of digital human twins

Pjotr L.J. Hilhorst, Sjeng Quicken, Frans N. van de Vosse, Wouter Huberts

Department of Biomedical Engineering, Eindhoven University of Technology, The Netherlands

Introduction

Digital human twins are becoming increasingly popular as a tool for clinical decision support. However, the data available for feeding these digital twins are constrained by the clinical workflow and are often not specifically collected for the digital twin. Therefore, most datasets are sparse and have a relatively large uncertainty. These input uncertainties propagate to uncertainties in model predictions which need to be quantified to assess model adequacy within the context of use. In tandem with uncertainty quantification (UQ), sensitivity analysis (SA) is typically done to identify the relative contributions of each model input, or their interactions, to the uncertainty in the model output. SA is widely recognized as an indispensable step during each phase of model development and model personalization. Insights obtained by SA help the modeler by prioritizing the model inputs to be measured more accurately, or by selecting the optimal balance between model complexity and data uncertainty.

Most state-of-the-art UQ and SA approaches applied to digital twins assume statistical independence between model inputs, though model inputs are often correlated. Potential reasons for the infrequent usage of SA that accounts for input correlation are the associated high computational costs, especially for models with many parameters, and the fact that it is difficult to assess the exact correlation structure within sparse clinical data. In this study, we propose an efficient SA method by applying a surrogate model-based approach and we will demonstrate how this approach can guide the modeler during model development and personalization.

Methods

The UQ and SA methodology proposed was applied to a 1D pulse wave propagation model (PWPM) of the human arterial tree while considering 23 model inputs. First, surrogate models of the PWPM were developed to efficiently calculate selected outputs of interest of the PWPM (e.g., aortic diastolic pressure, pulse wave velocity). Thereafter, a variance-based UQ and SA approach [1] that allows for considering correlations between inputs was executed using the surrogate model. Subsequently, this two-step SA approach was verified and evaluated in terms of efficiency. In addition, it was discussed how these results can be interpreted and guide the modelers during model development and personalization.

Results

Our two-step approach resulted in accurate SA results with a theoretically 27000 times lower computational costs than when using the PWPM instead of the surrogate model [2]. The connotation of the well-known Sobol indices change when considering correlations between inputs and we demonstrated that the amount of correlation affects the output uncertainty and the calculated sensitivity indices, advocating the need for identifying the correlation structure in the input data when this has a large relative contribution to the output.

Conclusions

In conclusion, we have introduced an efficient SA approach that is applicable to digital twins with many model parameters and can provide insights to the modeler as to whether the modeler should invest in more accurate measurements, assess the correlation structure, and/or should move to model order reduction. Moreover, it allows for efficiently estimating the uncertainty in the output caused by input uncertainties.

References

[1] Li et al. (2017), https://doi.org/10.1016/j.ast.2016.12.003
[2] Hilhorst et al. (2023), https://doi.org/10.1002/cnm.3797

A multi-scale, multi-physics approach to understand and prevent cardiovascular maladaptation in the Ross procedure

Nele Famaey, Lauranne Maes, Thibault Vervenne, Amber Hendrickx, Maïté Pétré, Lucas Van Hoof, Peter Verbrugghe, Filip Rega

Department of Mechanical Engineering & Department of Cardiovascular Sciences, KU Leuven, Belgium

Introduction

The Ross procedure is a surgical procedure in which a diseased aortic valve is replaced by the person's own pulmonary valve, as a so-called autograft. It is the only aortic valve substitute than can restore long-term survival and quality of life. It also presents a fascinating mechanobiological scenario in which the pulmonary autograft is assumed to have the potential to remodel into an aortic phenotype once exposed to systemic pressure conditions. However, one of the main pitfalls of the procedure is dilatation of the autograft wall due to a vicious cycle of maladaptation [1]. One option is to wrap the autograft with an external support, but pre-clinical results have shown that this can lead to undesired stress-shielding.

Methods

We present a multi-scale, multi-physics computational framework that allows to reproduce pulmonary autograft remodeling *in silico*. The cell-scale model consists of a network model that includes important signaling pathways and the relation between relevant transcription factors and their target genes. The resulting gene activity leads to changes in the mechanical properties at the tissue scale, modeled as a constrained mixture of collagen, elastin and smooth muscle cells. The models were calibrated based on previous experiments on sheep [2-4]. At the cell scale, we tested the effect of various pharmacological agents on the remodeling behaviour. At the tissue scale, we tested the effect of adding an external support to the autograft.

Results

At the tissue scale, progressive dilatation of the autograft without external support is observed, corresponding to the animal trials. An improved long-term outcome is predicted through the cell scale, by treatment with β-blockers and angiotensin-receptor blockers, although the improvement is limited in the former case. An even better outcome in terms of diminished dilatation is predicted by inhibition of the ETS1 transcription factor, a currently unexplored target for pharmacological treatment in this context. At the tissue scale, although preventing the increase of in vivo strains, the permanent external support inhibits mechanical compliance between diastole and systole, indeed leading to resorption of the vessel wall.

Conclusions

Our multiscale framework allows us to virtually reproduce the apparent remodeling phenomena and identify scenarios that favour positive remodeling over maladaptation. Future work involves the in silico based design and experimental testing of an optimized biodegradable support, and the further exploration of pharmacological treatment options, while simultaneously further improving the biofidelity and reliability of our framework according to the accepted VVUQ guidelines.

References

[1] Van Hoof, L. et al. (2022), Frontiers in Cardiovascular Medicine, 1-20.
[2] Vanderveken, E. et al.(2020), Sci Rep 10, 2724.
[3] Van Hoof, L. et al. (2021), Annals Of Cardiothoracic Surgery, 1-10.
[4] Vastmans, J., et al. (2018), J Mech Behav Biomed Mat, 78, 164-174.

The incremental value of computational fluid dynamics (CFD) in single ventricle congenital heart disease

Arno AW Roest

pediatric cardiologist

In SV-CHD, the ventricles are not suited for a biventricular circulation, due to hypoplasia, valve abnormalities and various other malformations. In these single ventricle patients, a palliative approach was introduced by professor Fontan to redirect the systemic venous return from the body to the pulmonary circulation. The initial Fontan circulation has undergone several modifications and currently both caval veins are connected to the pulmonary circulation. The final step in creating the Fontan circulation is connecting the inferior caval vein to the pulmonary circulation, either by placing a rigid conduit or constructing an atrial tunnel at the age of 2-4 years. Worldwide most centers use the extra cardiac conduit-a rigid goretex tube- with a diameter raging from 14-20mm- to complete the Fontan circulation and CFD has been used to further explore modifications in this final step.1

The focus of our research group is on the hemodynamics of the Fontan circulation longterm after Fontan completion with the use of the extra cardiac conduit. As the rigid conduit cannot meet somatic growth after Fontan completion at the age of 4 years, we are concerned that the plays a detrimental role in adverse outcomes, such as liver fibrosis and decrease exercise capacity.[2]

CFD proved to be of incremental value for understanding the complex interplay of flow patterns from the inferior caval vein and the liver veins. This is of importance as the so called “hepatic factor” is important to be distributed evenly to both lungs to prevent the development of arterio-venous fisteling.[3]

Furthermore, we used CFD to predict pressure gradients within the Fontan circulation during simulated exercise and used these predictions to develop cut-off values for adverse flow dynamics of the Fontan circulation.[4]

Finally, CFD allows us to predict the effect of virtual surgery, in which we virtually enlarged the extra cardiac conduit to adult sizes and proved that energy loss is decreased, but that the pulmonary arteries remain an important area of adverse hemodynamics.[5]

1. Energetics of Blood Flow in Cardiovascular Disease: Concept and Clinical Implications of Adverse Energetics in Patients With a Fontan Circulation.
Rijnberg FM, Hazekamp MG, Wentzel JJ, de Koning PJH, Westenberg JJM, Jongbloed MRM, Blom NA, Roest AAW.Circulation. 2018 May 29;137(22):2393-2407. doi: 10.1161/CIRCULATIONAHA.117.033359.PMID: 29844073

2. 4D flow cardiovascular magnetic resonance derived energetics in the Fontan circulation correlate with exercise capacity and CMR-derived liver fibrosis/congestion.
Rijnberg FM, Westenberg JJM, van Assen HC, Juffermans JF, Kroft LJM, van den Boogaard PJ, Terol Espinosa de Los Monteros C, Warmerdam EG, Leiner T, Grotenhuis HB, Jongbloed MRM, Hazekamp MG, Roest AAW, Lamb HJ.J Cardiovasc Magn Reson. 2022 Mar 28;24(1):21. doi: 10.1186/s12968-022-00854-4.PMID: 3534624

3. Non-uniform mixing of hepatic venous flow and inferior vena cava flow in the Fontan conduit.
Rijnberg FM, van der Woude SFS, van Assen HC, Juffermans JF, Hazekamp MG, Jongbloed MRM, Kenjeres S, Lamb HJ, Westenberg JJM, Wentzel JJ, Roest AAW.J R Soc Interface. 2021 Apr;18(177):20201027. doi: 10.1098/rsif.2020.1027. Epub 2021 Apr 7.PMID: 3382360

4. Haemodynamic performance of 16-20-mm extracardiac Goretex conduits in adolescent Fontan patients at rest and during simulated exercise.
Rijnberg FM, van 't Hul LC, Hazekamp MG, van den Boogaard PJ, Juffermans JF, Lamb HJ, Terol Espinosa de Los Monteros C, Kroft LJM, Kenjeres S, le Cessie S, Jongbloed MRM, Westenberg JJM, Roest AAW, Wentzel JJ.Eur J Cardiothorac Surg. 2022 Dec 2;63(1):ezac522. doi: 10.1093/ejcts/ezac522.PMID: 3634220

5. Virtual surgery to predict optimized conduit size for adult Fontan patients with 16-mm conduits.
Hut T, Roest A, Gaillard D, Hazekamp M, van den Boogaard P, Lamb H, Kroft L, Jongbloed M, Westenberg J, Wentzel J, Rijnberg F, Kenjeres S.Interdiscip Cardiovasc Thorac Surg. 2023 Nov 2;37(5):ivad126. doi: 10.1093/icvts/ivad126.PMID: 37522877

Efficient personalized lumped parameter modeling of pulmonary arterial hypertension

Sander JB Schomaker[1], Rolf MF Berger[2] , Tineke Willems[3], David J Nolte[1], Johannes M Douwes[2], Cristobal A Bertoglio[1]

[1]Bernouilli Institute for Mathematics, Computer Science and Artificial Intelligence, University of Groningen, Groningen, The Netherlands

[2]Department of Pediatric Cardiology, University Medical Center Groningen, Groningen, The Netherlands

[3]Department of Radiology, University Medical Center Groningen, Groningen, The Netherlands

Introduction

Mathematical models based on biophysical principles formalize the relationship between the properties of the cardiovascular system and its function. Therefore, by solving the inverse problem important parameters related to pulmonary arterial hypertension (PAH) can be extracted from clinical data. The right ventricular (RV) function is an important determinant of outcome in PAH. The aim of this research is to create a personalized model for different patients to better characterize RV adaptation and ventricular vascular coupling.

Methods

The proposed 0D lumped parameter model within this research is a closed-loop system consisting of the right heart, pulmonary circulation, left heart, and systemic circulation. The equations are solved for pressures and flow rates computationally using a tailor-made numerical method.

To create a personalized model the pressure data obtained by cardiac catheterisation and MRI flow rate data are used. The sum of the squared error (SSE) is minimized by using the BFGS algorithm. The gradient of the cost function is computed in an efficient and exact way. Overall, the whole computation of the inverse problems takes under a minute. Personalized models are created for 9 patients diagnosed with varying types of PAH. Important parameters related to PAH which are estimated with the model are resistances and compliance in the pulmonary artery, stiffness and contractility of the right ventricle.

Results

In figure 1 the adaptive pattern of the right ventricle in PAH is represented based on the estimated parameters for 7 patients. 3 groups can be identified depending on the resistance in the pulmonary capillaries, and RV contractility and stiffness. Furthermore, a higher resistance and lower compliance are found for the patients classified in WHO-FC* III compared to WHO-FC* II.

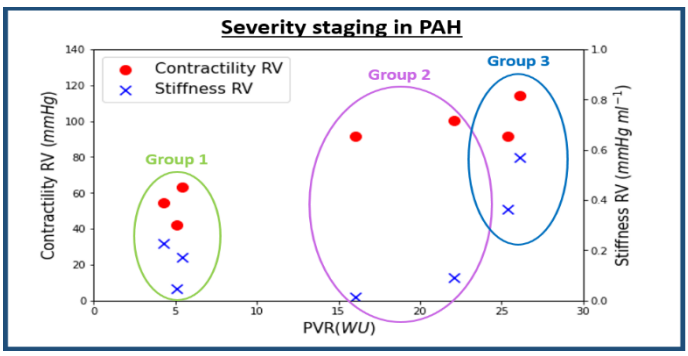

Figure 1: Adaptive pattern of the right ventricle in PAH with increasing pulmonary vascular resistance. The red dots represent the contractility of the right ventricle, and the blue crosses represent the stiffness of the right ventricle. On the horizontal axis, the modeled pulmonary vascular resistance is represented. In this plot, three groups of PAH patients can be identified. In group 2 and 3 there is an increased contractility of the right ventricle, in group 3 there is an increased stiffness of the right ventricle.

Conclusions

Multi-Scale Mechano-OMIC Interactions to Uncover Molecular Transducers for Vascular Protection

Tzung K. Hsiai, MD, PhD

Professor of Medicine and Bioengineering
UCLA Cardiovascular Engineering & Light-Sheet Imaging Laboratory
Director, Caltech/UCLA Bioengineering Training Program
Director, AHA Network Center for Science in Diversity of Clinical Trials

Abstract
During cardiovascular development, peristaltic contraction of the embryonic heart tube produces time-varying hemodynamic forces and pressure gradients across the atrioventricular canal. However, the relative importance of myocardial contraction and hemodynamic force to modulate cardiovascular morphogenesis in the non-Newtonian flow regime remain poorly understood. By using our custom-built 4-D light-sheet fluorescent microscope and post-imaging machine-learning algorithms, we recapitulate flow-mediated molecular transducers underlying the vascular injury and regeneration in the zebrafish vascular injury model. We further elucidate exercise training-mediated transcriptomic interaction underlying activation of endothelial SCD1 to catalyze anti-inflammatory metabolites. In this context, we integrate multi-scale mechano-transcriptomic interaction from zebrafish to mouse models and demonstrate flow-responsive molecular transducers as therapeutic targets for cardiovascular development, repair, and protection.

Acetylation permits arterial gene expression in a SMAD1/5-dependent manner in the pre-flow embryo

Margo Daems, Ljuba Ponomareva, Nadèche Geuens, Rita Simoes-Faria, Bart Ghesquière, An Zwijsen, Elizabeth A.V. Jones

Department of Cardiovascular Sciences, KU Leuven, Leuven, Belgium

Introduction
Notch signalling is widely accepted as the main driver of arterial identity and is a known mechanosensitive pathway. Mammalian arterial endothelial specification is observed before the onset of shear stress in the embryo however, however the role of Notch and other pathways before the onset of flow is poorly understood.

Methods
In situ hybridization and immunohistochemistry are used to look at expression of arterial genes before and after the onset of flow in dissected embryos. Ncx1-/- embryo are used to prevent the onset of blood flow in embryonic development. A combination of blocking antibodies, ligand trap proteins and genetic knockouts are used to block various pathways involved in arterial differentiation. Proxmity ligation assay is used to investigate acetylation of the transcription factor. Embryo culture with chemical inhibitors is used to investigate the role of acetylation.

Results
We establish that though Notch1 is expressed before flow, it is not activate nor is it necessary for the expression of some of the earliest arterial genes in the dorsal aortae (i.e. Hey1 and Gja4). Rather early expression of Hey1 and Gja4 requires Smad1/5 signalling in the mouse embryo. We demonstrate that Smad1/5 signalling is activated through the Alk1/Alk5/TGFβR2 receptor complex with TGFβ1 being a necessary ligand for pre-flow endothelial cells expression of Hey1 and Gja4. TGFβ is a weak ligand for SMAD1/5 signalling. We show that early arterial gene expression requires the acetylation of Smad1/5 proteins which renders them more sensitive to TGFβ1 stimulation. Blocking acetyl-CoA production blocks pre-flow arterial expression of Hey1 and Gja4 however preventing de-acetylation rescues the expression of these genes. Our results indicate that after the onset of flow, SMAD1/5 is no longer acetylated.

Conclusions
Early arterial identity is strictly dependent on the metabolic state of the endothelial cell and subsequent Smad1/5 acetylation. Our results indicate the onset of flow alters endothelial cell metabolism such that SMAD1/5 Is no longer sensitive to TGFβ signalling.

A.I. driven RNA therapeutics. Validation with a new CRISPR high throughput platform.

Zimpi Komo[1*], Arun Jaitly[1*], Shakeeb UI Hassan Ansari[1], Shayan Syed[1], Leila Towhidi[1], and Rob Krams[1]

Department of Science and Engineering[1], Queen Mary University London, London, United Kingdom.

Introduction
RNA therapeutics offer a new way to treat cardiovascular disease. We have created a new deep learning algorithm to generate new, synthetic miRNA which are more specific and offer better ways to specifically modify signaling pathways. These new drugs were tested on a newly developed high throughput CRISPR platform for toxicity, specificity, and sensitivity.

Methods
Non-coding RNA are ideal new drugs. Here, we describe a new AI algorithm (Transformers, CNN, RNN) which is capable of generating new synthetic miRNA that are signaling pathway specific and can work in tandem to gradually modulate specific signaling pathways. These new, synthetic drugs are tested for specificity and sensitivity on a high throughput CRISPR platform using in house knock out/in technology. The CRISPR-CAS9 platform consists of a highly efficiently designed electroporator for (reversed) gene transfection, an ultra-high precision robot dispenser, and a modular parallel plate chamber for experimental interventions which are functionalized involving a series of optimized procedures. Analysis was performed by in house developed single cell analysis software operating on a high throughput microscope. The platform was fully integrated in an AI approach which predicted.

Results
We created a huge data file with mRNA-miRNA canonical and non-canonical information. Entire genes were included to identify, new unknown information. After embedding with Word2vec, we trained a CNN-RNN network which accurately predict signaling pathways. To make more specific miRNA drugs, we generated thousands of in silico mutated miRNA and tested their specificity for pre-defined pathway inhibition. Our high throughput platform was then used to test the best selected synthetic miRNA for their property to specificity inhibit the signaling pathways under study.

Conclusions
This study introduced a novel integration of artificial intelligence and high throughput testing for evaluation of new RNA drugs, specifically designed to modify mechanosensitive signaling pathways.

Role of Mechanical Wall Stress in Coronary Atherosclerosis

Aikaterini Tziotziou [1], Eline Hartman [1], Suze-Anne Korteland [1], Aad van der Lugt [2], Antonius F.W. van der Steen [1], Joost Daemen [3], Daniel Bos [2,4], Jolanda Wentzel [1], Ali C. Akyildiz [1,5]

[1] Dept. of Cardiology, Biomedical Engineering, Cardiovascular Institute, Thorax Center, Erasmus Medical Center
[2] Department of Radiology & Nuclear Medicine, Erasmus Medical Center
[3] Department of Cardiology, Cardiovascular Institute, Thorax Center, Erasmus Medical Center
[4] Department of Epidemiology, Erasmus Medical Center
[5] Department of Biomechanical Engineering, Mechanical Engineering Faculty, Delft University of Technology

Introduction

Biomechanical factors are among the local risk factors for the focal onset, progression, and compositional change of atherosclerotic plaques [1]. Whereas the role of blood flow-induced wall shear stress (WSS) has been extensively studied, the other biomechanical factor, blood pressure-induced mechanical wall stress (MWS) has received limited attention. However, high MWS is known to activate numerous inflammatory pathways and promote extracellular matrix synthesis in the arterial wall [2,3]. To have a comprehensive understanding of the involvement of biomechanics in coronary atherosclerosis, we studied the individual and combined effects of MWS and WSS in atherosclerotic coronaries.

Methods

Computational (CFD and FEM) models of 34 non-culprit coronary arteries from 34 patients who presented acute coronary syndrome were constructed to assess MWS and WSS, based on optical coherence tomography, near-infrared spectroscopy intravascular ultrasound, and computed tomography angiogram data. Twelve months after this baseline imaging, the arteries were reimaged (follow-up time point). To study the local effects, the arteries were divided into sectors of an angle of 45° in the circumferential direction and a length of 1.5 mm in the longitudinal direction. Potential associations of baseline WSS tertiles and MWS tertiles with wall thickness change (ΔWT) over 12 months at the sector level were evaluated using Linear Mixed Models, to account for intra-artery dependency of the sectors.

Results

From the 34 coronaries (13 LADs, 11 RCAs, and 10 LCXs), 6527 sectors were obtained. At baseline, 63% (n = 4112) of the sectors were identified as plaque-free (WT <0.5 mm). In plaque-free sectors, ΔWT had a positive correlation with baseline luminal MWS and a negative correlation with baseline WSS (Figure – A). The remainder of the sectors were identified as plaque sectors (WT <0.5 mm) at baseline. In plaque-sectors, ΔWT had a negative correlation with both baseline luminal MWS and baseline WSS Figure – B). The highest ΔWT was observed in the plaque sectors with high luminal MWS and high WSS.

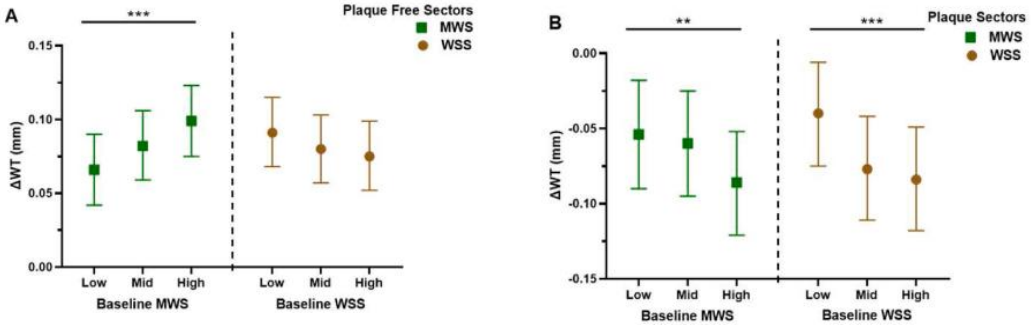

Figure: Baseline luminal MWS and WSS vs. ΔWT in plaque-free sectors (A) and in plaque sectors (B)

Conclusions

Our study demonstrated significant associations of both WSS and MWS, the latter having been largely overlooked so far, to plaque formation and development in coronary arteries.

References

[1] C. Costopoulos et al., Impact of combined plaque structural stress and wall shear stress on coronary plaque progression, regression, and changes in composition, Eur. Heart J. 40 (2019) 1411–1422
[2] J.D. Humphrey et al., Central artery stiffness in hypertension and aging, Circ. Res. 118 (2016) 379–381
[3] S. Lee et al., Effects of statins on coronary atherosclerotic plaques, J. Am. Coll. Cardiol. Img. 11 (2018) 1475–84

The Maastricht acquisition platform for studying mechanisms of cell-matrix crosstalk (MAPEX): Emerging insights on ascending thoracic aortic aneurysm formation

Berta Ganizada, Shaiv Parikh, Pepijn Saraber, *MUMC-TAA Student Team*, Mitch Ramaekers, Gijs Debeij, Cengiz Akbulut, Armand Jaminon, Ehsan Natour, Jos Maessen, Michael Jacobs, Alessandro Giudici, Bart Spronck, Simon Schalla, Joachim Wildberger, Tammo Delhaas, Leon Schurgers, Elham Bidar, Koen Reesink

Cardiovascular Research Institute Maastricht (CARIM) and Heart & Vessel Center, Maastricht UMC+, The Netherlands

Introduction
Current management guidelines for ascending thoracic aortic aneurysms (aTAA) consider diameter and growth rate. However, about half of aTAA dissections and ruptures occur before the surgical intervention threshold is reached. During aTAA repair surgeons observe and experience considerable variations in tissue strength, thickness, and stiffness that are not fully explained by patient risk factors.

Methods
To improve our understanding of aTAA pathophysiology, we established a multi-disciplinary research infrastructure: The Maastricht acquisition platform for studying mechanisms of tissue-cell crosstalk [1]. The scientific focus of this infrastructure is on elucidating the dynamic interactions between vascular smooth muscle cells (VSMC) and extracellular matrix (ECM), playing an essential role in aortic mechanical homeostasis. We have included over 190 patients (aTAA, aTAAD, control) and our current analysis is based on 90 patients, involving extensive histomorphometric, in-situ biaxial wall strain, and MR 4D-flow shear stress characterizations.

Results
Current key findings are: **A.** Considerable heterogeneity among aTAA cases in relative wall thickness (thinning or thickening), elastin structural integrity (degraded), VSMC density (increased) and phenotype (away from contractile); n=90. **B.** An overall lack of constitutive differences (thickness, ECM, VSMC) across the circumference of the max dilated part of the aneurysm (n=60), though at individual level considerable variations are noticed. **C.** A consistent (n=67) proximal-to-distal difference in circumferential strain but no difference in axial strain between inner and outer bend (of the ascendens). **D.** Tendency for co-localization of increased wall shear stress and elastin degradation (n=18).

Conclusions
MAPEX' present findings indicate that wall stress homeostasis may not be fully dysfunctional in aTAA but rather involves variations of adaptive wall remodeling and changes in smooth muscle function. Hence, VSMC repurposing appears as a promising personalized strategy in patients with developing aortopathy.

References

[1] Ganizada BH, Reesink KD, Parikh S, Ramaekers MJFG, Akbulut AC, Saraber PJMH, Debeij GP, Mumc-Taa Student Team, Jaminon AM, Natour E, Lorusso R, Wildberger JE, Mees B, Schurink GW, Jacobs MJ, Cleutjens J, Krapels I, Gombert A, Maessen JG, Accord R, Delhaas T, Schalla S, Schurgers LJ, Bidar E. The Maastricht Acquisition Platform for Studying Mechanisms of Cell-Matrix Crosstalk (MAPEX): An Interdisciplinary and Systems Approach towards Understanding Thoracic Aortic Disease. Biomedicines. 2023 Jul 25;11(8):2095. doi: 10.3390/biomedicines11082095.

[2] Parikh S, Ganizada B, Debeij G, Natour E, Maessen J, Spronck B, Schurgers L, Delhaas T, Huberts W, Bidar E, Reesink K. Intra-Operative Video-Based Measurement of Biaxial Strains of the Ascending Thoracic Aorta. Biomedicines. 2021 Jun 11;9(6):670. doi: 10.3390/biomedicines9060670.

Real-Time Quantification of Patient-specific Wall Stress in Diseased Coronary Arteries

Amir Rouhollahi[1], Karim Kadry[2], Elazer R. Edelman[2], Farhad R. Nezami[1]

[1]Department of Surgery, Brigham and Women's Hospital, Harvard Medical School, Boston, USA

[2]Institute for Medical Engineering and Science, Massachusetts Institute of Technology, Cambridge, USA

Introduction

Coronary artery disease is a major global health issue, leading to serious heart events. Current imaging techniques fall short in diagnosing and predicting the complex mechanical responses underlying plaque destabilization. Although 3D biomechanics simulations offer accurate wall stress predictions, they are resource-intensive and slow, taking hours to analyze a single patient's data.

Methods

We developed a neural network surrogate model for rapid prediction of arterial wall stress in atherosclerotic lesions. Intravascular optical coherence tomography (OCT) was utilized for quantifying lesion micro-morphology using convolutional neural networks (CNN) [1]. Labeled images were processed to create simulation-ready digital twins (Fig.1A) [2]. Lesion-specific computational modeling for 10+ coronary patients coupled lesion morphology to mechanics, providing ground truth for training/testing a stress-predicting tool. Soft tissues were modeled hyperelastically while calcium was assumed to behave linear elastically (Fig.1B) [3]. Results from 3D simulations were partitioned into 2D heatmaps, akin to OCT frames, to train and test a surrogate U-Net created by TensorFlow and Keras frameworks. The model, optimized to minimize mean absolute error, incorporates dropout layers and hyperparameter tuning to prevent overfitting and leverages the Adamax optimization algorithm for training.

Results

Training the U-Net model was performaed with 238 pairs of images and binary labels, with a separate set of 38 pairs for validation purposes. The extensive training converged after 30 epochs, achieving a validation dice loss metric of 0.97, reflecting the model's enhanced predictive accuracy and its adeptness in deciphering the nuances of biomechanical stress analysis. Our results show that calcium morphology modifies wall stress distribution, particularly creating high-stress areas where rigid, calcified plaques meet softer, non-calcified tissues. This imbalance in stress can significantly increase the likelihood of plaque rupture, potentially triggering serious heart conditions like acute coronary syndromes or heart attacks.

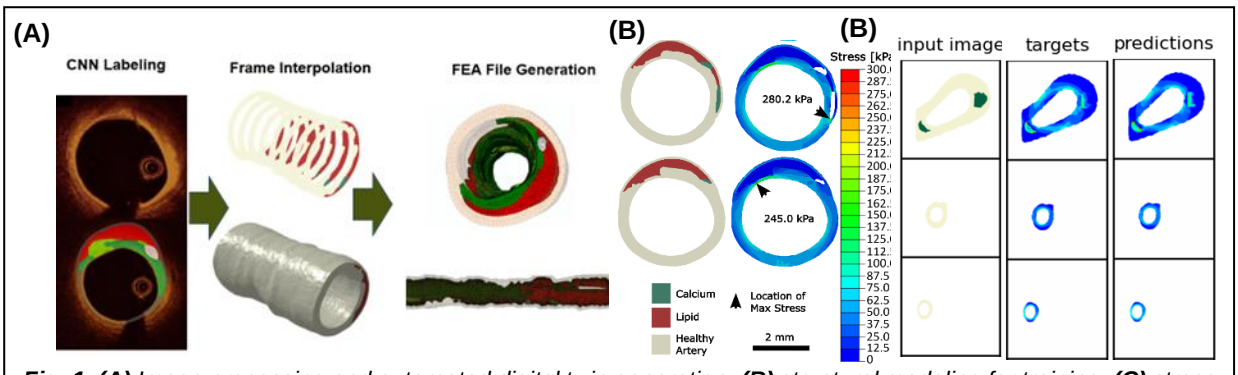

Fig. 1. (A) *Image processing and automated digital twin generation,* ***(B)*** *structural modeling for training,* ***(C)*** *stress map prediction using machine learning*

Conclusions

Stress distribution in a diseased coronary artery is a complex function of plaque micromorphology. Machine learning tools hold the potential to automate the generation of digital twins and enable real-time quantification of such intricate wall stress pattern to predict clinical events, specifically rupture.

References

[1] ML Olender, Y Niu, D Marlevi, ER Edelman, FR Nezami, Impact and implications of mixed plaque class in automated characterization of complex atherosclerotic lesions, CMIG, Volume 97, 2022.

[2] R Straughan, K Kadry, SA Parikh, ER Edelman, FR Nezami, Fully automated construction of three-dimensional finite element simulations from Optical Coherence Tomography. *Comput Biol Med*. 165:107341, 2023.

[3] K Kadry K, ML Olender, D Marlevi, ER Edelman, FR Nezami, A platform for high-fidelity patient-specific structural modelling of atherosclerotic arteries: from intravascular imaging to 3D stress distributions, *JRSI*,18(182), 2021.

Impact of thrombus mechanical properties on virtual thrombectomy procedures

Virginia Fregona[1], Giulia Luraghi[1], Behrooz Fereidoonnezhad[2], Frank JH Gijsen[2,3], José Félix Rodríguez Matas[1], Francesco Migliavacca[1]

[1]Department of Chemistry, Materials and Chemical Engineering 'Giulio Natta', Politecnico di Milano, Italy

[2]Department of Biomechanical Engineering, Delft University of Technology, Delft, The Netherlands

[3]Department of Biomedical Engineering, Erasmus MC, Rotterdam, The Netherlands

Introduction

Endovascular thrombectomy (EVT) with stent-retriever is a minimally invasive treatment for acute ischemic stroke, aiming at removing a clot from a large cerebral vessel. After being navigated up to the occlusion site crimped in a microcatheter, the stent-retriever is deployed, and the stent with the captured clot is retrieved. Literature suggests that clots are formed mainly by red blood cells (RBCs), platelets, and fibrin, in variable percentages among patients [1]. Fibrin-rich clots may be more difficult retrieve [2] while RBC-rich clots may be more prone to fragmentation [3]. Here, after the development of a material model for clots of different compositions, finite-element simulations of the EVT are performed varying the clot composition.

Methods

With a methodology validated through the comparison with *in vitro* experiments [4], the entire EVT procedure with stent-retriever (stent crimping in the microcatheter, microcatheter tracking, stent deployment, and retrieval) was replicated *in silico* in Ansys LS-DYNA. An ideal cerebral vasculature anatomy is created taking the average values of the morphological features reported in [5] and modelled as a rigid shell. A clot of 13.5 mm of length (median length in [6]) is positioned in the distal M1 (most frequent location in [7]). The clot is modelled as a hyperelastic foam exploiting the experimental uniaxial stress-strain curves in compression and tension (Figure 1). Three different clot compositions are considered (0%, 1% and 40% RBCs). For each composition three simulations are run changing the design of the stent-retriever, discretized with beam elements and modelled with a shape-memory material.

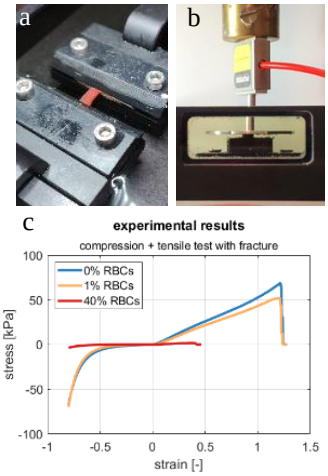

Figure 1 Experimental setup for clot a) tensile test b) compression test. c) experimental stress-strain curves.

Results

Preliminary data show that the clot composition and the device design have an impact on the in silico EVT outcome, in terms on success of the retrieval. EVTs performed on identical clot but with different stent-retriever design do present different outcomes, as for EVTs performed with the same device and different clots. In some cases, indeed, the clot is lost during the retrieval or fragmented as in Figure 2. As expected, fragmentation is more likely to happen for the RBCs-rich clots (here, 40% RBCs).

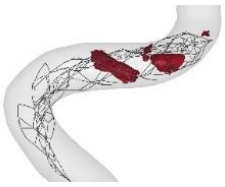

Figure 2 Fragmented clot.

Conclusions

Having the clot a central role in the procedure, knowing its mechanical properties and its interaction with different devices, and thus understating its influence on the EVT outcome is crucial to improve the selection of retrieval devices and intervention strategies.

References

[1] N. Boodt *et al.*, *Stroke*, no. August, pp. 2510–2517, 2021.
[2] I. Yuki *et al.*, *Am. J. Neuroradiol.*, vol. 33, no. 4, pp. 643–648, 2012.
[3] B. Fereidoonnezhad *et al.*, *Acta Biomater.*, vol. 127, pp. 213–228, 2021.
[4] G. Luraghi *et al.*, *Interface Focus*, vol. 11, no. 1, p. 20190123, 2021.
[5] S. Bridio *et al.*, *Appl. Sci.*, vol. 13, no. 18, 2023.
[6] N. Boodt *et al.*, *Stroke*, vol. 51, no. 6, pp. 1727–1735, 2020.
[7] B. G. Dutra *et al.*, *Stroke*, vol. 50, no. 8, pp. 2057–2064, 2019.

HEG1 Protects Against Atherosclerosis by Regulating Stable Flow-Induced KLF2/4 Expression in Endothelial Cells.

Ian A. Tamargo*, Kyung In Baek*, Chenbo Xu, Yerin Kim, Christian Park, Shoutaro Tsuji, and Hanjoong Jo

Coulter Department of Biomedical Engineering, Emory University and Georgia Tech, USA

Introduction
Atherosclerosis preferentially occurs in arterial regions of disturbed blood flow, and stable flow (s-flow) protects against atherosclerosis by incompletely understood. Our single-cell RNA-sequencing data using the mouse partial carotid ligation model was reanalyzed, which identified Heart-of-glass 1 (HEG1) as an s-flow–induced gene. Here, we studied the role of HEG1 in endothelial function and athesclerosis (1).

METHODS:
HEG1 expression was studied by immunostaining, quantitive polymerase chain reaction, hybridization chain reaction, and Western blot in mouse arteries, HAECs (human aortic endothelial cells), and human coronary arteries. A siRNA (small interfering RNA)-mediated knockdown of HEG1 was used to study its function and signaling mechanisms in HAECs under various flow conditions using a cone-and-plate shear device. We generated endothelial-targeted, tamoxifen-inducible HEG1 knockout ($HEG1^{iECKO}$) mice. To determine the role of HEG1 in atherosclerosis, $HEG1^{iECKO}$ and littermate-control mice were injected with an adeno-associated virus–PCSK9 [proprotein convertase subtilisin/kexin type 9] and fed a Western diet to induce hypercholesterolemia either for 2 weeks with partial carotid ligation or 2 months without the surgery.

RESULTS:
S-flow induced HEG1 expression at the mRNA and protein levels in vivo and in vitro. S-flow stimulated HEG1 protein translocation to the downstream side of HAECs and release into the media, followed by increased messenger RNA and protein expression. HEG1 knockdown prevented s-flow–induced endothelial responses, including monocyte adhesion, permeability, and migration. Mechanistically, HEG1 knockdown prevented s-flow–induced KLF2/4 (Kruppel-like factor 2/4) expression by regulating its intracellular binding partner KRIT1 (Krev interaction trapped protein 1) and the MEKK3-MEK5-ERK5-MEF2 pathway in HAECs. Compared with littermate controls, $HEG1^{iECKO}$ mice exposed to hypercholesterolemia for 2 weeks and partial carotid ligation developed advanced atherosclerotic plaques, featuring increased necrotic core area, thin-capped fibroatheroma, inflammation, and intraplaque hemorrhage. In a conventional Western diet model for 2 months, $HEG1^{iECKO}$ mice also showed an exacerbated atherosclerosis development in the arterial tree in both sexes and the aortic sinus in males but not in females. Moreover, endothelial HEG1 expression was reduced in human coronary arteries with advanced atherosclerotic plaques.

Conclusions
HEG1 is a novel mediator of atheroprotective endothelial responses to flow and a potential therapeutic target.

References
[1] Tamargo IA, Baek KI, Xu C, Won Kang D, Kim Y, Andueza A, Williams D, Demos C, Villa-Roel N, Kumar S, Park C, Choi R, Johnson J, Chang S, Kim P, Tan S, Jeong K, Tsuji S, **Jo H.**. Circulation. 2023 Dec 15. doi: 10.1161/CIRCULATIONAHA.123.064735. Online ahead of print.

Role of Endothelial Cell Shape and Orientational Order in Angiogenic Sprouting

Abdul I. Barakat[1], Sara Barrasa-Ramos[1], Carles Blanch-Mercader[2]

[1]LadHyX, CNRS, Ecole Polytechnique, Institut Polytechnique de Paris, Palaiseau, France

[2]Laboratoire PCC, Institut Curie, Universite PSL, Sorbonne Université, CNRS UMR168, Paris, France

Introduction
Angiogenesis is the emergence of new microvessels from pre-existing vessels. Favoring or thwarting this process is essential in fields as diverse as cancer, cardiovascular disease, and tissue engineering. However, the mechanisms through which endothelial cells (ECs) integrate different pro- and anti-angiogenic signals remain incompletely understood. A well-established pro-angiogenic protein, vascular endothelial growth factor (VEGF), has been shown to induce spatially heterogeneous changes in EC elongation and alignment. Independently, recent studies have provided insight into various morphogenetic events by appealing to the framework of active liquid crystals. Inspired by these investigations, we aim to explore the role of VEGF-induced changes in EC shape and alignment in modulating the out-of-plane transition that initiates angiogenic sprouting.

Methods
Human umbilical vein ECs (HUVECs) were cultured to confluence on the surface of a flat fibronectin-coated Type I collagen hydrogel. VEGF (50 ng/ml) was subsequently added to the culture medium for 66 h. Some experiments explored the impact of the following cytoskeletal-altering agents: nocodazole, blebbistatin, Y27632, calyculin A, cytochalasin D, and latrunculin A. Other studies involved patterning of the hydrogel free surface using a PRIMO (Alveole) system. Immunostained samples were observed under confocal and widefield fluorescence microscopy. Analysis was performed using both open-source and custom-made codes in FIJI, Matlab, and Python.

Results
VEGF elicited striking changes in EC shape as well as the formation of sprouts that grow into the collagen hydrogel. Interestingly, sprouts are significantly more likely to initiate close to *wedge* regions, defined as singularities in cell orientational order at the interface between highly ordered (i.e. elongated and aligned) and more isotropic cell clusters. Interestingly, these areas are also observed to correlate with wrinkling of the underlying hydrogel. We are currently exploring if this wrinkling is a consequence of mechanical stresses around wedges. We are also investigating the possible links between gel wrinkling and angiogenic sprouting. The results of the cytoskeleton disruption studies suggest that the VEGF-induced changes in EC morphology are mediated by a competition between microtubules (MTs), which promote cell elongation, and actomyosin contractility, which counteracts it. The results also indicate that MT disruption alters the nature of gel deformation by the cells, transforming the “wrinkles” to more circular “dimples”. This appears to correlate with a reduced incidence of angiogenesis. Patterning the hydrogel surface with 100 to 400 μm-wide adhesive lines provides geometrical confinement of the EC monolayer. Progressively thinner line patterns induce increased global cellular elongation, thereby reducing the cell morphological heterogeneities induced by VEGF. Preliminary findings suggest reduced angiogenic sprouting in this case.

Conclusions
The present results suggest that local heterogeneities in EC shape and orientation play an important role in the initiation of sprouting angiogenesis. The observed substrate deformation in these zones is suggestive of local forces acting at the wedge level, which may provide a link between cell orientational order and angiogenic sprouting. The observation that MT disruption alters both EC shape and the nature of substrate deformation is consistent with existing literature pointing to a central role for MTs in sprouting angiogenesis through induction of cell polarity. Our ongoing studies focus on using traction force microscopy to measure the force distribution in the EC monolayer and to combine these measurements with theoretical modeling to better understand the resulting hydrogel deformations. We are also further pursuing gel patterning studies in an effort to provide tools for physical control of angiogenic sprouting.

Bioprinting of 3D vascular models.

Biofabrication Process and Preliminary Results using FRESH technique

Franca Scocozza, Michele Conti

Department of Civil Engineering and Architecture, University of Pavia, Pavia, Italy

michele.conti@unipv.it

Introduction

Vascular grafting is a commonly used method for treating severe cardiovascular diseases or damage that leads to the loss of a vessel [1]. While 3D printing technologies have enabled new approaches for creating vascular grafts, producing vessels that range in size from large (> 6mm) to small (< 1mm), while also mimicking the biomechanical properties, geometric organization, and complexity of the cellular and extracellular microenvironment, remains a challenge [2]. To address this issue, the Freeform Reversible Embedding of Suspended Hydrogels (FRESH) method has been developed. This method is effective in controlling geometry and fluid flow [3]..

Methods

The FRESH method was utilized as a temporary support solution to prevent the collapse and deformation of the constructs during the printing process. A gelatine-based bath and a low-viscosity sodium alginate with ionic crosslinking were used as biomaterial ink for printing. The bioink was printed using a pneumatic extrusion bioprinter.

The biofabrication process consists of three main steps: pre-printing, FRESH printing, and post-printing. During pre-printing, the biomaterial ink and support bath were developed. FRESH printing involved the fabrication of a vessel-like structure, while post-printing involved melting the support bath and coating the printed structure to provide greater resistance.

Optimal bioprinting conditions were defined by varying the pressure between 3 kPa and 20 kPa and evaluating two nozzle diameters of 0.4 mm and 0.5 mm. The shape fidelity of the printed construct was analyzed qualitatively using ImageJ software and quantitatively using micro-CT. Additionally, an uniaxial compression test was performed to evaluate the mechanical properties of the printed vessel. The sterility of the biofabrication process was evaluated, and a preliminary biological test was conducted using the rat osteosarcoma (UMR) line. Finally, the vessel was connected to a perfusion system to evaluate the construct's resistance to low pressures.

Results

We have successfully created a blood vessel using the FRESH method. After conducting several tests, we found that the optimal bioprinting conditions were a printing speed of 15 kPa and a needle size of 0.4 mm. We discovered that the model's geometry and walls became more regular and homogeneous after coating. Our mechanical characterization results showed that the constructs printed at different times had similar behavior and low data dispersion, although they did not reflect the vessels' mechanical-physiological behavior. We also found that the printed constructs were not contaminated for up to 21 days, had a high number of cells in the coating layer, and the cells were uniformly distributed.

Conclusions

The FRESH method shows potential for creating blood-like structures to replicate a healthy and hypertensive vessel microenvironment.

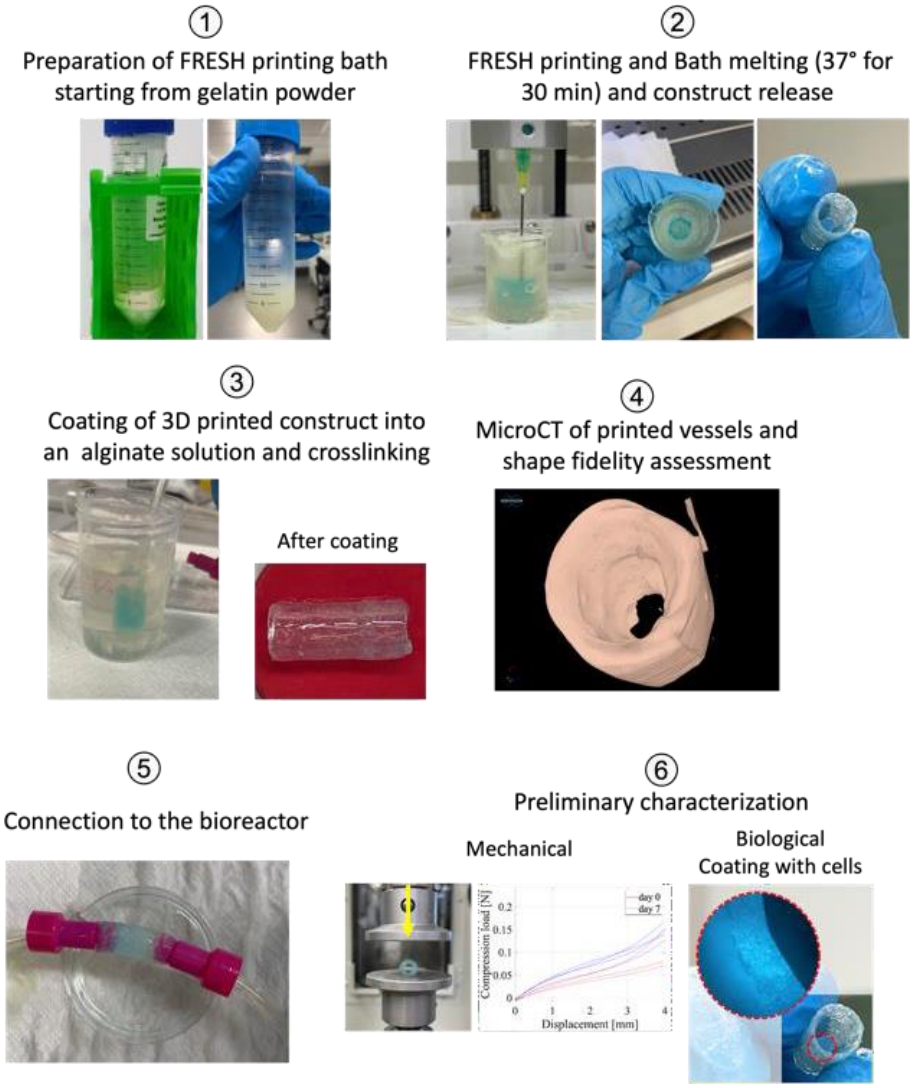

References

[1] Fazal F et al., Recent advancements in the bioprinting of vascular grafts, Biofabication 13.3:032003, 2021.

[2] Shiwarski D. et al., FRESH 3D Bioprinted Collagen-based Resistance Vessels and Multiscale Vascular Microfluidics, The FASEB Journal, 36, 2022.

[3] Cao X. et al., Bioprinting of small-diameter blood vessels. Engineering, 7.6:832-844, 2021.

A tissue-engineered model of the atherosclerotic plaque cap with microcalcifications

Imke L Jansen[a], Hanneke Crielaard[a], Tamar B Wissing[a], Carlijn VC Bouten[b,c], Frank JH Gijsen[a,d], Ali C Akyildiz[a,d], Eric Farrell[e], Kim van der Heiden[a]

a Department of Biomedical Engineering, Erasmus MC, University Medical Center Rotterdam, the Netherlands
b Department of Biomedical Engineering, Eindhoven University of Technology, Eindhoven, The Netherlands.
c Institute for Complex Molecular Systems, Eindhoven University of Technology, Eindhoven, The Netherlands.
d Department Biomechanical Engineering, Delft University of Technology, Delft, The Netherlands
e Department of Oral and Maxillofacial Surgery, Erasmus MC, University Medical Center Rotterdam, the Netherlands

Introduction
Rupture of the cap of an atherosclerotic plaque can lead to thrombotic cardiovascular events, such as stroke and myocardial infarction. The cap overlying the atherosclerotic lipid pool is often characterised by a heterogenous composition, and can among others contain inflammation and microcalcifications (diameter < 50 µm) embedded in a collagenous matrix. Current computational models suggest that microcalcifications in the atherosclerotic cap can increase the risk of cap rupture, but experimental verification of the mechanical effect of microcalcifications is lacking. In this study, we make use of a tissue-engineered (TE) model of the atherosclerotic plaque cap with microcalcifications to assess the impact of microcalcifications on collagen organisation and cap mechanics.

Methods
Firstly, human carotid plaque caps obtained from carotid endarterectomy (CEA) samples were histologically analysed to determine the distribution and particle size of microcalcifications in cap tissue. Hydroxyapatite (HA) particles were then used as mimic of microcalcifications in the TE-cap, since HA is the main component of microcalcifications in human plaques. Human myofibroblasts were cultured in 1 x 1.5 cm-sized fibrin-based constrained gels, according to previously established protocols. At the start of the culture, clusters of hydroxyapatite particles were injected in the fibrin gel. During a 21-culture period, the myofibroblasts deposited a collagenous matrix around these particles. At day 21, samples were exposed to multiphoton microscopy with second harmonic generation (SHG) to determine the local collagen fiber orientation, which was done using a fiber orientation analysis tool (FibLab). In combination with the SHG imaging, hydroxyapatite particles were visualized using a hydroxyapatite-targeting probe (IVISense Osteo 680). After vital imaging, the samples were subjected to uniaxial tensile tests until rupture to assess global mechanical properties.

Results
In CEA samples microcalcification particles were found to be present in clusters. The majority of the particles were observed to be 2 - 15 µm (84%), while only 3% was larger than 30 µm. HA particles with similar size and distribution were used to mimic microcalcifications in the TE constructs and verified against the human situation. SHG revealed higher local collagen fiber dispersion in regions of hydroxyapatite clusters compared to control samples. Uniaxial tensile testing showed that engineered caps with HA particles demonstrated lower stiffness and ultimate tensile stress than control samples, suggesting increased rupture risk in atherosclerotic plaques with microcalcifications. Furthermore, sample stiffness negatively correlated with dispersion of collagen fibers, highlighting the effect of fiber orientation, due to microcalcifications, on tissue mechanics.

Conclusions
In this study, we have created a TE fibrous cap model with a mimic of microcalcifications to study the effect on cap mechanics and collagen organisation. This model supports previous computational findings regarding a potential harmful role for microcalcifications on cap rupture risk, due to a lowered ultimate tensile stress and stiffness. Ongoing research focusses on the effect of various microcalcification characteristics, such as size, shape and density on cap rupture mechanics. The model can be further deployed to elucidate tissue mechanics in pathologies with calcifying soft tissues.

Funding
This work was funded by a NWO-Vidi grant (18360)

Image-based flow and structural simulation of platelet aggregates under low, medium, and high shear flow conditions

Yue Hao[1], Gabor Zavodszky[1]

[1]Computational Science Lab, Informatics Institute, University of Amsterdam, Amsterdam, The Netherlands

Introduction

The initial step of thrombus formation involves the aggregation of a pro-thrombotic agonist, the platelets. The characteristics of this initial platelet aggregate are strongly impacted by the local blood flow conditions [1], including shape, porosity, and mechanical properties. Such local morphological differences in turn impact the flow and the subsequent clot formation process [2]. In this work we combine two imaging modalities to capture morphological information on initial platelet aggregates forming in low, medium, and high shear flow envionments. This infomarion is used to build a computational model that can proble the local flow and mechanical microenvironment (fluid stresses, various molecular weight agonist transport, structural stresses in the aggregates). Such detailed information is currently not available via experimental methods. Finally, using this method we demonstrate correlations between the morphology of the aggregates and the fluid mechanical environment in which they formed.

Methods

The platelet aggregates have been recorded in 3D using stack of differential interfecence contrast (DIC) microscopy and fluorescence microscopy [3]. The former defines the shape of the aggregate while the latter yields the porosity distribution. The combination of these images is used to build a finite element model of the aggregates, that is subjected to flow, where the effect of the aggregate is imposed by the Darcy term added to the Navier-Stokes equation. The magnitude of this term is then used to define force interaction between fluid (whole blood) and solid (platelet aggregate). A a simple neo-Hookean material model is then applied to the aggregate to estimate the distribution of internal stresses.

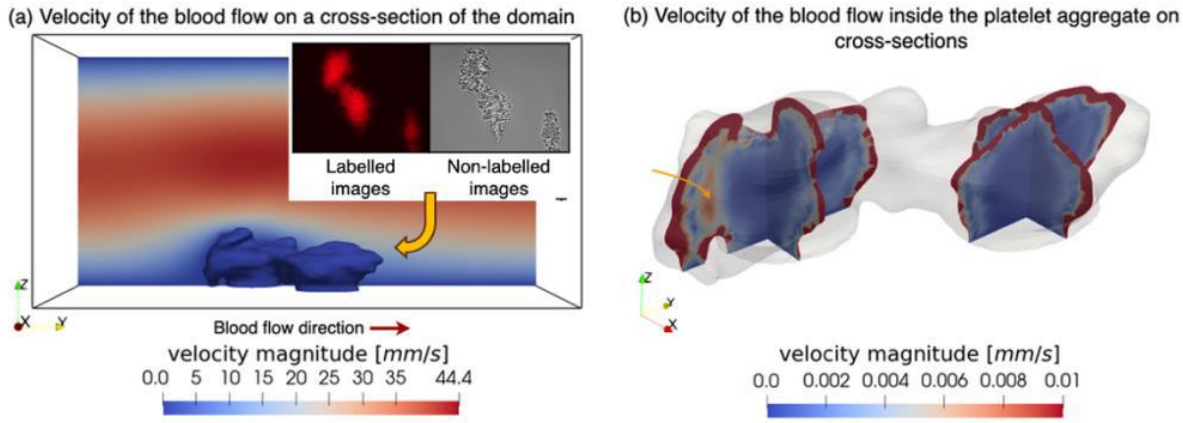

Results

The morphology of aggregates differs substantially under the different shear regimes. The internal density (and the size of the ‘core’ region) increases with shear. The typical shape of the aggregates is influenced: low shear aggregates tend to grow along the coated surface of the microfluidic chamber, while high shear ones tend to grow more perpendicular, into the flow, leading to much faster occlusion.

Conclusion

The study highlights the impact of the fluid mechanical microenvironment on the growth and morphology of the initial platelet aggregates and demonstrates a way to combine in vitro and in silico techniques to access high-detail information on this environment.

References

[1] Casa, L.D., Ku, D.N.: Thrombus formation at high shear rates. Annual Review of Biomedical Engineering 19(1), 415–433 (2017).

[2] D. A. Kim and D. N. Ku, “Structure of shear-induced platelet aggregated clot formed in an in vitro arterial thrombosis model,” Blood Advances, vol. 6, no. 9, pp. 2872–2883, May 2022.

[3] Y. Hao, G. Závodszky, C. Tersteeg, M. Barzegari, and A. G. Hoekstra, “Image-based flow simulation of platelet aggregates under different shear rates,” PLOS Computational Biology, vol. 19, no. 7, p. e1010965, Jul. 2023.

Spatial transcriptomics of remodeling brain arteries reveals potential molecular signals for dystrophic versus eutrophic responses to flow

John Kolega, Kerry E. Poppenberg, Liza C. Gutierrez, Sricharan S. Veeturi, Adnan H. Siddiqui, Vincent M. Tutino

Departments of Pathology & Anatomical Sciences and Neurosurgery, SUNY at Buffalo, Buffalo, NY, USA

Introduction

When blood flow exerts elevated wall shear stress (WSS) on an artery, it can induce wall growth to enlarge the lumen. However, in brain aneurysms, high WSS with a positive spatial gradient induces destructive remodeling that thins and weakens the vessel wall[1]. Because WSS is sensed by the intima, but remodeling occurs primarily in the media, we hypothesize that aneurysm-inducing hemodynamics cause the intima to produce different signals than those produced during eutrophic enlargement. This study identifies WSS-sensitive intimal signals that distinguish eutrophic and dystrophic remodeling.

Methods

New Zealand white rabbits underwent bilateral carotid ligation to increase flow in the basilar artery (BA) or sham surgery with no ligation. Hemodynamics in the BA, where eutrophic growth occurs, and the basilar terminus (BT), where aneurysms form, were mapped by computational fluid dynamics as previously described[1]. 24 hours post-surgery, the BA and BT were dissected and 10-micron frozen sections in the plane of the bifurcation were collected onto Visium Spatial Gene Expression Capture Slides. Sections were permeabilized and reverse transcribed in situ to generate barcoded cDNA. Illumina sequencing libraries were constructed with unique molecular identifiers (UMIs) incorporated, then sequenced to an average 20,000 reads/spot. Reads were aligned to the rabbit genome and UMI counts were quantified for each spot using the Cell Ranger Spatial pipeline (10X Genomics). Spots on intima and media were identified on histology in the Loupe browser. Differentially expressed genes were identified by modified F-test (p-value<0.1). To predict signals between intima and media, Pearson correlation coefficients were calculated in Python for every possible intima-media gene pair across all spots and conditions[2]. All genes with a p-value<0.1 and expressed in at least half of samples in both intima and media groups were included. Gene pairs with absolute correlation coefficient >0.9 and p-value< 0.01 were considered significantly correlated.

Results

85% of reads mapped to the genome and identified 3,339 genes. Comparing expression in eutrophic vs dystrophic intima (BA vs BT), 101 genes were differentially expressed (81 higher, 20 lower in the BT). In the media, 335 genes were differentially expressed (294 higher, 41 lower in BT). Potential upstream regulators of smooth-muscle cells during dystrophic remodeling were predicted from the medially expressed genes using Ingenuity Pathway Analysis (IPA; Qiagen Inc). Regulators were considered significant if z>2. Predicted regulators were then mapped to hubs and key genes in networks of potential interactions generated in IPA for the differentially expressed intimal genes at the BA and BT. Networks were considered significant if their p-scores were >21. This analysis suggested that the TGFβ1 signaling pathway could mediate dystrophic remodeling. Correlation analysis revealed 486 gene pairs (involving 97 unique intimal genes) whose expression were significantly correlated between intima and media. One of the intimal genes with the most media correlates was BMP4, a member of the TGF-β superfamily.

Conclusions

Correlative expression analysis of intimal and medial genes can reveal novel signals that may regulate flow-induced arterial remodeling. Pathway analysis of differentially expressed genes and correlation analysis implicate TGF-β superfamily in dystrophic remodeling.

References

[1] Metaxa, E, Tremmel, M, Natarajan, S., Xiang, J, Paluch, R, Mandelbaum, M, Siddiqui, AH, Kolega, J, Mocco, J, Meng, H. Characterization of critical hemodynamics contributing to aneurysmal remodeling at the basilar terminus in a rabbit model. *Stroke* 41: 1774-1782, 2010.

[2] Kolega, J, Poppenberg, KE, Lim, H-W, Gutierrez, LC, Veeturi, SS, Siddiqui, AH, Rajabzadeh-Oghaz, H, Tutino, VM, Identification of intima-to-media signals for flow-induced vascular remodeling using correlative gene expression analysis. *Sci. Rep.,* 11: 16142, 2021.

Mechanical wall stress and wall shear stress are associated with atherosclerosis development in coronary arteries

Aikaterini Tziotziou[1], Eline Hartman[1,2], Ayla Hoogendoorn[1], Suze-Anne Korteland[1], Aad van der Lugt[3], Antonius F.W. van der Steen[1], Joost Daemen[2], Daniel Bos[3,4], Jolanda J Wentzel[1], Ali C Akyildiz[1,5]

1. Department of Biomedical Engineering, Erasmus Medical Center, Rotterdam, the Netherlands;
2. Department of Cardiology, Erasmus Medical Center, Rotterdam, the Netherlands;
3. Department of Radiology & Nuclear Medicine, Erasmus Medical Center, Rotterdam, the Netherlands;
4. Department of Epidemiology, Erasmus Medical Center, Rotterdam, the Netherlands.
5. Department of Biomechanical Engineering, Delft University of Technology, Delft, the Netherlands;

Introduction

Atherosclerotic plaque development in coronary arteries is affected by a local biomechanical factor; the blood flow induced wall shear stress (WSS) [1]. However, the potential role of another biomechanical factor, the blood pressure induced wall mechanical stress (WMS) has been mainly overlooked. In this study, we investigated the individual and combined effect of WMS and WSS in atherosclerosis progression in human and porcine coronary arteries.

Methods

Human Coronaries: Thirty-four coronary arteries were analyzed using near-infrared spectroscopy intravascular ultrasound (NIRS-IVUS) and optical coherence tomography (OCT) at baseline and after 12 months [2]. *Porcine Coronaries:* Thirty coronary arteries (ten male pigs) under high-fat diet were imaged with NIRS-IVUS and OCT at 3 months, 6 months and 12 months later [3]. The lumen, vessel wall, and lipid-rich necrotic core (LRNC) geometries were reconstructed for all time points in both datasets. WSS was computed with Computational Fluid Dynamics and WMS with finite element analysis using artery-specific blood flow and pressure [2,3]. The individual and combined effect of WSS and MWS on local wall thickness (WT) change over time, was evaluated in 3mm/45^{o} arterial sectors using Generalized Linear Mixed Models (GLMM) in SPSS, correcting for baseline measurements on each individual dataset.

Results

Plaque sectors in human coronaries demonstrated wall thickness reduction over time, likely due to the medical therapy, where higher levels of WSS and WMS, individually and combined, ($p<0.05$) were associated with a greater reduction (Fig. 1). Same trend was observed in porcine coronaries where lower levels of WSS and WMS were associated ($p<0.05$) with greater increase in WT over time (Fig. 1). In both datasets, sectors exposed to low MWS combined with high WSS demonstrated moderate WT change with the highest LRNC percentage increase ($p<0.05$), suggesting a potential transformation into higher-risk phenotypes.

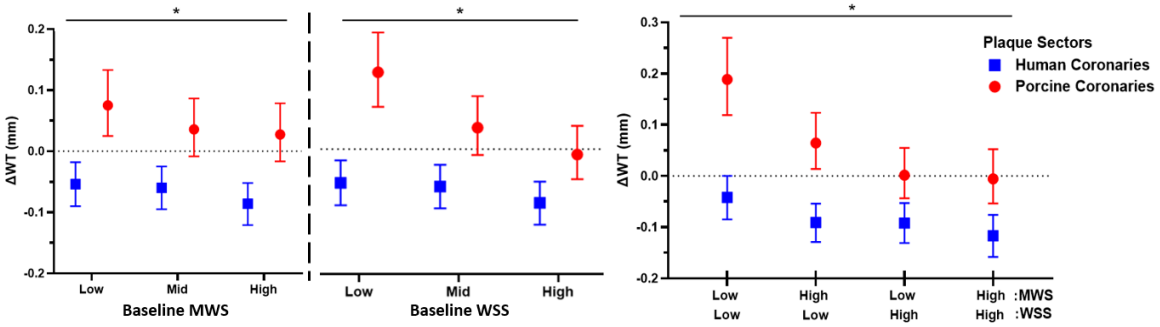

Figure 1. Association of WMS and WSS with ΔWT based on GLMM. (Data are presented as mean with 95% CI).

Conclusions

Our findings demonstrate that atherosclerotic disease development is not only associated with the well-accepted WSS but also with MWS, highlighting the importance of the local biomechanical analysis and local plaque composition assessment.

References

[1] Hartman, E et al., *J. of Cardiovasc. Trans. Res.*, 14:416–425, 2021.
[2] Tziotziou, A et al., *Atherosclerosis*, 387:117387, 2023.
[3] Hoogendoorn A, et al., *Cardiovasc Res*, 116:1136-46, 2020.

In-depth calcification morphometrics in carotid arteries are associated with cerebrovascular events, sex and cardiovascular risk factors

Aikaterini Tziotziou[1], Federica Fontana[2], Suze-Anne Korteland[1], Eline Kooi[3], Aad van der Lugt[4], Antonius F.W. van der Steen[1], Jolanda J Wentzel[1], Daniel Bos[4,5], Ali C. Akyildiz[1,2]

[1] Department of Biomedical Engineering, Erasmus Medical Center, Rotterdam, the Netherlands;
[2] Department of Biomechanical Engineering, Delft University of Technology, Delft, the Netherlands;
[3] Department of Radiology and Nuclear Medicine, Maastricht Medical Center+, Maastricht, the Netherlands;
[4] Department of Radiology & Nuclear Medicine, Erasmus Medical Center, Rotterdam, the Netherlands;
[5] Department of Epidemiology, Erasmus Medical Center, Rotterdam, the Netherlands.

Introduction

Carotid atherosclerosis is the underlying cause of many ischemic stroke events and calcium is a highly prevalent structural component within carotid plaque [1]. Carotid calcifications have been analyzed so far for their prevalence, volume, or calcium score [2] but we still lack a comprehensive description and understanding of carotid calcification morphology, its change over time, and its role in cerebrovascular events.

Methods

One-hundred forty-four non-severely stenotic carotid arteries from 72 symptomatic patients were imaged using multi-detector computed tomography angiography (MDCTA) at baseline and 2-year follow-up [3]. The lumen, vessel wall, and calcifications were delineated based on Hounsfield Units (HU) (Fig. 1). A comprehensive morphometric assessment of carotid calcifications was performed, including length, shape, size, proximity to the lumen, and number of calcifications (Fig. 1). Potential associations of calcification morphometric parameters at baseline and follow-up with symptomatic and asymptomatic side, recurrent cerebrovascular events, sex and cardiovascular risk factors were investigated, using Generalized Linear Mixed Models (GLMM).

Results

The baseline data showed that the asymptomatic carotids had less calcification bodies, located closer to the lumen with larger calcification area and width compared to symptomatic side ($p<0.05$) (Fig. 1). Carotid calcifications in women were thicker, wider, larger and located closer to the lumen than those of men ($p<0.05$). At follow-up, after adjusting for baseline measurements, calcifications in asymptomatic side had still larger width and width-to-thickness ratio with shorter length ($p<0.05$) (Fig. 1). Women still had thicker, wider, larger, and longer calcifications, which were closer to the lumen ($p<0.05$).

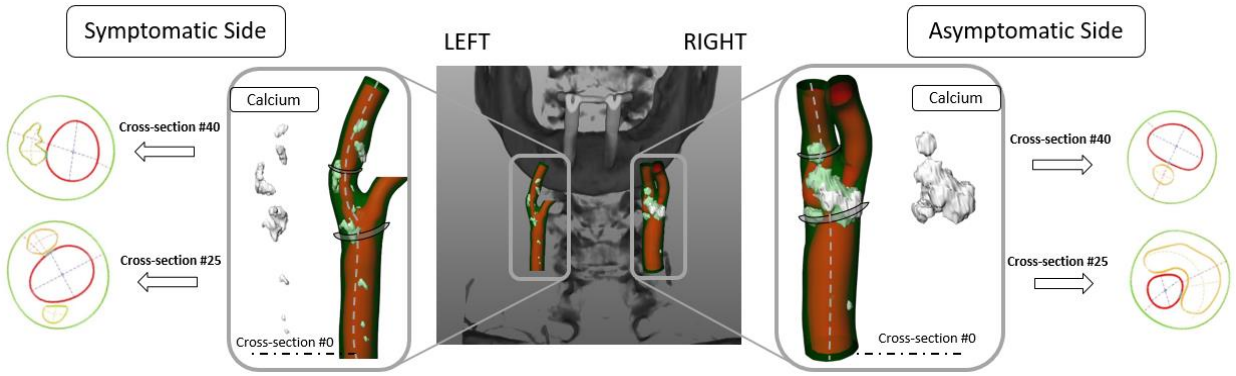

Figure 1. Pipeline of calcium morphometric analysis at baseline.

Conclusions

Our findings may suggest that measuring only calcification volume or score in carotid arteries may not be sufficient to describe the calcification morphology, its change over time, and to understand their role in acute cerebrovascular events.

References

[1] Bos, D et al., *J Am Coll Cardiol.,* 77(11):1426-1435, 2021.
[2] Van Dam-Nolen, DHK et al., *Stroke*, 53(2):370-378, 2022.
[3] Truijman, MTB et al., *Int. J. Stroke*, 9:747–54, 2014.

In vivo evaluation of the hemodynamic consequences of carotid endarterectomy by using ultrafast ultrasound-based blood flow imaging

Janna Ruisch[1,2], Suzanne Holewijn[2], Michel M.P.J. Reijnen[2,3], Chris L. de Korte[1,4] and Anne E.C.M. Saris[4]

1. *Department of Vascular Surgery, Rijnstate, Wagnerlaan 55, 6815 AD Arnhem, The Netherlands*
2. *Medical Ultrasound Imaging Center, Radboud university medical center, 6500 HB Nijmegen, The Netherlands*
3. *Multi-Modality Medical Imaging, University of Twente, 7522 NB Enschede, The Netherlands*
4. *Physics of Fluids, University of Twente, 7522 NB Enschede, The Netherlands*

Introduction

Approximately 20% of strokes originate from an atherosclerotic plaque rupture in the carotid artery. To reduce the risk of stroke recurrence, symptomatic patients can undergo surgical plaque removal, i.e. carotid endarterectomy (CEA). However, restenosis after CEA was reported to range between 5- 22%. Clinical associations are unknown, but CEA changes the carotid geometry and might induce an abnormal, atheroprone hemodynamic condition. The advent of ultrafast ultrasound makes continuous tracking of blood flow in all directions feasible. In this project, we aim to evaluate the hemodynamic consequences of CEA by using ultrafast ultrasound blood flow imaging..

Methods

Blood flow imaging of the carotid bifurcation is performed in patients that recently underwent CEA with patch repair and age-matched healthy subjects without cardiovascular diseases. We compared peak systolic velocities (PSV) and blood flow-related parameters such as time-averaged vector complexity (TA-VC), time-averaged wall shear stress (TA-WSS) and vortex duration as percentage of the cardiac cycle.

Results

Initial flow analysis is performed in twelve patients (11 males, median age 71.5 [55.0–87.0] years) and ten healthy subjects (5 males, median age 71.0 [67.0–75.0] years). PSV's in CCA in patients after surgery (44.2 [26.5–71.8] cm/s) were similar compared to healthy subjects (49.6 [25.8 – 69.7] cm/s) (p=1.00). No differences were observed in TA-VC values (0.29 [0.07–0.71] in patients versus 0.23 [0.10–0.39] (p=0.14) in healthy subjects) and TA-WSS values (0.23 [-0.06 – 0.42] in patients versus 0.24 [-0.02 – 0.66] (p=0.58) in healthy subjects). A vortex was detected in all patients, and present in 50% of healthy subjects (Figure 1). Moreover, a higher vortex duration was observed in patients (35.4 [2.3–71.2] %) compared to healthy subjects (1.1 [0.0–99.1] %) (p=0.011).

Conclusions

These preliminary results show that patients after recent CEA with patch repair have a larger vortex zone of longer duration, despite normal PSV values. A larger vortex might indicate an abnormal condition, but this was not reflected in the TA-WSS. Expanding the dataset is needed to confirm these results and provide more insight in the hemodynamic consequences of surgical carotid plaque removal and repair using a patch.

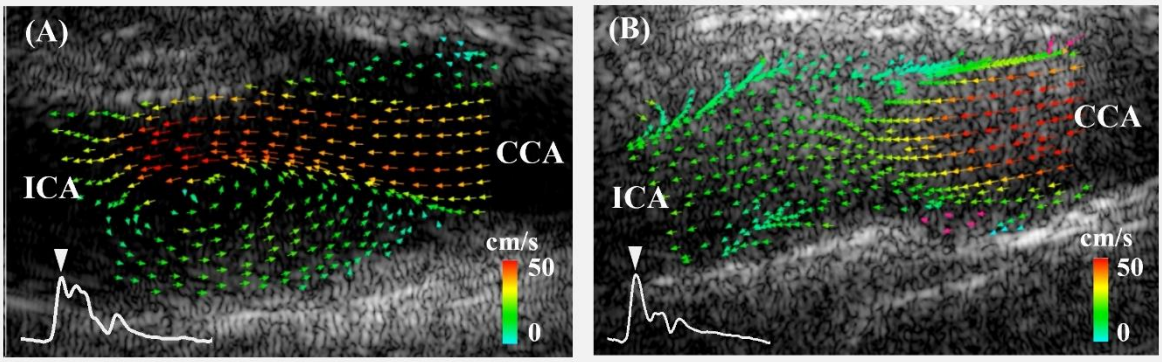

Figure 1: Vector flow Imaging of the carotid bifurcation during peak systole. Flow profile in (A) a patient (male, 63 years) after recent carotid endarterectomy with patch-repair showing a recirculation and (B) a healthy volunteer (male, 67 years).

References

-

Stiffening of the Large Arteries in Healthy Aging

Cemre Çelikbudak Orhon (1), Dionysios Adamopoulos (2), Lindsey A. Crowe (2), Miklos Kassai (2), Ibtisam Aslam (2), Jean-François Deux (2), Jean-Paul Vallée (2), Nikolaos Stergiopulos (1)

1. Ecole Polytechnique Fédérale de Lausanne (EPFL), Switzerland; 2. Hopitaux Universitaires de Genève (HUG) et Université de Genève, Switzerland

Introduction

With age, major arteries such as the aorta lose their elasticity and their capability to cushion pulsatile load decreases as a natural process [1]. However, early arterial stiffening could be a marker of cardiovascular risk factors or future cardiovascular diseases. Aortic stiffness is commonly evaluated with the carotid to femoral pulse wave velocity (c-f PWV), eventhough it does not consider the stiffness of the proximal aorta which is a main contributor to the total arterial compliances. Also, c-f PWV approximates the distance between the measurement sites with a superficially measured length without considering the patient- and age-dependent changes on the aortic geometry. Since the carotid artery is an elastic artery like the aorta and anatomically located close to the proximal aorta [2], in this study, we investigated whether the stiffening of the carotid artery could be a better surrogate of stiffening of proximal aorta in healthy aging.

Methods

The present study included 33 healthy volunteers in total, 11 people from each of the age categories of young (<35), middle-aged (35-55) and elderly (>55) without having any cardiovascular diseases or risk factors. Carotid pressure waveform and c-f PWV were recorded by using SphygmoCor. Aortic pressure waveforms derived from carotid pressure waveforms were taken from SphygmoCor. Echocardiogram (ECHO) was performed on the right common carotid artery. Extracted ECHO images are then converted to M-mode ECHO using Fiji software and the changes in the cross-sectional area of carotid artery during the cardiac cycle were tracked by using a custom-made code in Matlab. 2D gradient echo velocity-encoded PC MR was performed on the ascending aorta (AAO) and the changes in the cross-sectional area of aorta were exctracted using CVI (Circle Cardiovascular Imaging) software. The distensibility of the carotid artery and ascending aorta were calculated by linear fitting of the pressure and area changes until to their systolic peaks. Carotid PWV and AAO PWV were then calculated from Bramwell-Hill equation using the distensibilities. All statistical analysis was performed in Matlab. Correlations of different PWV methods were calculated using Pearson correlation coefficient (R). Differences in the mean PWV values of age groups were evaluated with the paired t-test and considered statistically significant for $p<0.05$ unless otherwise stated.

Results

The present study showed that both carotid PWV ($R=0.74$, $p<0.001$) and AAO PWV ($R=0.72$, $p<0.001$) has stronger correlation with the age comparing to the correlation of c-f PWV ($R=0.37$, $p<0.05$) with aging in healthy individuals. Similarly, the association between the carotid PWV and AAO PWV ($R=0.63$, $p<0.001$) was much stronger than that of c-f PWV and AAO PWV ($R=0.34$, $p=0.05$). According to the paired t-test, carotid PWV was 0.54 m/s higher than AAO PWV (95%CI [1.42 0.34]) on average for young people (<35). However, there was no statistically significant difference between carotid and AAO PWV values for the middle-aged (35-55) and elderly (>55) group.

Conclusions

This study demonstrated that the stiffness of carotid artery is a better surrogate for stiffness of the proximal aorta in healthy individuals compared to c-f PWV. Similarly, stiffening of the carotid artery can better estimate the stiffening of the proximal aorta with healthy aging and could be used to understand the underlying mechanism of large artery stiffening in healthy aging. Assessment of the carotid artery with ECHO tracking is a much simpler and cheaper method comparing to the evaluation of the aortic stiffness based on magnetic resonance imaging, therefore carotid artery stiffness offers great potential to be used as a marker of proximal aortic stiffness in healthy individuals.

References

[1] Segers P, Rietzschel ER, Chirinos JA, How to Measure Arterial Stiffness in Humans, *ATVB* 40: 1034–1043, 2020.
[2] Sung S-H, Liao J-N, Yu W-C, Cheng H-M, Chen C-H, Common Carotid Artery Stiffness Is Associated with Left Ventricular Structure and Function and Predicts First Hospitalization for Acute Heart Failure, *Pulse* 2: 18–28, 2014.

Lipid-Rich Plaque Progression in Human Coronary Arteries can be Predicted Combining Multimodal Imaging and Computational Hemodynamics

Giuseppe De Nisco[1], Eline M. Hartman[2], Elena Torta[1], Diego Gallo[1], Claudio Chiastra[1], Joost Daemen[2], Umberto Morbiducci[1], Jolanda J. Wentzel[2]

[1]PolitoBIOMed Lab, Department of Mechanical and Aerospace Engineering, Politecnico di Torino, Turin, Italy
[2]Department of Biomedical Engineering, Erasmus MC, Rotterdam, The Netherlands

Introduction

Plaque composition and wall shear stress (WSS) magnitude act as well-established players in coronary plaque progression [1]. However, relying solely on WSS magnitude is insufficient to fully describe the biomechanical stimuli affecting atherosclerosis evolution, as endothelial cells experience also changes in the spatiotemporal configuration of WSS on the luminal surface. This study explores WSS profile and lipid content signatures of plaque progression to identify biomarkers of coronary atherosclerosis in a human follow-up study.

Methods

Thirty-eight non-culprit human coronary segments were imaged by coronary computed tomography angiography (CCTA), intravascular ultrasound (IVUS), near-infrared spectroscopy (NIRS), and optical coherence tomography (OCT) at time point T1 and at 1 year follow-up (T2). Baseline coronary artery geometries were reconstructed from IVUS and CCTA, and were combined with patient-specific flow information to perform CFD simulations assessing the time-average WSS magnitude (TAWSS) and the variability in the WSS contraction/expansion action on the endothelium along the cardiac cycle, quantified in terms of topological shear variation index (TSVI) [2,3]. Plaque progression was measured as IVUS-derived plaque atheroma volume change (ΔPAV) between T2-T1. Plaque composition was classified as lipid rich, fibrous or plaque free (PFW) based on NIRS and OCT images.

Results

An explanatory case of luminal distribution of TAWSS, TSVI and ΔPAV is presented in Figure 1A. Overall, the luminal exposure to high TSVI at T1 was associated with significantly higher ΔPAV in the T2-T1 time interval (4.00±0.69%) than sectors exposed to low or mid TSVI at T1 (Figure 1B). A clear trend emerged also for the exposure to low TAWSS at T1 and high ΔPAV (3.60±0.62%). Plaque phenotype acted synergistically with TAWSS or TSVI regarding plaque progression: at low TAWSS or high TSVI sectors in combination with lipid rich plaque, ΔPAV values were significantly higher than when considering the individual contribution of hemodynamics (≥5.90%, p<0.01; Figure 1C).

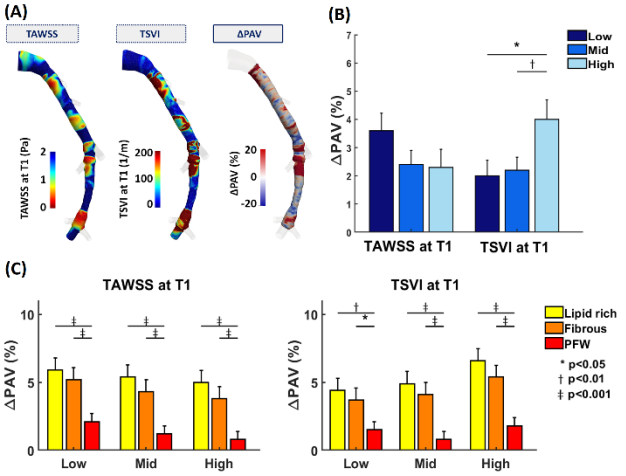

Figure 1: (A) TAWSS, TSVI and ΔPAV maps; (B) TAWSS and TSVI vs. estimated ΔPAV: (B) solely; (C) in combination with plaque phenotypes.

Conclusions

Luminal exposure to high TSVI, solely or combined with a lipid rich plaque phenotype, is associated with enhanced plaque progression at 1-year follow-up. Where plaque progression occurred, low TAWSS was also observed. These findings indicate TSVI, in addition to low TAWSS, as a potential biomechanical predictor for plaque progression, offering promise for clinical translation to enhance patient prognosis.

References

[1] Hartman EMJ et al., Wall shear stress–related plaque growth of lipid-rich plaques in human coronary arteries: an near-infrared spectroscopy and optical coherence tomography study. Cardiovasc Res,119: cvac178, 2022.
[2] Candreva A et al., Risk of myocardial infarction based on endothelial shear stress analysis using coronary angiography, Atherosclerosis, 342:28-35, 2022.
[3] Mazzi V et al., Early Atherosclerotic Changes in Coronary Arteries are Associated with Endothelium Shear Stress Contraction/Expansion Variability. Ann Biomed Eng, 49:2606-2621, 2021.

Fluid-structure interaction simulations for the investigation of coronary artery disease

Vittorio Lissoni, Marco Stefanati, Francesco Migliavacca,
Gabriele Dubini, Jose F Rodriguez Matas, Giulia Luraghi

Department Chemistry, Materials and Chemical Engineering “Giulio Natta”, Politecnico di Milano, Italy

Introduction

Computational simulations have emerged as a valuable tool to investigate coronary artery disease (CAD). Structural and computational fluid-dynamic (CFD) simulations have been used to investigate, respectively, the risk of plaque rupture, through plaque structural stress and arterial shear stress [1] and the risk of infarction, through the calculation of fractional flow reserve (FFR), a non-invasive index [2]. Only a few studies in the literature investigated pathological conditions through fluid-structure (FSI) interaction models. This work describes a methodology to assess CAD by calculating patient-specific coronaries blood flow with FSI simulations including arterial pre-stress.

Methods

Coronary models accounting for the main epicardial branches and plaque elements were segmented using Medis (Medis Medical Imaging Systems B.V., NL) from patient-specific images and then meshed using ANSA (BETA CAE Systems, Greece). To account for the arterial pre-stress, the zero-pressure configuration [3] was loaded up to diastolic condition in the first simulated cardiac cycle. Simulations were implemented with an ALE, strong and two-way coupling method using the commercial finite element solver LS-DYNA 971 Release 14.0. Physiological aortic pressure curve was prescribed at the inlet of each coronary, while a five-elements lumped parameter model retrieved from the literature [4] was used to simulate the distal microvasculature behaviour.

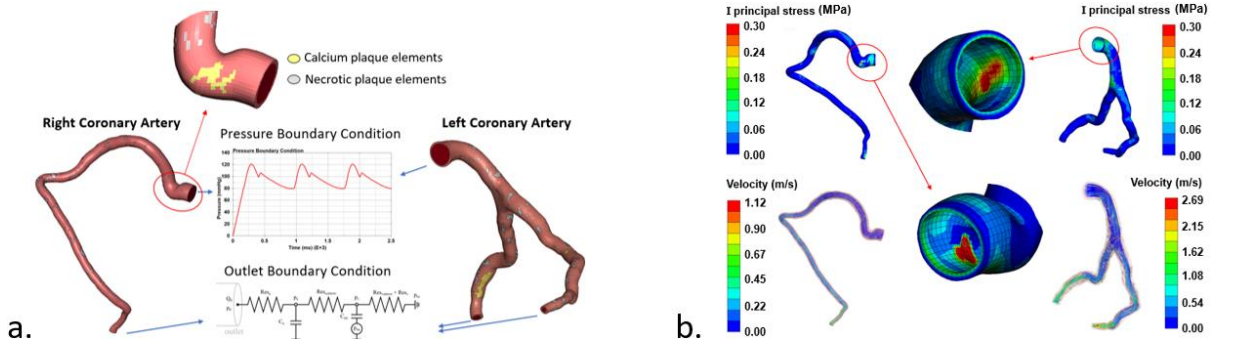

Figure 3. a) Examples of the right and left coronary artery meshes and the boundary conditions applied with detail of the mesh. b) First principal stress and blood velocity during systole in two right and left coronaries investigated.

Results

The resulting pressure/flow rate curves were compared against the theoretical ones retrieved from the literature (maximum flow error in the peak flow instant of 4.2%) [5]. Our initial results indicate accurate quantification of both structural and fluid dynamic results. The highest stress values were found in the calcium plaque elements with peak I principal stress of 0.9 MPa in systole for the first left coronary vessel investigated. Shear stress values on the coronaric lumen are consistent with the ones found in a similar work [1] with an average value of 3.0 Pa (results not shown).

Conclusions

This methodology quantifies blood flow in patient-specific diseased coronary vessels. Comparing results with standalone CFD or structural simulation suggests FSI implementation for accurate CAD risk assessment. Further investigation is needed.

References

1. Fandaros, M. et al. Med Biol Eng Comput, vol. 61, no. 6, pp. 1533–1548, Jun. 2023
2. Taylor, C. A., et al. Journal of the American College of Cardiology vol. 61 2233–2241 (2013).
3. Ramella, A. et al., Biomech Model Mechanobiol, (2023).
4. Sankaran, S. et al. Ann Biomed Eng 40, 2228–2242 (2012).
5. Calcaterra, D. et al. Aorta (Stamford). 5(1):1-10 (2017)

Biomechanical exploRation of Ischemic Stroke risK amoNg athEroSclerotic carotidS - a BRISKNESS pilot study

Brian BP Berghout[a,b], Suze-Anne Korteland[c], Daniel Bos[a,d], Jolanda J Wentzel[c], M. Kamran Ikram[a,b]

[a]Department of Epidemiology
[b]Department of Neurology
[c]Department of Biomedical Engineering
[d]Department of Radiology & Nuclear Medicine, Erasmus MC, Rotterdam, The Netherlands

Introduction

Arterial wall shear stress (AWSS) is implicated in the pathophysiology of coronary atherosclerotic plaques[1], significantly contributing to an increased risk of acute cardiovascular disease. However, its role in stroke is relatively unexplored. Large population-based studies allow for the exploration of factors associated with the longitudinal risk of diseases such as stroke, but no population-based effort has systematically assessed AWSS in the association with the risk of stroke, perhaps due to the computational resource demanding nature of estimating AWSS using computational fluid dynamics. In this pilot study, we investigated carotid AWSS profiles from fifteen elderly participants from a population-based cohort study who developed ischemic stroke during follow-up, to determine the feasibility of assessing carotid AWSS profiles on a population-wide scale.

Methods

Between 2007 and 2012, 1740 participants from the Rotterdam Study[2], a long-running population-based observational cohort study, underwent 1.5T MRI imaging of the carotid bifurcation based on the presence of carotid atherosclerosis on ultrasounds. These participants were subsequently followed-up over time for the development of ischemic stroke until January 1, 2020. The MRI black-blood sequences were used for generating AI-based lumen segmentations of common and internal carotid arteries[3], and these were used to create 3D reconstructions of the carotid bifurcations. Common carotid bloodflow was estimated based on MRI phase-contrast sequences, and applied as input for steady-state blood velocity simulations to obtain the local AWSS profiles in the carotid arteries. AWSS parameters from culprit arteries that would lead to the stroke were compared with contralateral non-symptomatic sides using paired t-tests. Fifteen patients (aged 70.2 (IQR 63.5-80.9) years, 53.3% female) with comparable common and internal carotid artery lengths on MRI field of view were selected.

Results

A total of 121 (7.0%) participants developed a first-ever ischemic stroke during follow-up. The time between imaging and stroke diagnosis was 4.1 (IQR 1.8-8.1) years. Inter-rater agreement for the assessment of bloodflow velocity produced an intraclass correlation coefficient of 0.89 [0.61-0.97]. Average bloodflow was 4.0 (IQR 3.4-4.8) ml/s, and was similar among culprit (4.1, IQR 3.5-5.2) and contralateral carotids (3.7, IQR 3.0-4.7, P=0.07). Minimal lumen area (MLA) measured across the arteries was a median 12.0 (IQR 9.1-14.5) mm², and was similar between culprit and contralateral carotids (P=0.07). The AWSS gradient at MLA was 4.3 (IQR 1.8-6.0) Pa, and was similar between culprit and contralateral carotids, see figure 1.

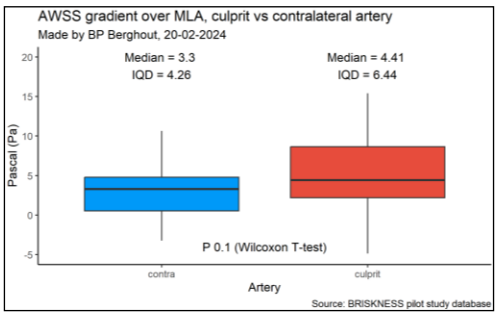

Conclusions

We developed a method of assessing carotid AWSS profiles tailored for application in a large population-based study, which shows great potential in unraveling the role of AWSS in the development of ischemic stroke. Initial results from this pilot study illustrate how the AWSS gradient over the MLA of the carotid arteries could be associated with the risk of future ischemic stroke.

References

1: Bourantas, CV, et al. (2020). JACC. Cardiovascular imaging, 13(10), 2206–2219.
2: Ikram, MA, et al. (2024). The Rotterdam Study. Design update and major findings between 2020 and 2024, European journal of epidemiology. Advance online publication.
3: Isensee, F., et al. (2021). nnU-Net: a self-configuring method for deep learning-based biomedical image segmentation. Nature methods, 18(2), 203-211.

In-Silico Modeling of Atherosclerosis: An Agent-Based Modeling Approach

Caballero R, Martínez M.Á. and Peña E.

Aragón Institute of Engineering Research (I3A). University of Zaragoza, Spain

Introduction

Atherosclerosis, a primary factor in cardiovascular diseases[1], is a major challenge in biomedical research. In this study, we present an in-silico model that combines a hybrid approach of continuous convection-diffusion-reaction model and agent-based model to predict atheroma plaque growth in coronary arteries.

Methods

Our hybrid model has three coupled modules: computational fluid dynamics (CFD), mass transport, and agent-based modeling (ABM). The CFD module starts from a 3D coronary artery geometry, in which hemodynamics are calculated using the Navier-Stokes equations. Then, several 2D cross-sectional surfaces are selected in the zone of least wall shear stress (WSS) of the 3D model, and the plasma filtration process is reproduced using Darcy's Law. The mass transport module models the transport of substances using the convection-diffusion-reaction equations. Low-density lipoprotein (LDL) leakage through the endothelium is evaluated using the three-pore model[2], which considers three pore sizes: small, normal, and large.

The ABM module imports both the 2D geometry and the WSS and LDL concentration values from the CFD and mass transport modules. This module is responsible for predicting arterial wall remodeling using conditional and stochastic behavioral rules, which calculate the probability of occurrence for each cellular process. The cellular processes included: mitosis and apoptosis of cells; production and degradation of extracellular matrix; production, phagocytosis, and necrosis of macrophages, becoming foam cells (FCs) due to excess LDL in the wall; and the change of phenotype of smooth muscle cells (SMCs) from contractile to synthetic.

To couple both models, a segmentation process is performed on the ABM output image, identifying the different layers that form the arterial wall. Then, with this information, the 3D geometry is reconstructed, and the process is repeated.

Conclusions

Our agent-based model (ABM) demonstrates promising capabilities in predicting the growth of atheroma plaques, particularly in areas with lower wall shear stress (WSS). It is important to note that these findings are preliminary and require further validation. This work represents an early exploration of the complex dynamics involved in cardiovascular disease progression.

References

[1] Roth G. et al., The Lancet, 392 (10159): 1736 – 1788, 2018
[2] C. C.; CURRY, F. E. Microvascular permeability. Physiological Reviews, 1999

Machine Learning-Based Estimation of Wall Shear Stress using Small Data

Julian Suk[1], Eline M.J. Hartman[2], Suze-Anne Korteland[2], Jolanda J. Wentzel[2], Jelmer M. Wolterink[1]

[1]Mathematics of Imaging & AI, University of Twente, Enschede, The Netherlands
[2]Department of Biomedical Engineering, Erasmus MC, Rotterdam, The Netherlands

Introduction

Wall shear stress (WSS) is related to plaque progression and arterial remodelling. WSS estimation is performed in-silico, using computational fluid dynamics (CFD). CFD can be time-intensive and might be too slow for some practical applications, rendering machine learning (ML) an interesting alternative. In prior work, we have generated a large set (2,000 samples) of synthetic single coronary arteries and bifurcations, performed CFD in the arteries, and used this data for training and validation of an ML model for WSS estimation [1]. Real arteries are complex and contain branching points, stenoses, and pathology. Clinical application of our method should be able to handle such variation, but extending our model to such data sets poses challenges: data is limited and samples significantly vary. In this study, we establish an ML baseline for the estimation of WSS in anatomically plausible 3D coronary artery shapes.

Methods

Data of 49 arteries scanned and reconstructed to 3D models (each ~100,000 vertices) in the IMPACT study [2] were included. Previously obtained WSS using CFD was used as a reference. The data set contained variation in anatomical location (18 LAD, 13 LCX, and 18 RCA). Moreover, for each reference CFD simulation, personalized boundary conditions were included. We trained a Transformer model with a PointNet++-based tokenizer using geometric input features, vertex normals and geodesic distances to the inlet and outlet. The model estimated time-averaged WSS vectors.

Results

Preprocessing failed in three cases. In the remaining 46 cases we performed a direct quantitative analysis using normalized mean absolute error (NMAE) and 23-fold cross validation. The Figure shows results on two arteries in the test set. Cross-fold average NMAE was 3.6 % (compared to 0.6 % on the synthetic single and 1.2 % on the synthetic bifurcating arteries in [1]) and cross-fold standard deviation was 1.1 %, suggesting decent approximation. We observed larger errors (right) when arteries had a unique shape that stood out from the rest of the dataset, indicating limited generalization to complex cases.

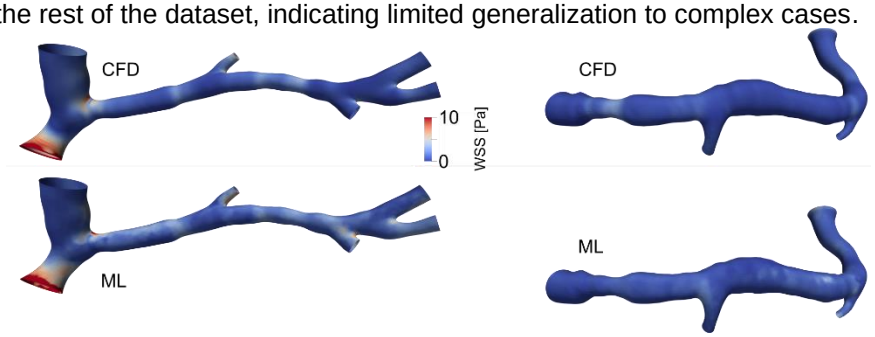

Conclusions

Results indicate that training and validation of an ML model solely on a limited-size real-world data with high variability is feasible. However, we were not able to reach similar performance as on our large, idealized, synthetic data set. We hypothesize that in future work, incorporating additional anatomical priors and physics constraints is likely to improve generalization, in addition to the collection of larger data sets, if possible.

References

[1] Suk, J., Haan, P. D., Lippe, P., Brune, C., & Wolterink, J. M. (2021, September). Mesh convolutional neural networks for wall shear stress estimation in 3D artery models. In International Workshop on Statistical Atlases and Computational Models of the Heart (pp. 93-102). Cham: Springer International Publishing.

[2] De Nisco G, Chiastra C, Hartman EMJ, Hoogendoorn A, Daemen J, Calò K, Gallo D, Morbiducci U, Wentzel JJ. Comparison of Swine and Human Computational Hemodynamics Models for the Study of Coronary Atherosclerosis. Front Bioeng Biotechnol. 2021 Aug

Mechanical stress in coronary atherosclerotic plaques: Comparison of 2D vs. 3D computational strategies

Sara Zambon[1], Aikaterini Tziotziou[2], Eline MJ Hartman[2], Claudio Chiastra[1], Umberto Morbiducci[1], Jolanda J Wentzel[2], Diego Gallo[1]

1. PolitoBIOMed Lab, Department of Mechanical and Aerospace Engineering, Politecnico di Torino, Turin, Italy
2. Department of Biomedical Engineering, Erasmus MC, Rotterdam, The Netherlands

Introduction

Biomechanical factors are suspected to play a crucial role in the initiation and progression of coronary atherosclerotic plaques. Recent evidences suggest that high mechanical wall stress (MWS) is associated with wall thickness progression in plaque-free regions of coronary wall and reduction in lipid-rich necrotic core (LRNC) size in plaque regions [1]. Furthermore, it is reported that high MWS hot spot values may act as potential trigger for plaque rupture [2]. Most of the emerged evidences rely on finite-element (FE)-based 2D structure-only computational analyses, an approach that may simplify the 3D nature of the atherosclerotic arterial structure. Expanding the current approach, here we analyze the effect of 2D vs. 3D FE-based modelling of mechanical stress in atherosclerotic coronary vessels using patient-specific imaging data.

Methods

Acute coronary syndrome patients, enrolled at the Erasmus MC (Rotterdam, NL), underwent invasive pressure measurement, computed tomography angiography (CTA), optical coherence tomography (OCT) and intravascular ultrasound (IVUS) imaging of a non-culprit coronary artery [1]. Coronary 2D cross-sections were obtained by combining co-registered IVUS and OCT frames. Lumen and external elastic lamina were segmented from IVUS images. The adventitia was assumed to have constant thickness [1]. The LRNC inner edge was segmented on OCT images, while the outer edge was reconstructed adopting a previously validated approach [4]. The arterial 3D geometry was reconstructed combining IVUS lumen segmented contours and the vessel centerline extracted from CTA images. FE-based structural simulations were carried out in Abaqus/Standard (Dassault Systemes), assuming intima and media, adventitia, and LRNC components as nonlinear hyperelastic materials [1]. The backward incremental method [3] was applied to calculate the initial diastolic stress distribution and the patient-specific systolic blood pressure was prescribed. The 2D vs. 3D comparison was carried out in terms of von Mises stress distribution.

Results

When considering three plaque-free cross-sections and one cross-section containing a LRNC, (Fig. 1), comparable MWS contours are obtained in 2D vs. 3D simulations (data not shown). The 2D simulations overestimated the maximum MWS values for all four cross-sections, compared with 3D simulations, with percentage differences in the range 15%–47% (Table, Fig. 1). The location of the maximum MWS differs in two out of the four considered cross-sections (sections A and B in Fig. 1). Focusing on the cross-section containing a LRNC (Fig. 1), differences in maximum MWS emerge in the cap region.

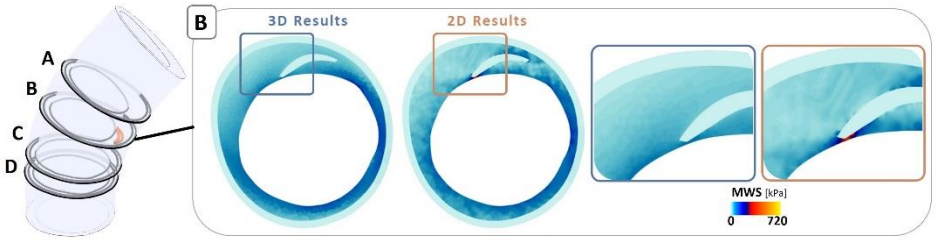

Maximum luminal MWS [kPa]

Slice	2D	3D	Δ_{2D-3D}
A	195.5	129.7	33.7%
B	333.4	176.3	47.1%
C	313.9	192.1	38.8%
D	357.3	303.6	15.0%

Figure 4 – 3D representation of the investigated coronary artery model. MWS contours are shown for cross-section B containing a LRNC. Maximum luminal MWS values and 2D vs. 3D differences (Δ_{2D-3D}) are reported in the table.

Conclusions

The biomechanical assessment of the MWS in coronary plaques based on 2D vs. 3D structure-only FE simulations highlighted that the 2D strategy could overestimate maximum MWS at the cap, but they may still capture the maximum MWS location, warranting further investigation. Future advancements will include the implementation of fluid-structure interaction to consider the synergistic action between MWS and hemodynamic stresses on disease initiation and evolution.

References

[1] Tziotziou A, et al., *Atherosclerosis*, 387:117387, 2023. [2] Pedrigi R, et al., *Arterioscler Thromb Vasc Biol*, 34(10):2224-31, 2014. [3] Akyildiz A, et al., *Comput Methods Biomech Biomed Engin*, 19(7):771-9, 2016. [4] Kok A, et al., *Biomed Eng Online*, 15(1):48, 2016.

In-silico modelling of cerebral vasculopathy among pediatric patients with sickle cell disease

Weiqiang Liu[1], Lazaros Papamanolis[2], Christian Kassasseya[3], Kim-Anh Nguyen-Peyre[4,5], Morgane Garreau[6], Nour Bekeziz[4], Corentin Provost[7], Jean-Frédéric Gerbeau[8], Suzanne Verlhac[9], Pablo Bartolucci[3,4], Irene Vignon-Clementel[6]

[1]McGill University, Canada; [2]Stanford University, USA; [3]Hôpital Henri Mondor, Créteil, France; [4]IMRB, Créteil, France; [5]EFS, Créteil, France; [6]INRIA, Saclay, France; [7]Centre Hospitalier Saint-Anne, Paris, France; [8]INRIA, Rocquencourt, France; [9]Hôpital Robert Debré, Paris, France

Introduction

Sickle cell disease (SCD) is an inherited blood disorder associated with severe complications such as cerebral vasculopathy. It can result in strokes due to stenosis or occlusion, most frequently observed in young patients aged 2 to 5 years (yrs). Transcranial Doppler imaging has been demonstrated as an efficient method to screen the patients at high risk of stroke, in particular if they present a time-averaged maximum velocity (TAMV) exceeding 200 cm/s [1]. In this work, hemodynamic metrics obtained from blood flow simulations are investigated to understand the development of arterial lumen narrowing.

Methods

MRA images of the internal carotid arteries (ICA) with cerebral branches are obtained for 15 patients: 5 of them are under 5 yrs, 5 are between 5 and 18 yrs and 5 are adults. After segmentation of the geometries, 3D hemodynamics simulations are conducted for a pulsatile inflow with mean flow rate 10 mL/s.

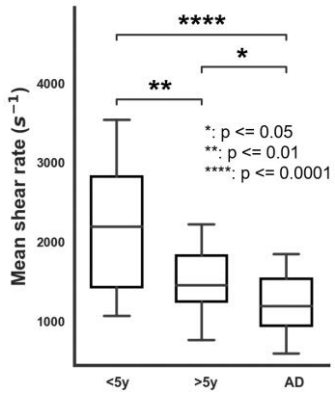

Figure 5. Mean shear rate.
<5y: patients under 5, >5y: patients between 5 and 18, AD: adults

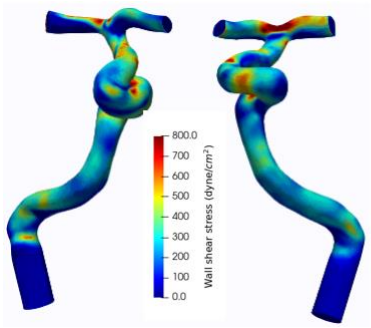

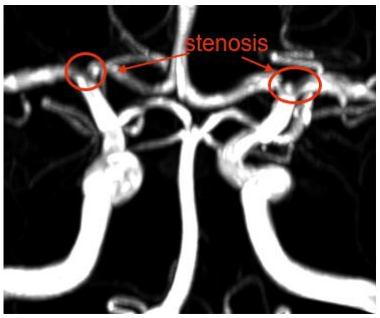

Figure 2. Left: WSS distribution at age X**.**
Right: MRA at age X+7 years.

Results

A significantly higher mean shear rate is found in patients under 5 yrs as illustrated in Figure 1. Moreover, children under 5 yrs present a wider area (in %) of high mean wall shear stress (mean WSS > 400 dyne/cm^2) than the other groups. The regions of high WSS are mostly located in the carotid siphon and branch intersections. The longitudinal study case presented in Figure 2 shows the WSS distribution in healthy state (left) and the stenosis formation at the same position after 7 years (right).

Conclusions

Our results demonstrate that high and alternating shear stress might be linked with development of stenosis in SCD. Younger patients present higher shear rate compared to older patients under the same boundary conditions, which indicate that the arterial geometrical complexity in different age groups are at play in the development of vasculopathy, even though additional experimental validation is needed.

References

[1] Adams R, McKie V, Nichols F, et al. The use of transcranial ultrasonography to predict stroke in sickle cell disease. N Engl J Med 1992;326:605–610.

Complex Aortic Arch Repair: a Fluid-Structure Interaction analysis

Sampad Sengupta[1], Xiao Yun Xu[2]

[1]Department of Fluids & Environment, University of Manchester, Manchester, UK

[2]Department of Chemical Engineering, Imperial College London, London, UK

Introduction

Thoracic endovascular aortic repair (TEVAR) provides a minimally invasive option for aortic arch and thoracic aortic surgery, whilst potentially improving the outcome compared to conventional methods. Endografts used in TEVAR are designed to mimic a patient's anatomy as closely as possible and like most implanted devices, they present with their own set of complications that can arise due to improper fixation of the device or due to pathological developments affecting the efficacy of the device. Complications in the delivery process can cause inaccurate deployment or damage to the vessel wall, whilst the pulsating nature of the aorta can also impact the stability of endografts and lead to malalignment or migration. Haemodynamic and biomechanical indices such as wall shear stress (WSS) and von Mises wall stresses are important for evaluating the local response to TEVAR in the arch. A Fluid-Structure Interaction (FSI) investigation has been conducted to incorporate the effects of wall motion alongside pulsatile flow through the lumen and investigate their effects on one another.

Methods

A post-TEVAR scenario was modelled where the patient was treated for an aortic arch aneurysm using a single-branched NEXUS^{TM} endograft. Retrospective CT images were used to faithfully reconstruct the patient geometry. Fluid and solid mechanics simulations were carried out with the configuration shown in Figure 1, with a strong two-way coupling method implemented to ensure reliable convergence of the fluid and solid field solutions and to capture the reciprocal nature of the two domains for the FSI analysis.

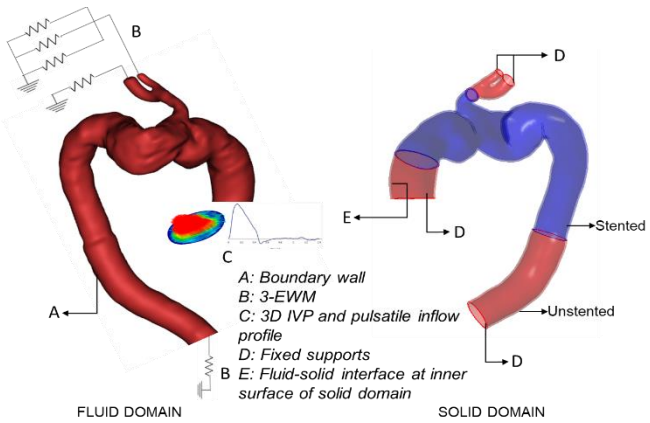

Figure 1: An overview of the boundary conditions prescribed for the fluid domain (left) and solid domain (right).

Results

The FSI simulation was able to predict flow and wall mechanics in detail, allowing quantification of the effect of wall motion on the haemodynamics and the effect of pulsatile flow on wall deformation. It should be noted that whilst the overall flow patterns did not change much, accounting for wall compliance resulted in altered predictions of WSS metrics within the pulsating aorta. For the case investigated here, the most significant difference between the FSI and rigid wall CFD simulation results was over-prediction of peak flow velocities, which in turn influenced the WSS prediction in both models.

Conclusions

TEVAR in the aortic arch remains a difficult procedure, primarily due to the geometric complexity of the region in question. The findings of this study strengthen the need to incorporate a combination of structural and fluid dynamics whilst analysing a vascular response to TEVAR. This investigation quantified the effect of wall deformation on pulsatile flow patterns and vice versa. FSI provides more physiologically relevant results but should be utilised based on the requirements of the study due to the greater degree of complexity in preprocessing and increased computational time.

Altercations of aortic hemodynamics during aortic valve stenosis leading to subclinical hemolysis: A subject-specific analysis using 4D Flow MRI-based CFD techniques

Tianai Wang[1], Christine Quast[2], Florian Bönner[2], Malte Kelm[2,3], Teresa Lemainque[4], Ulrich Steinseifer[1], Michael Neidlin[1]

(1) Department of Cardiovascular Engineering, Institute of Applied Medical Engineering, Medical Faculty, RWTH Aachen University, Aachen, Germany, (2) Department of Cardiology, Pulmonary Diseases and Vascular Medicine, Heinrich-Heine University, Düsseldorf, Germany, (3) CARID, Cardiovascular Research Institute Düsseldorf, Heinrich-Heine University, Düsseldorf, Germany, (4) Department of Diagnostic and Interventional Radiology, University Hospital RWTH Aachen, Germany

Introduction

Subclinical hemolysis, i.e. subclinical release of free hemoglobin from a small fraction of red blood cells (RBC), was recently discovered in patients with aortic valve stenosis (AS). Abnormal hemodynamics are hypothesized to be the cause for this membrane damage. However, an in-depth analysis of these pathological flow structures and their impact on RBCs in comparison to healthy blood flow is missing. In this study, we aimed to elucidate the hemodynamic changes induced by aortic valve stenosis through 4D Flow MRI and CFD for a selection of healthy subjects (H) and patients suffering from severe AS.

Methods

Computational models of subject-specific aortic geometries were created using in-vivo medical imaging data. Temporally and spatially resolved boundary conditions taken from 4D Flow MRI measurements were implemented. After validation of the in-silico results with in-vivo data, the resulting aortic flow fields were investigated regarding their hemodynamic characteristics, in particular shear stresses and helicity. These insights were used to determine the potential cause of flow-induced subclinical hemolysis in AS.

Results

The accuracy of the 4D Flow MRI-based CFD model was proven with excellent agreement between two velocity fields and an R2 of 0.9 ($p<0.001$). Figure 1 shows the numerically derived total shear stress (TSS) evolution and distribution of an AS patient for a cross-sectional plane in the ascending aorta (AAo). A pathological high TSS region in the bulk flow is visible during late systole with an increase by 125 % compared to the maximum value for the healthy individual.

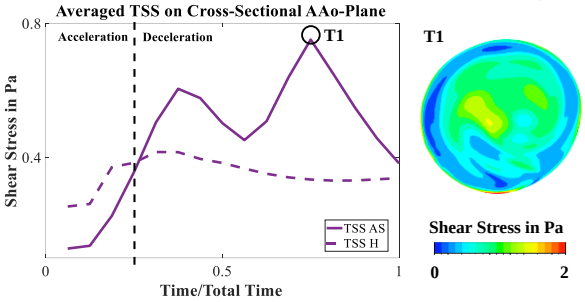

Fig.1 *Left: TSS for AS and H case on cross-sectional plane in AAo. Right: Cross-sectional total shear stress contour at T1.*

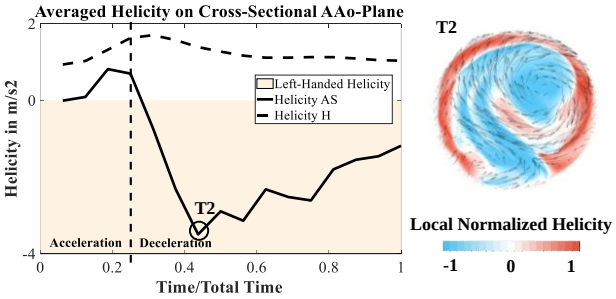

Fig.2 *Left: Helicity for AS and H case on cross-sectional plane in AAo. Right: Cross-sectional local normalized helicity contour at T2.*

Physiological aortic flow form a Dean-like, bihelical pattern with predominantly right-handed helices at late systole. However, the AS flow in our study displays a dominant left-handed helical structure (see Figure 2), accompanied by elevated turbulent kinetic energy in areas of accumulated left-handed helicity.

Conclusions

In conclusion, the validated, subject-specific 4D Flow MRI-based CFD models of healthy and AS patients have shown that altered turbulent and helical structures in the bulk region of the flow may be the cause for increased damaging forces acting upon the RBCs, leading to the subclinical membrane damage in AS patients. Differences in TSS and helicity between AS and H were observed. Future work will investigate the capabilities of aortic valve replacements to shift pathological flow profiles towards physiological ones, improving long-term outcomes of patients undergoing such procedures.

In Vitro Model Mimicking Early-Stage Tissue Formation in *in situ* Tissue-Engineered Vascular Access Grafts

Mattia Manenti[a,b], A.I.P.M. Smits[a,b], N.A. Kurniawan[a,b], C.V.C. Bouten[a,b]

[a] Department of Biomedical Engineering, Eindhoven University of Technology, Eindhoven, The Netherlands
[b] Institute for Complex Molecular Systems, Eindhoven University of Technology, Eindhoven, The Netherlands

Introduction

Chronic kidney disease (CKD) significantly reduces life quality, forcing CKD patients to undergo hemodialysis therapy for blood detoxification. This requires long-term access to the patient's vasculature using vascular access grafts. *In situ* tissue-engineered vascular access grafts (TEVAGs) may offer durable, living graft alternatives that can be designed to circumvent current grafts' high failure rates due to stenosis and neointima hyperplasia (NIH). Our research concentrates on understanding NIH in *in situ* TEVAGs for subsequent graft scaffold optimization. NIH, particularly at the vein-anastomotic site, involves the hyperproliferation and migration of (myo)fibroblast and vascular smooth muscle cells (VSMCs), leading to abnormal thickening of the tunica intima and potential occlusion of the graft. Recent evidence underscores the critical role of the interaction between recruited cells and the graft's hemodynamic environment. When exposed to a non-physiological flow environment, endothelial cells (ECs) can trigger VSMCs migration and proliferation, potentially increasing the risk of NIH development[1]. Here, we aimed to (i) set up an *in vitro* model of *in situ* small-diameter vascular graft remodelling, to (ii) understand the role of endothelium in the early stages of cell responses, tissue formation, and NIH.

Methods

A small-diameter polycarbonate bis-urea (PC-BU) tubular scaffold was produced via electrospinning and morphologically characterized using scanning electron microscopy. Scaffolds were seeded with human THP-1 monocytes (~$3.5x10^6$ cells/scaffold) with and without an intima layer of primary human umbilical vein endothelial cells (~$2.3x10^6$ cells/scaffold) embedded in a fibrin-gel environment. Constructs were cultured statically for 7 days and then dynamically for 72h, while subjected to different hemodynamic conditions, mimicking *in vivo* flow conditions present at the vein-graft anastomosis[2]: low shear stress (~0.1 Pa), high shear stress (~3 Pa) and high, oscillatory shear stress (~3 Pa, 1 Hz). Flow experiments were carried out with a vascular bioreactor[3] connected to an IBIDI perfusion system. Samples were collected and analysed via *en-face* immunofluorescence (IF) to assess the surface coverage percentage of the lumen and via immunohistochemistry (IHC) and histology (H&E) to check the cell penetration.

Results

All the scaffolds were electrospun on a 3 mm mandrel, with a wall thickness in the range of 250-300 µm and with randomly oriented fibers with an average diameter of 4 µm. The first pilot experiment was carried out to demonstrate both the robustness of the flow system and the effectiveness of the *in vitro* model, comparing low-shear stress conditions to no-flow conditions. Throughout the flow perfusion, no leakages and no pressure drops occurred; moreover, at the end of the dynamic stimulation, all the cell-seeded constructs were intact with no signs of contamination and cell detachment. All the flow-stimulated grafts showed a (near-)confluent endothelium layer on the luminal side, comparable with the no-flow condition, and a homogeneous monocyte penetration throughout the wall thickness.

Conclusions

An *in vitro* model mimicking the early stages of *in situ* tissue-engineered vascular access graft remodelling has been established and characterized. Current studies focus on unraveling the role of ECs in neo-tissue formation, including potential neointimal hyperplasia.

Acknowledgments

This study is financially supported by the Gravitation Program "Materials Driven Regeneration," funded by the Netherlands Organization for Scientific Research, grant # 024.003.013

References

[1]. Newby, A. C. & Zaltsman, A. B. J. Pathol. 2000.
[2]. Quicken, S. et al. Int. J. Numer. Methods Biomed. 2021.
[3]. Pennings, I. et al. Biofabrication. 2019.

The left ventricular strain-volume loop in a healthy Dutch population: age- and sex related differences

Robert R Zwaan[1], Zoë A Keuning[1], Thijs P Kerstens[2], Daniel J Bowen[1], Alexander Hirsch[1,3], Hendrik J Vos[1], Arie PJ van Dijk[4], Dick H. J. Thijssen[4], Jolien W Roos-Hesselink[1] and Annemien E van den Bosch[1]

[1] Erasmus MC, Cardiovascular Institute, Thorax Center, Department of Cardiology
[2] Department of Physiology, Radboud University Medical Center, Nijmegen, Netherlands
[3] Department of Radiology and Nuclear Medicine, Erasmus University Medical Center, Rotterdam, the Netherlands
[4] Department of Cardiology, Radboud University Medical Center, Nijmegen, the Netherlands

Introduction

By combining left ventricular (LV) global longitudinal strain (GLS) with LV volume during the cardiac cycle, LV strain-volume loops can be generated. LV SV-loop derived parameters provide new insights into the interaction between cardiac contraction and volume in a variety of cardiac diseases (1,2) and may even have prognostic value. (3,4) Reference values for healthy individuals with attention to sex- and age-related differences have not been established yet. Therefore, the aim of this study is to provide reference ranges in a healthy adult population and investigate potential sex- and age-related differences of LV SV-loop characteristics.

Methods

In 125 healthy volunteers aged 18-72 years, apical 2-, 3- and 4-chamber views were acquired to measure GLS. Custom software was used to combine strain and volume data to construct SV-loops. Different parameters were derived: (i)linear slope of systolic strain-volume relation (S-Slope); (ii) early linear slope of systolic strain-volume relation (ES-Slope); (iii) early linear slope of diastolic strain-volume relation (ED-Slope); and (iv) uncoupling between systolic and diastolic strain-volume relation (UNCOUP).

Results

For the systolic strain-volume relation higher values were observed in females as compared with males with S-Slope values of 0.19 [0.17-0.22] %/mL m^{-2} and 0.13 [0.11-0.15] %/mL m^{-2} respectively. ED-Slope was higher in females as compared with males with values of 0.18 [0.09-0.28] %/mL m^{-2} and 0.12 [0.06-0.18] %/mL m^{-2} respectively. Relative coupling of the systolic and diastolic strain-volume relation was observed with a mean value of 0.34 ± 1.1. UNCOUP was correlated with age with a value for *r* of 0.4.

Conclusions

Higher values for the systolic and early-diastolic strain-volume relation in females can be reflective of different cardiomechanics as LV contraction is not only comprised of longitudinal but also circumferential and radial deformation. In line with current literature our custom software found relative coupling of the systolic and diastolic strain-volume relation in our cohort of healthy subjects. Towards older age relative uncoupling of the systolic and diastolic strain-volume relation was found.

References

1. Oxborough D, Heemels A, Somauroo J, McClean G, Mistry P, Lord R, et al. Left and right ventricular longitudinal strain-volume/area relationships in elite athletes. *Int J Cardiovasc Imaging*. 2016;32(8):1199-211.
2. Lord R, George K, Somauroo J, Stembridge M, Jain N, Hoffman MD, et al. Alterations in Cardiac Mechanics Following Ultra-Endurance Exercise: Insights from Left and Right Ventricular Area-Deformation Loops. *J Am Soc Echocardiogr*. 2016;29(9):879-87 e1.
3. Hulshof HG, van Dijk AP, Hopman MTE, Heesakkers H, George KP, Oxborough DL, et al. 5-Year prognostic value of the right ventricular strain-area loop in patients with pulmonary hypertension. *Eur Heart J Cardiovasc Imaging*. 2021;22(2):188-95.
4. Zoë A. Keuning, Thijs P. Kerstens, Robert R. Zwaan, Daniel J. Bowen, Arie P. J. van Dijk, Jolien W. Roos-Hesselink et al. Left ventricular strain-volume loops in bicuspid aortic valve: new insights in hemodynamics and prognostic value. [*Submitted*]

Gaussian processes improve rapid estimates of physics-based artificial intelligence predictors of 3D velocity, shear stress and pressure fields in pig and human coronary arteries.

Lam Wing Hei[1], Amal Roy Murali[2], Ben Morgan[1], Christos Bourantas [4,5], Ryo Torii [3], Anthony Mathur[4,5], Andreas Baumbach[4,5], Marc C Jacob[2], Sergey Karabasov[1], and Rob Krams[1]

[1] Department of Science and Engineering, Queen Mary University London

[2] Laboratoire de Mécanique des Fluides et d'Acoustique UMR5509, INSA Lyon, Ecole Centrale de Lyon, University of Lyon, University of Claude Bernard Lyon 1, CNRS, 69130, Ecully, France.

[3] Department of Mechanical Engineering, UCL, London

[4] Centre for Cardiovascular Medicine and Devices, William Harvey Research Institute, Queen Mary University of London, London, UK;

[5]Department of Cardiology, Bart's Heart Centre, Bart's Health NHS Trust, London, UK

Introduction

Abnormal blood flow patterns are strong predictors of atherosclerotic lesion location, progression, and plaque rupture. Patient-specific blood flow patterns are often obtained from 3D-imaging-based computational fluid dynamics. However, the high computational cost makes these methods impractical. Here, we describe a new technique which is capable of producing accurate, patient-specific blood flow patterns in seconds.

Methods

We developed a semi-automatic pipeline producing a large dataset of randomly perturbed meshes (n=3,500) obtained from atherosclerotic pig coronary arteries (n=7) to numerically simulate blood flow in the classical way for reference (with Abaqus). This dataset was decomposed with Singular Value Decomposition (SVD) to obtain "eigen" modes of the variation of flow solutions with respect to the variation in the geometry shape, analogous to the common-base Proper Orthogonal Decomposition (cPOD). From the obtained eigen modes, 10 modes were selected to represent >90% of signal variance with respect to geometry variation. Next, for dimensionality reduction of mesh geometries, t-Stochastic Neighbour Embedding (t-SNE) was employed to represent each mesh with approximately 110,000 nodes in a low dimensional space with variable dimensionality. A Bayesian regression method based on Gaussian Process Regression was then used to obtain a surrogate model of the cPOD mode coeffients as a function of the t-SNE representation of meshes. The hyperparameters for the surrogate model were then optimised using in 70% of data randomly chosen from the available dataset and evaluated on the remaining 30% for accuracy as validation set.

Results

The developed architecture was capable of predicting the dominant 10 POD-mode coefficients, within few seconds. The RMSE (Root Mean Square Error) for regression over first mode was of 5.2% with for a 2D tSNE in the training dataset, and 7.2% for the test set. Increasing dimensionality of the tSNE decreased the error (Figure 1) with a best performance (lowest RSME) for 4D t-SNE. A plot of variation of the training and validation errors for t-SNE dimensions 3 and 4 for all 10 cPOD modes are also given in Fig 2. and 3. The errors in the higher modes decreased, and as their energetic contribution to the overall signal also decreased rapidly, their contribution to the overall error was neglectable.

Conclusions

We have developed a very fast and highly accurate CFD solver for patient-specific studies in the catheterization laboratories.

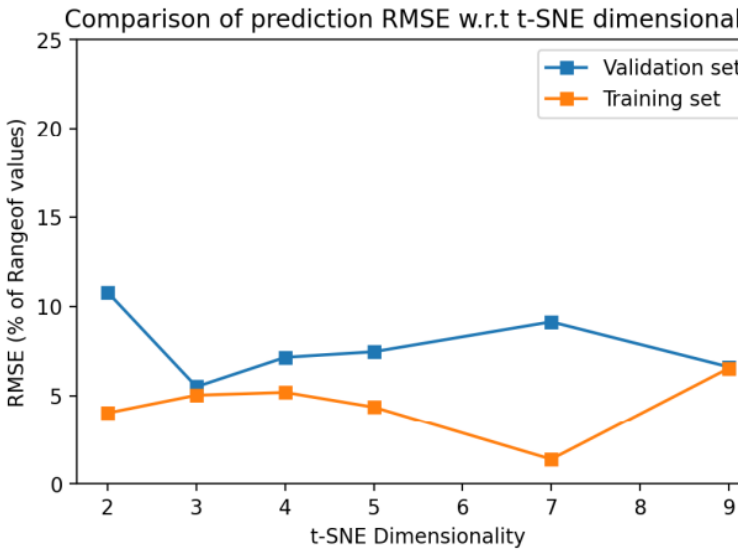

Figure 6: Comparison of RMSE across different t-SNE dimensions for the 1st cPOD mode coefficient

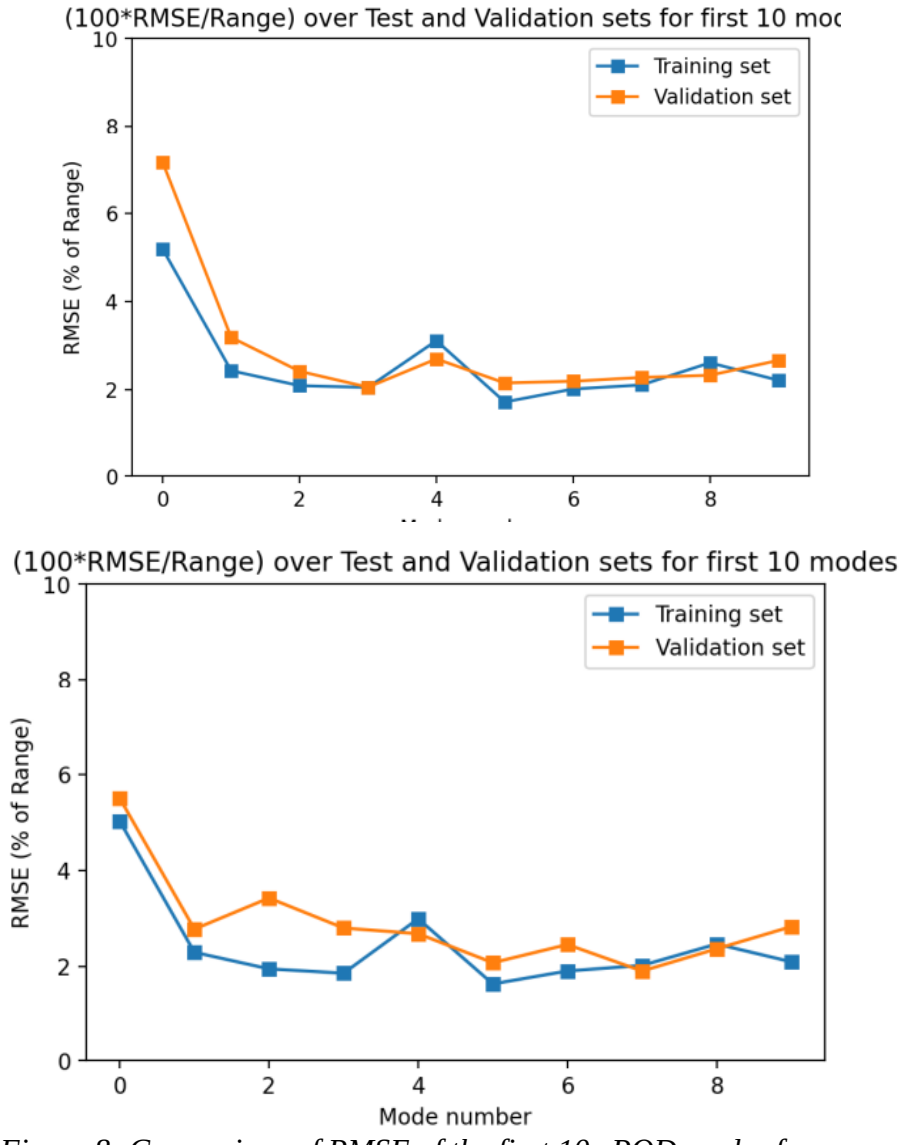

Figure 8: Comparison of RMSE of the first 10 cPOD modes for regression over 3D t-SNE dimensionality.

A fully automated vulnerable plaque classifier for OCT accurately predicts vulnerable plaques in human coronary arteries.

Luis Alberto Marcelo Chamorro[7], Zimpi Komo [7], Ali Bashir Ali[7], Ryo Torii[2], Christos Bourantas[3], Qianni Zhang[1], Anthony Mathur[3,8], Andreas Baumbach[3,8,] Ryan M. Pedrigi, PhD[4]; Ranil de Silva, MBBS, PhD[5,6], and Rob Krams, MD, PhD[7]

[1]Dept of Electronical Engineering, Queen Mary University, UK

[2]Dept of Mechanical Engineering, University College London, UK
[3] Centre for Cardiovascular Medicine and Devices, William Harvey Research Institute, Queen Mary University of London, London, UK
[4]School of Engineering, University of Nebraska, USA
[5]National Heart and Lung Institute, Imperial College London, UK, [6]Institute of Cardiovascular Medicine and Science, Royal Brompton and Harefield NHS, UK
[7]Department of Science and Engineering, Queen Mary University, UK
[8]Department of Cardiology, Bart's Heart Centre, Bart's Health NHS Trust, London

Introduction
The high mortality rates of coronary artery disease (CAD) is predominantly associated with a rupture of the thin cap overlying a vulnerable plaque. Intracoronary optical coherence tomography (OCT) is a high resolution, catheter based invasive imaging system that allows the evaluation of atherosclerotic plaques at the requested high spatial resolution. Currently, plaque characterization and classification are done by visual evaluation, making diagnosis of OCT images subjective and time-consuming. Initial AI classifiers suffer from the fact they cannot detect the plaque embedded in healthy tissue. In this study, we overcome this problem, and propose to fully automate OCT-based atherosclerotic plaque diagnosis using a validated experimental pig model. In order to validate the AI architecture in patients, we apply an active learning approach.

Methods
A PCSK transgenic pig model was instrumented with a stenotic stent to expedite advanced plaque formation. For validation 10 patients were studied before and after stent implementation. OCT images of the plaques were acquired and carefully co-registered with its histology (pigs) or stents (humans) using a previously developed and validated 3D histological method. Labelling was performed by two trained pathologists into 5 classes (IT, XA, PIT, FCA, TCFA). As this led to an unbalanced dataset, we performed data augmentation. Pre-processing, speckle noise reduction (ELF, BM3D) and segmentation (K-means, Gaussian mixture models) were applied in a variety of combinations to evaluate their contribution to classification by five different pretrained ultradeep convolutional neural networks (ResNet-50, VGG-16, VGG-19, Inception-V3 and DenseNet-121). Saliency maps were implemented to visualize the prediction of the classification. As the human data were devoid of histology we are using an active learning approach to train and test the network including human data.

Results
The accuracy of ResNet-50 was poor, 40%, but VGG-16, VGG-19, Inception-V3, and DenseNet-121 performed well, achieving 69%, 66%, 78%, and 80% prediction accuracy. Pre-processing appeared essential to obtaining a high accuracy. Further fine tuning of DenseNet-121 led to a training and testing accuracies of 95% and 92%. Saliency maps indicated that DenseNet-121 automatically identified diseased, atherosclerotic plaques, even when they only partially affected the vessel wall.

Conclusions
Ultradeep learning classifiers when trained with histological data are capable of robust classification of vulnerable plaques even when the plaques are partially affecting the cross section of the vessel wall. This is the first, fully automatic, accurate OCT based vulnerable plaque classifier.

Twist1 deletion influences atherosclerotic plaque size and composition

Blanca Tardajos Ayllón, Mannekomba Diagbouga, Paul C. Evans

William Harvey Research Institute, Queen Mary University of London, London, UK

Introduction
Atherosclerotic plaques progress towards instability and rupture, triggering myocardial infarction or stroke. Plaque instability is characterised by several features, including reduced collagen content and increased inflammation. Although it is known that disturbed blood flow influences plaque instability by altering endothelial cell (EC) physiology, the molecular pathways driving this process are incompletely understood. TWIST1, a transcription factor, has been linked to coronary artery disease and stroke in human genetic studies. Additionally, TWIST1 expression is induced in atheroprone areas exposed to disturbed flow. Although endothelial *Twist1* promotes early atherogenesis, the role of *Twist1* in atheroprogression and plaque stability is unknown, and is a focus of the current study.

Methods
ApoE$^{-/-}$ mice with an inducible EC-specific *Twist1* knockout (*Twist1*$^{fl/fl}$ *ApoE*$^{-/-}$ *Cdh5*$^{CreERT2/+}$; called *Twist1*$^{EC\text{-}KO}$) and control mice (*Twist1*$^{fl/fl}$ *ApoE*$^{-/-}$ *Cdh5*$^{+/+}$; called *Twist1*$^{EC\text{-}WT}$) were generated. At 8-10 weeks of age, mice were exposed to a Western diet for 8 weeks to generate plaques, then given tamoxifen to activate Cre, and fed a Western diet for a further 6 weeks to drive atheroprogression. Aortic EC (CD31^{+} CD45^{-}) were isolated by FACS and analysed by single-cell RNA sequencing (scRNAseq), to assess the influence of *Twist1* on downstream targets and EC phenotype. Additionally, plaque histological studies were performed in brachiocephalic arteries.

Results
Twist1 deletion in aortic EC was validated by qRT-PCR, revealing a >90% reduction in *Twist1*$^{EC\text{-}KO}$ mice. scRNAseq identified 10 EC subtypes in mouse aortas. *Twist1* deletion had a major effect on EC heterogeneity by suppressing three of these subtypes (clusters 2, 7 and 8), which highly expressed low shear stress markers. Gene ontology analysis revealed that these clusters are associated with endothelial-to-mesenchymal-transition (endMT) (cluster 8), development, cell proliferation and migration (cluster 7) and extracellular matrix organisation (cluster 2, 8). Studies of brachiocephalic plaques show that *Twist1* EC deletion reduces plaque size and collagen content (feature of stability), while it increases macrophage content and necrotic core area (feature of instability).

Conclusions
Altogether, our results show that Twist1 controls EC heterogeneity in atherosclerosis to increase plaque growth and concomitantly enhance features of plaque stability, suggesting that endMT may have some beneficial roles in atherosclerosis.

Endothelial GATA4 in Atherosclerosis Progression

Siyu Tian[1,2], Paul C. Evans[1,2]

[1]Centre for Biochemical Pharmacology, William Harvey Research Institute, Queen Mary University London, UK.

[2]Department of Infection, Immunity and Cardiovascular Disease, University of Sheffield, Sheffield, UK.

Introduction

Atherosclerosis plaques rupture is driven by the disturbed blood flow which induces multiple pathological changes in endothelial cells (ECs). GATA4 is a pleiotropic transcription factor that regulates fundamental cellular processes including survival, migration, proliferation, inflammation and EndMT. Our investigation unveiled the expression of GATA4 at sites of disturbed flow in the murine aorta, and EC-specific deletion of GATA4 demonstrated its role as a driver of EC turnover and early atherosclerosis. However, the GATA4 gene and regulatory networks that specifically play roles in atherosclerosis are unknown.

Methods

In this study, we employed cultured human aortic endothelial cells subjected to an ibidi flow system in vitro and utilized RNA-seq to probe into the involvement of GATA4 and regulatory genes in atherosclerosis.

Results

En face staining of EC in the murine aorta revealed that GATA4 is enriched at sites of disturbed blood flow that are prone to atherosclerosis initiation. A significant upregulation of the GATA4 gene expression in human aortic endothelial cells exposed to disturbed flow, encompassing both low shear stress (LSS) and low oscillatory shear stress (LOSS) conditions. Silencing of the GATA4 gene in ECs attenuated this increase under disturbed flow. Furthermore, RNA-seq analysis was employed to dissect the functional role of GATA4 and its associated gene networks under LSS and LOSS conditions.

Conclusions

Our findings will be compared with in vivo data to elucidate the role of GATA4 in driving pathogenic EC subsets and gene networks. This will be achieved through the analysis of plaques from GATA4 EC knockout mice and control groups using single-cell RNA-seq techniques.

Characterizing TWIST1 signalling pathway in atheroprogression

Mannekomba R Diagbouga[1,2], Blanca Tardajos Ayllon[1,2], Paul C Evans[1,2]

1.William Harvey Research Institute, Queen Mary University of London, London, UK. 2.Department of Infection, Immunity and Cardiovascular disease, University of Sheffield, Sheffield, UK.

Introduction

The transcription factor TWIST1 regulates fundamental cellular processes including migration, proliferation, inflammation, and endothelial-to-mesenchymal transition (EndMT), all contributing to atherosclerosis. We previously demonstrated that TWIST1 is enriched in endothelial cells (ECs) at atheroprone low oscillatory shear stress (LOSS) regions of the aorta and promotes atherogenesis. Moreover, TWIST1 is abundantly expressed in human and mouse atherosclerotic plaques, suggesting a role in plaque biology and in atheroprogression. Despite its significance, the precise signalling pathways of TWIST1 in the context of atherosclerosis remain incompletely understood. In this study, we aimed to characterize the downstream targets of TWIST1, focusing on their roles in regulating proliferation and migration.

Methods

We used unbiased RNA-seq to capture TWIST1 downstream targets. Human aortic ECs (HAoECs) silenced for *TWIST1* or non-targeting control were exposed to LOSS for 72h using Ibidi system. The RNA-seq data were integrated with *Twist1*-regulated genes from murine plaque endothelium and common genes were studied by gene silencing and functional analyses. Additionally, ATAC-seq was employed to investigate chromatin accessibility changes associated with *TWIST1* silencing and shear stress levels.

Results

RNA-seq analysis identified 293 genes whose expression levels were altered in absence of TWIST1. Integration with the transcriptome of murine plaque endothelium identified 45 common genes of which 10 (*AEBP1*, *COL4a1*, *DLL4*, *FKBP10*, *KDELR3*, *MTX2*, *RSP7*, *SEC23*, *PELP1*, and *USP14*) were subsequently demonstrated to regulate proliferation, with *PELP1* additionally regulating migration. AEBP1, COL4a1, FKBP10 and PELP1 regulation by TWIST1 was confirmed at the protein level via immunostaining or western blot. Further RNA-seq analysis of *PELP1* and *AEBP1* silenced cells confirmed their roles in regulating cell migration, extracellular matrix, and cell division, sharing common downstream targets with TWIST1. Furthermore, HAoECs cultured on Collagen IV matrix and exposed to LOSS show no difference in proliferation level in *TWIST1* silenced *vs.* control cells. Thus, collagen IV particularly its constituent protein COL4a1, may play a crucial role in mediating TWIST1 regulation of proliferation. To assess the potential impact of TWIST1 on chromatin remodelling, we conducted ATAC-seq analysis. The results indicated that *TWIST1* silencing alone may not significantly alter chromatin accessibility in HAoECs, as there were no notable differences in open chromatin regions between *TWIST1* silenced and control cells. However, when examining the effects of shear stress, we found that *TWIST1* silencing had a discernible impact. Comparing *TWIST1* silenced cells under LOSS *vs.* HSS, we observed 37 significantly different open chromatin regions. In contrast, comparing control cells under LOSS *vs.* HSS, we identified 400 significantly different open chromatin regions. These results suggest that TWIST1 silencing may modulate chromatin accessibility in response to changes in shear stress levels.

Conclusions

Altogether, our results support TWIST1 as a driver of EC proliferation, migration and EndMT in atherosclerosis disease. Our mechanistic studies add to the understanding of endothelial TWIST1 signalling. The identification of key regulators of this pathway, including AEBP1, COL4a1, FKBP10 and PELP1 provides potential therapeutic targets and insights into disease pathogenesis. Furthermore, our ATAC-seq data give insight into the dynamic chromatin accessibility changes associated with TWIST1 silencing and WSS levels, providing additional layers of understanding in the molecular regulation of atherosclerosis progression.

Arterial arcades and collaterals regress under hemodynamics-based diameter adaptation: a computational and mathematical analysis

Wieger Kuppers[1], Vivi Rottschäfer[2,3], Ed van Bavel[1]

[1] Department of Biomedical Engineering and Physics, Amsterdam University Medical Center, The Netherlands
[2] Mathematical Institute, Leiden University, The Netherlands
[3] Korteweg de Vries Institute for Mathematics, University of Amsterdam, The Netherlands

Introduction

Wall shear stress (WSS) is considered to be a major drive for regulation of arterial caliber, shaping arterial trees from large entrance vessels to increasingly smaller branches. Yet, arterial networks are not trees but rather contain many arcades and collateral connections. These loop-like structures provide alternative routing for flow in the presence of upstream obstructions. Here, we use simulation and mathematical analysis to evaluate WSS-driven adaptation of such networks.

Methods

Adaptation of arterial radius (r) to WSS was modeled as: $\frac{dr}{dt} = k_{reg} r(|WSS| - WSS_{ref})$ with WSS_{ref} the reference value for adaptation and k_{reg} the rate of adaptation. We assumed Newtonian fluid and non-ideal pressure sources and sinks. A large range of model variations were simulated in small topologies with extensive sweeping of parameters and initial states. In addition, the model was applied to large human coronary [1] and mouse cerebral arterial networks [2].

Simulation results

The example shows a triangular topology with adapting colored segments connected to three sources. The simulation starts close to an equilibrium where all segments obtain WSS_{ref}. Yet, this equilibrium is unstable, leading to regression of one of the segments and conversion to a mere tree with the remaining segments at WSS_{ref}. While equilibria could generally be found in small networks, these were unstable and adaptation to WSS caused regression of loops in all 8756 tested models, including generalized local hemodynamics as stimulus, different adaptation rates for arterial shrinkage and growth, heterogeneous WSS_{ref}, dynamic pressure gradients, and 100-fold sweeps of model parameters. Loss of arterial loops was also found in the human coronary network, containing 101,223 segments and 3202 initial loops, for tested WSS_{ref} between 1 and 30 Pa. A similar loss of loops was found in adaptation models of the cerebral circulation of BALBc and C57BL6 mice.

Optical Coherence Tomography versus Computed Tomography Angiography in the stented femoropopliteal tract for Computational Fluid Dynamics

Lisa Rutten[1,2,3,4], Kartik Jain[3], Michel Versluis[2], Michel MPJ Reijnen[1,4]

[1]Multi-Modality Medical Imaging group, TechMed Center, University of Twente, Enschede, the Netherlands

[2]Physics of Fluids group, TechMed Center, University of Twente, Enschede, the Netherlands

[3]Engineering Fluid Dynamics group, University of Twente, Enschede, the Netherlands

[4]Department of vascular surgery, Rijnstate, Arnhem, the Netherlands

Introduction

In-stent restenosis (ISR) in the femoropopliteal tract remains a challenging problem. Computational fluid dynamics (CFD) models can be used to better understand and possibly predict ISR. Computed tomography angiography (CTA) is often used to obtain the vessel geometry, but the limited resolution (~300 µm) and blooming artifacts cause uncertainty that affect the CFD result. Intravascular optical coherence tomography (OCT) can be used to improve the geometry as it has a better resolution (15-20 µm) and minimal artifacts, but OCT is invasive and has a limited field of view of 10 mm in diameter. In this study, post stent placement OCT and CTA scans of the femoropopliteal tract are compared to identify the differences in geometrical features between both scans.

Methods

Post stent placement OCT and CTA scans of the femoropopliteal tract, obtained from a prospective, single-center study, will be used. The stented segments are determined to match positions in the OCT and CTA scans. The stent area (proximal, mid and distal in the stent) and the native vessel area (1 cm proximal/distal to the stent) are quantified and reported as mean [min max]. Further analysis of the scans is performed to identify potential unique differences between both imaging modalities. OCT- and CTA-based CFD simulations will be performed and the corresponding differences in flow quantities, velocity and wall shear stress, will be quantified.

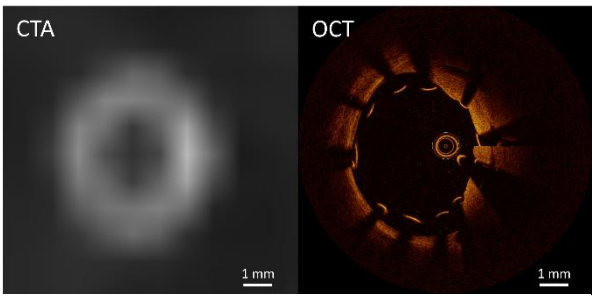

Figure 1: CTA and OCT scan of the same position. OCT shows stent strut malapposition, not observed with CTA.

Results

So far sixteen patients were included in the clinical study and one patient case was analyzed. The stent area was larger in the OCT scan (15.46 mm^2 [13.78 18.08]) compared to the CTA scan (9.08 mm^2 [8.47 9.43]). The native vessel area was smaller in the OCT scan (mean area: 14.08 mm^2 [12.38 15.77]) than in the CTA scan (mean area: 14.63 mm^2 [10.53 18.73]). The stent structure and apposition of the stent against the vessel wall were visualized with OCT, but could not be observed with CTA, see Figure 1. A preliminary CTA-based CFD result shows complex flow phenomena, including flow separation and boundary tripping, see Figure 2.

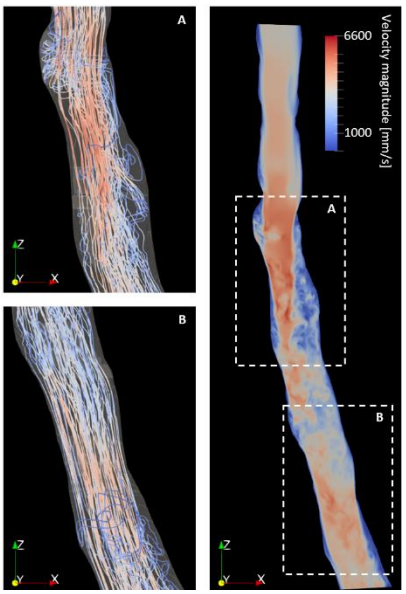

Figure 2: CTA-based CFD showing boundary tripping and flow separation. Velocity magnitude in mm/s.

Conclusions

These preliminary results show that OCT clearly captures better anatomical features than CTA, resulting in larger in-stent lumen measurements. The complex flow phenomena observed in the CTA-based CFD simulation could be even more complex in the OCT-based CFD simulations. Patient inclusion and our work on detailed CFD to quantify differences in flow quantities is ongoing. These quantitative differences will steer us towards corresponding association with pathology of ISR.

Fibrin clot formation modeling: from in vitro validation to 3D simulations

JMH Cruts[1], A Rachid[2], FN van de Vosse[2], M Rezaeimoghaddam[2], FJH Gijsen[1,3]

[1] Department of Biomedical Engineering, Erasmus MC, Rotterdam, The Netherlands
[2] Department of Biomedical Engineering, Eindhoven University of Technology,Eindhoven, the Netherlands
[3] Department of BioMechanical Engineering, Delft University of Technology, Delft, the Netherlands

Introduction

After a blood vessel is damaged, clot formation will be initiated and the stabilizing fibrin network will be formed due to coagulation. *In silico* coagulation models offer a means to investigate this complex mechanism. However, existing models are often computationally expensive or fail to account for individual variations in blood composition, therefore neglecting potential complications such as accelerated clot growth in thrombotic plasma. To address this, our aim is to introduce a fast reduced coagulation model, validated on a personalized basis, and test this in a real 3D clot environment.

Methods

A biophysical model of a fibrin-rich clot is developed based on previously developed framework [1]. This model employs a reduced 0D coagulation model, solving for the concentrations of factors IX, X, prothrombin, and thrombin. Personalized parameters are determined through curve fitting against *in vitro* thrombin generation test data (Fig. 1A). Subsequently, these parameters are integrated into a 1D *in silico* model in MATLAB, including a system of coupled reaction-diffusion equations, additionally solving for fibrinogen and fibrin concentrations (Fig. 1B). The bottom wall in Fig. 1B represents a tissue factor (TF) coated surface, initiating coagulation. Thrombin-fibrin(ogen) binding is added to the model to improve correspondence with *in vitro* observations from thrombodynamics assays [2]. Next, the personalized coagulation model is implemented in a 3D blood vessel geometry (d=30µm) (Fig. 1C) using FLUENT 2021R1, featuring a TF-coated surface, pre-adhered static platelets, and a parabolic velocity inlet ($\dot{\gamma}$=20s^{-1}).

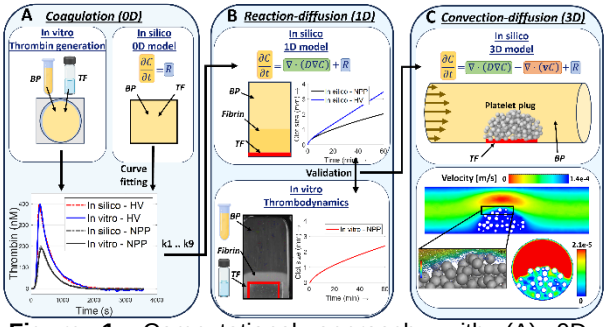

Figure 1: Computational approach, with (A) 0D coagulation model, (B) 1D model validation, and (C) 3D clot environment simulations. BP = blood plasma, TF = tissue factor, NPP = normal pooled plasma, HV = healthy volunteer plasma.

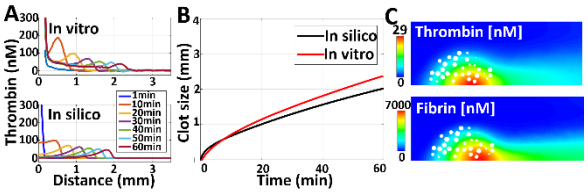

Figure 2: 1D *in silico* vs. *in vitro* thrombin (A) and fibrin (B) spatio-temporal dynamics for NPP. C) thrombin and fibrin concentration after 30min.

Results

The 1D results for NPP reveal that the thrombin wave speed and final thrombin peak height were 27µm/min and 39.2nM *in vitro*, and 22.4µm/min and 45.2nM *in silico* (Fig. 2A). Clot size at 30min and stationary growth rate were 1.5mm and 38µm/min *in vitro*, and 1.3mm and 30.9µm/min *in silico* (Fig. 2B). 3D simulations showed that thrombin and fibrin primarily concentrate within the platelet plug and extend further downstream (Fig. 2C).

Conclusions

Consistency was observed between *in vitro* and *in silico* observations. Our model offers potential to investigate patient-specific fibrin clot formation, and aid in tailoring treatments such as anticoagulant therapy, thereby reducing thrombotic risks. Further validation with additional plasma samples is underway.

References

[1] Bouchnita, A., et al. (2020). *PloS one*, 15(7), e0235392.
[2] Dashkevich, N. M., et al. (2012). *Biophysical journal*, 103(10), 2233-2240.

Acknowledgements: The EU funded project In Silico World, grant number 101016503.

The importance of patient-specific boundary conditions in pulmonary artery models

CH Armour[1,2], D Gopalan[3], B Statton[4], D O'Regan[4], Lawrie, A[1] and XY Xu[2]

[1]National Heart and Lung Institute, Imperial College London, London; [2]Department of Chemical Engineering, Imperial College London, London; [3]National Pulmonary Hypertension Service, Imperial College Healthcare NHS Trust, London; [4]Medical Research Council, Laboratory of Medical Sciences, Imperial College London, London

Introduction: Computational fluid dynamics (CFD) continues to unearth valuable insight into the mechanistic workings of cardiovascular disease. Many aortic studies have shown the use of a patient-specific 3D inlet velocity profile (IVP) derived from 4D-flow MRI data is essential to accurately capture flow and wall shear stress (WSS) patterns, particularly in the ascending aorta (AAo)[1,2]. Given the anatomical similarities between the AAo and pulmonary aorta (PA) being the two primary arteries in the body, it can be hypothesised that the choice of IVP is also important in PA studies. However, this has yet to be reported, and the complexity of the PA (numerous bifurcations close together) may add to the impact of IVP choice on flow fields and further derived parameters. This study was conducted to elucidate the influence of IVP choice in PA simulations.

Methods: The PA from a patient diagnosed with pulmonary hypertension was segmented from a CT scan, beginning just distal to the pulmonary valve and extending into both the left and right PA down to the 3rd branching level. Three simulations were run using 1: a 3D IVP derived from the patients 4D-flow MRI data, 2: a 2D through-plane derived from the 3D IVP, and 3: a flat profile derived by a generic PA flow waveform extracted from literature[3] tuned to match the patients stroke volume (measured from cardiac MR) and heart rate (extracted from echocardiogram). The choice of outlet boundary condition was explored by testing flow split conditions based on branch area and 3-element Windkessel models tuned to each branch. Simulations were run in Ansys CFX with a timestep of 0.001 s for 5 cycles to ensure periodicity, with the final cycle used for analysis.

Results: Figure 1 shows peak systolic velocity fields for both a 3D and flat IVP, as an example. Velocity extracted directly from 4D-flow MRI is also shown as the gold standard for comparison. The velocity fields are very well matched between the 3D IVP simulation and the 4D-flow MRI data, while the flat IVP fails to capture areas of high velocity in the main and first branch level of the PA. This discrepancy results in significantly different predictions of TAWSS, with the 3D IVP predicting an average TAWSS roughly 2.9x greater than the flat IVP. The choice of boundary condition was less impactful on flow patterns due to the small size of the vessels.

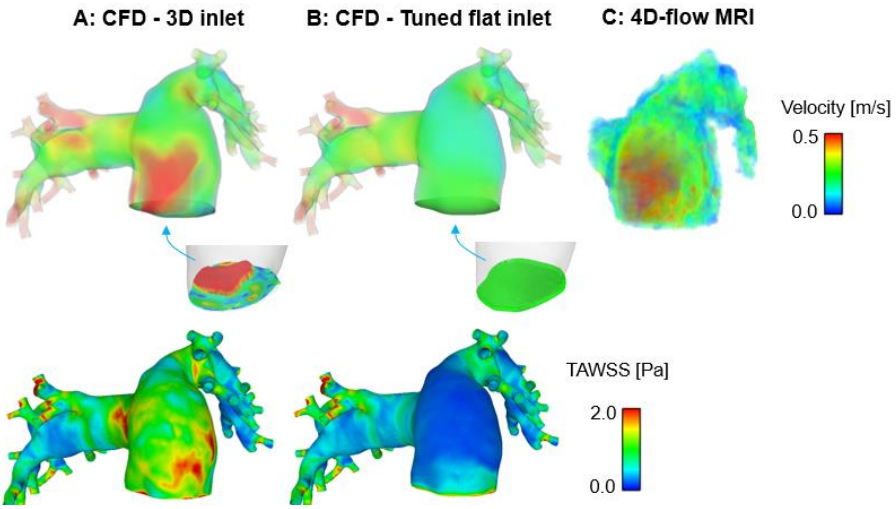

Figure 9: Velocity fields and time-averaged wall shear stress (TAWSS) predicted by CFD simulations using (A) a 3D and (B) flat inlet velocity profile. (C) 4D-flow MRI velocity field.

Conclusion: This work clearly demonstrates the importance of using a patient-specific 3D IVP when simulating the PA for accurate assessment of WSS. These results will be highly valuable to researchers when designing future studies, and when interpreting the results of previous studies which have utilised idealised conditions.

References: [1.] Armour et al. 2020 *Biomech Mod Mechanbiol* 20:481-490; [2.] Pirola et al. 2017 *APL Bioeng* 2(2):026101. [3.] Fanni et al. 2023 *Comp Fluids* 260:105912.

Aortic Annuloplasty: a Methodology to integrate Experimental Data, In-silico Analysis, and 4D-flow MRI Validation

Luca Bontempi[1,2], Anna Ramella[1], Francesco Migliavacca[1], Steffen Ringgaard[3,4], Won Yong Kim[3,5], Peter Johansen[6,7], Monika Colombo[2]

1. Dept. of Chemistry, Materials and Chemical Engineering, Politecnico di Milano, Italy
2. Dept. of Mechanical and Production Engineering, Aarhus University, Denmark
3. Dept. of Clinical Medicine, Aarhus University, Denmark
4. Dept. of MR Research Centre, Aarhus University Hospital, Denmark
5. Dept. of Cardiology, Aarhus University Hospital, Denmark
6. Dept. of Electrical and Computer Engineering, Aarhus University, Denmark
7. Dept. of Cardiothoracic and Vascular Surgery, Aarhus University Hospital, Denmark

Introduction

Aortic annuloplasty involves the implantation of a ring external to the aortic root, aiming to reduce annular dimensions in conditions such as aortic valve regurgitation. This project introduces a methodology to validate a computational fluid-structure interaction (FSI) model, through the comparison with magnetic resonance imaging (MRI) analysis of an experimental setup. The primary objective is to create a tool to assist clinicians in pre-surgical planning: specifically, to aid in selecting the optimal device geometry and mechanical properties, ensuring an optimal sinotubular junction (STJ) – annulus ratio in post-operative conditions. In order to validate this tool, the synthesis of experimental measurements, computational analyses, and clinical imaging necessitates a multidirectional and systematic coupling.

Methods

The initial steps involved the analysis of idealized aortic root phantoms, constructed through CAD-modeling to obtain both a 3D-printed phantom to be integrated in the in-vitro flow-loop and an in-silico geometry used for computational simulations. Two phantoms were created using an elastic resin with material properties similar to the aortic root wall: one representing physiological conditions and another one for post-operative conditions, with an idealized ring implanted downstream of the valve. To gather essential boundary conditions for the computational model, the phantoms were incorporated into a flow meaurement setup, where a pulsatile flow is maintaned. A glycerol-water mixture was used as testing fluid to simulate blood viscosity. Flow and pressure sensors-based collected data from the flow-loop were then applied within the numerical model to define the strong two-way FSI simulation, replicating the entire aortic root under physio-pathologic and post-annuloplasty conditions. The model couples the deformable aortic wall domain with hemodynamic behaviors. Simulations were performed on 20 CPUs of an Intel Xeon64 with 120 GB of RAM using the commercial finite element solver LS-Dyna 971 R14.0. To validate the simulation, 4D-flow MRI scans of the experimental flow-loop were employed to collect fluid velocity-field data.

Results

Both the 3D-printed phantoms were integrated into the experimental mock circuit. Experimental sensor-based data were collected and implemented with the in-silico simulation. 4D-flow MRI data of the mock circulatory loop were compared with the velocities obtained through the FSI simulation.

The qualitative comparison between the computational and imaging outcomes has shown that the implantation of the annuloplasty ring leads to higher aortic pressures, due to the increase in resistance caused by the presence of the ring, resulting in a subsequent increase in the leaflet coaptation height.

The outlined methodology was proven feasible and has been applied to a preclinical study using ex-vivo porcine aortic roots.

Conclusions

To develop an in-silico model of aortic annuloplasty applicable to patient-scale scenarios and reduce the time-consuming nature of in-vitro testing, preliminary steps are essential to ensure the reliability of obtained results. Integrating experimental parameters, in-silico analysis, and clinical imaging data enables the prediction of surgical outcomes and assists surgeons in assessing surgical feasibility and planning.

Examining the range of Constrained Mixture Modelling in predicting Adaptation and Maladaptation in Arterial Mechanics

Yousof MA Abdel-Raouf[1], Lauranne Maes[2], Mathias Peirlinck[3], Nele Famaey[2], Patrick Sips[4], Julie De Backer[4,5], Jonathan Weissmann[6], Jay D Humphrey[6,7], Patrick Segers[1]

[1]Institute of Biomedical Engineering and Technology - BioMMedA, Ghent University, Ghent, Belgium
[2]Biomechanics Section, Department of Mechanical Engineering, KU Leuven, Leuven, Belgium
[3]Department of BioMechanical Engineering, Delft University of Technology, Delft, the Netherlands
[4]Center for Medical Genetics Ghent, Department of Biomolecular Medicine, Ghent University, Ghent, Belgium
[5]Department of Cardiology, Ghent University Hospital, Ghent, Belgium
[6]Department of Biomedical Engineering, Yale University, New Haven, CT, USA
[7]Vascular Biology and Therapeutics Program, Yale School of Medicine, New Haven, CT, USA

Introduction

The arterial wall, a dynamic environment of cells and extracellular matrix, plays a crucial role in maintaining artery structure and enabling cells to sense local stress. Connective tissue diseases and aging impact the extracellular matrix, making computational models vital for predicting disease progression by simulating elastic constituent changes.

Methods

We apply a general case of stress-driven smooth muscle cell mass production within the bilayer artery model comprising a (constrained) mixture of four constituents namely elastin, collagen (four fiber families), smooth muscle cells (SMCs), and glycosaminoglycans (GAGs) [1]. Elastase is replicated by reducing elastin mass fraction linearly with time, and the effect of inhibition of collagen cross-linking -via administration of beta-aminopropionitrile (BAPN)- is replicated by reducing collagen prestretch [2][3]. Additionally, we present a scenario where we assume that GAGs (with subsequent Donnan Swelling) are produced by SMCs with the aim of maintaining interlamellar spacing occupied by the latter with attachment to the elastin lamellae [4][5].

Results.

The model demonstrates behaviour of arteries in-line with previously reported experiments where compromised elastin (shown in dashed blue in Figure below) causes adequate dilation of the artery, but collagen compromise disrupts advemtitial rescue and collagen recruitment at higher stiffness. Implementation of growth laws also shows elastin+collagen compromise causes acute SMC production, and when compensatory swelling through GAG production is added, the total circumferential stress in the media is lower (312 MPa) compared to the absence of swelling (380 MPa).

Conclusions

Constrained mixture models offer greater utility to applications of constituent specific maladies.

References

[1] Roccabianca S, Bellini C, Humphrey JD. 2014 J. R. Soc. Interface 11: 20140397.
[2] Li DS, Cavinato C, Latorre M, Humphrey JD. 2023 Proc. R. Soc. A 479: 20230116.
[3] Weiss D, et al. 2021 Acta Biomaterialia 134: 422-434: 202107059.
[4] Cavinato C, et al. 2021 Front. Cardiovasc. Med. 8:800730.
[5] Yousef S, Matsumoto N, et al. 2021 Scientific Reports 11:13185.

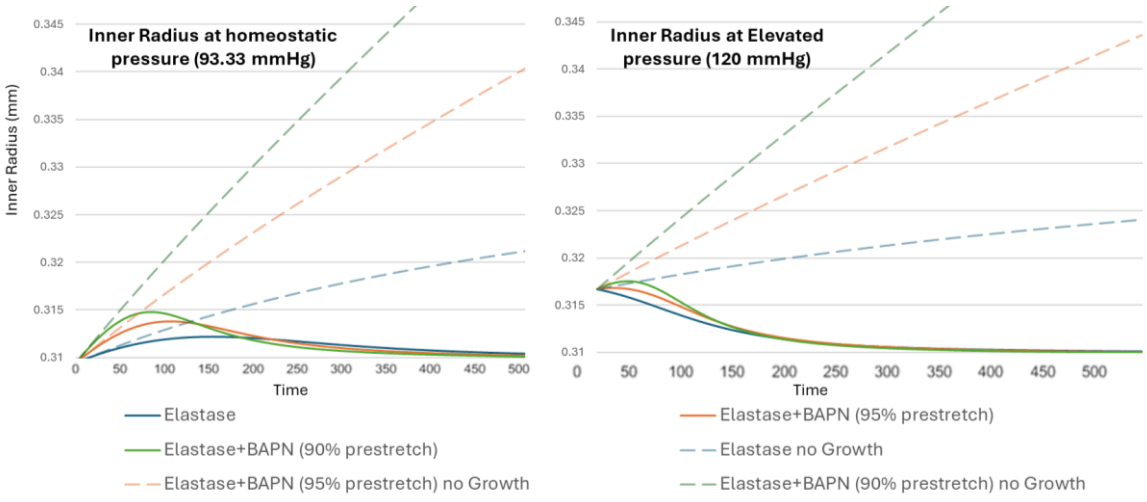

Mechanical characterization of thrombi by studying shear and friction

Sanne van Kuijk, Behrooz Fereidoonnezhad, Frank Gijsen

Department of Biomedical Engineering, Erasmus MC, Rotterdam, The Netherlands
Department of Biomechanical Engineering, TU Delft, Delft, The Netherlands

Introduction

Stroke, caused by large vessel occlusions, is the second leading cause of death worldwide. Large vessel occlusions are the result of thrombosis, the undesired coagulation of blood within the vasculature. Due to this coagulation, a vessel can get blocked, prohibiting blood flow to areas distal from the occlusion, with all the serious consequences that may ensue. Since 2015, mechanical thrombectomy procedures have been widely accepted as a successful treatment technique to remove thrombi from the vasculature. However, complete reperfusion is only reached in 50% of acute ischemic stroke cases. To successfully remove a thrombus from the vasculature, it is necessary to apply a specific retrieval force. This force must exceed the opposing forces, including the impaction force generated by the blood pressure gradient across the thrombus and the interaction forces between the thrombus and the vessel wall. Multiple studies have focused on tensile and compressive properties of thrombi. However, little is known about shear loading of the thrombus and about the interaction properties of the thrombus-vessel wall interface. Therefore, the aim of this study is to gain a better comprehension of thrombus biomechanics by studying the shear behavior of thrombi and the interaction of the thrombus-vessel wall interface *in vitro*.

Methods

In order to perform these *in vitro* studies, two custom-made test setups have been designed and developed. The friction test setup contains a plate of which the angle can be inclined slowly. By placing a thrombus-vessel wall sample on top of this plate, it is aimed to determine the static and kinetic coefficient of friction of the thrombus-vessel wall interface. Furthermore, it is aimed to determine the effect of time on this interaction. The thrombus-vessel wall interface was created by obtaining a piece of vein and blood from pigs. To study the shear behavior of thrombi a shear test setup has been developed. Two thrombi types have been utilized for this study, red blood cell- and fibrin-rich. Within the shear test setup it is possible to perform shear experiments under different normal loading conditions. A comprehensive analysis of the data acquired from experiments performed with both test setups has been conducted. Furthermore, a computational model has been developed to fit towards the experimental data obtained from the shear experiments.

Results

The friction experiments suggest that time positively influences the bonds formed between a thrombus and the vessel wall as the coefficients of friction increase with an increased waiting time. Furthermore, a strong positive correlation was found between the static and kinetic coefficient of friction. This result was also found when doing an extensive analysis of the data obtained from the shear experiments. Additionally, the shear experiment showed that the thrombus composition influences its mechanical properties. Higher shear moduli and kinetic coefficients of friction were found for the fibrin samples, compared to the red blood cell samples.

Conclusions

The results obtained from the friction and shear experiments provide valuable insights into thrombus biomechanics. By extending the performed studies a better comprehension on thrombus mechanics and the thrombus-vessel wall interaction can be achieved.

CFD assisted Machine Learning for blood flow prediction in patient-specific aorta geometries

Daiqi Lin, Saša Kenjereš

Department of Chemical Engineering, Faculty of Applied Science, Delft University of Technology, The Netherlands

Introduction

Blood flow patterns and associated hemodynamical parameters like wall shear stress (WSS) have been linked to aorta pathologies and aortic dysfunction [1]. Combining Computation Fluid Dynamic and Neural Networks is a promising and efficient method to predict flow fields. The shape-driven method has been applied to predict velocity and pressure [2]. However, whether such results are good enough to calculate WSS hasn't been explored and tested. In this study, the neural networks have been trained on 1000 virtual aorta geometries based on the available 4D Flow MRI measurements to predict velocity and pressure fields separately. Furthermore, in the post-processing phase, we derived the WSS from velocity predictions and evaluated the error of WSS against ground-truth results.

Methods

In total 40 patient-specific aorta geometries are obtained from MRI dataset. Details about the MRI dataset can be found in our previous study [1]. In this study, in contrast to Pajaziti et al. [2], we did not clip the geometries to maintain the same length, which makes the scenario more realistic. To extend the limited number of available geometries, we conducted the data augmentation to generate in total 1000 virtual aorta geometries using the Statistical Shape Model (SSM). CFD simulations are run for these virtual geometries to generate a dataset of velocity and pressure. The laminar flow model is used to simplify the problem and to reduce calculation time. The neural networks of Multilayer perceptron (MLP) are built and trained to predict velocity and pressure fields based on the reported structure [2]. Then, additional in-house codes are developed to calculate the WSS from the predicted velocity using PvPython (a Python interface of ParaView). The predicted WSS and ground-truth WSS are patched and mapped onto the surface to analyze the performance.

Results

We demonstrated that the neural networks can predict the CFD flow fields (pressure and velocity magnitude) for 100 cases within 0.135 sec on the NVIDIA A4500 GPU, which is much faster than the traditional calculation method (~1h per case). In terms of subject-wise MAEs (Mean Absolute Errors), the average MAE is 198.8 Pa and 0.11 m/s for the prediction of pressure and velocity-magnitude. For the derived WSS, the averaged MAE is 0.43 Pa and, the MAEs for the best and worst case are 0.26 Pa and 1.20 Pa, respectively. After mapping the WSS onto an aortic surface, we find that generally, the predicted WSS agrees well with the ground-truth value. However, the predicted WSS cannot reflect the finest WSS distribution characteristics. In the worst cases, the error of WSS usually exists near the inlet and outlet zones, which is a result of the unequal-length geometries.

Conclusions

The neural network of multilayer perceptron can predict 3D velocity and pressure within seconds. The developed neural network is also good enough to predict the wall shear stress with an error of 13.18%. In some cases, the predicted WSS may lose the finest local distributions. Significant errors are usually located in the proximity of the inlet and outlet. In this study, we only consider the dataset of healthy aorta geometries without considering side-branches. For future studies, more aorta pathologies, such as the aortic aneurysm and coarctation, and the blood flow in the aorta branches will be taken into consideration. To predict the finest local distributions of WSS, the pixel-to-pixel method could be applied to bridge the gap.

References

[1] R. Perinajova *et al.*, "Geometrically induced wall shear stress variability in CFD-MRI coupled simulations of blood flow in the thoracic aortas," *Comput Biol Med,* vol. 133, p. 104385, Jun 2021, doi: 10.1016/j.compbiomed.2021.104385.

[2] E. Pajaziti *et al.*, "Shape-driven deep neural networks for fast acquisition of aortic 3D pressure and velocity flow fields," *PLoS Comput Biol,* vol. 19, no. 4, p. e1011055, Apr 2023, doi: 10.1371/journal.pcbi.1011055.